

KOBELCO TECHNOLOGY REVIEW

No. **38** Mar. 2020

Feature- I : Automotive Weight Reduction

Feature- II : Iron and Steel Manufacturing Technology

Contents

Feature- I Automotive Weight Reduction

Global Business Expansion of Wire Rods and Sheets 1
Takaaki MINAMIDA, Kuniyasu ARAGA

Global Marketing Strategies for Automotive Aluminum Sheet, Extrusion and Forged
Suspension Businesses 5
Dr. Yasuo TAKAKI, Shogo SAKAMOTO, Takashi OKA, Narikazu HASHIMOTO

Global Expansion of Copper Rolled Product Business for Automotive Terminals and
Connectors 11
Yosuke MIWA

Technical Trends in Aluminum Alloy Sheets for Automotive Body Panels 16
Yosuke OTA, Dr. Tetsuya MASUDA, Shinpei KIMURA

Technical Trends in Copper Alloys and Plating for Automotive Terminals 21
Hiroshi SAKAMOTO

Hot-dip Galvanized Steel Sheet of 980MPa Grade Having Excellent Deformability in
Axial Crush 28
Michiharu NAKAYA, Shinjiro KANETADA, Michitaka TSUNEZAWA

Multi-material Automotive Bodies and Dissimilar Joining Technology to Realize
Multi-material 32
Dr. Junya NAITO, Dr. Reiichi SUZUKI

Feature- II Iron and Steel Manufacturing Technology

Outline of Steel Production System 38
Tsutomu HAMADA

Decreasing Coke Rate under All-Pellet Operation in Kobe No.3 Blast Furnace ... 46
Hitoshi TOYOTA, Tomonori MAEDA, Nayuta MITSUOKA, Kota TANAKA

Establishment of Special Steel Production System at Kakogawa Works
-Construction of No.3 Secondary Refining Equipment and No.6 Continuous Caster- ... 53
Yasumasa YOSHIDA, Hideya OKADA, Hiroaki SAKAI, Hiroyuki ONODA, Dr. Takehiro NAKAOKA

Improving Control Accuracy of Steel Plate Temperature by Accelerated Cooling
with Columnar Water Jets 60
Takahiro OHARA, Keiichi YAMASHITA, Kiichiro TASHIRO, Kensuke UENISHI, Taketsugu OSAKA, Dr. Masahiko MITSUDA

On-line Inter-stand Tension Monitor System for Bar Mill 67
Dr. Masanori KOBAYASHI, Tomohide TAIRA, Masakazu KATO, Hiroshi NAKAMURA, Dr. Yoshio MORIMOTO, Dr. Shusuke YANAGI

Technology for Reducing Strip Meandering in Tandem Cold Mill 72
Shigeto KOIZUMI, Dr. Shusuke YANAGI, Dr. Masanori KOBAYASHI

Influence of Modified Oxide Inclusions on Initiation of Rolling Contact Fatigue Cracks in
Bearing Steel 80
Masaki SHIMAMOTO, Dr. Eiichi TAMURA, Akihiro OWAKI, Akihiro MATSUGASAKO

Editor-in-chief :
Yuichiro GOTO
Associate Editor :
Hiroyuki TAKAMATSU

Editorial Committee :
Nobuyuki FUJITSUNA
Takao HARADA
Hiroshi HASHIMOTO
Koichi HONKE
Atsushi INADA
Haruyuki KONISHI
Yasushi MAEDA
Michihiro MATSUZAKI
Hiroki SANARI
Hirohisa WATANABE

Published by

**Technical Development Group
Kobe Steel, Ltd.**

5-5, Takatsukadai 1-chome,
Nishi-ku, Kobe, HYOGO 651-2271, JAPAN
<https://www.kobelco.co.jp>

Editorial Office: **Shinko Research
Co., Ltd.**

2-4, Wakinohama-Kaigandori 2-chome,
Chuo-ku, Kobe, HYOGO 651-8585,
JAPAN
Fax: +81-78-261-7843
E-mail: rd-office@kobelco.com

Global Business Expansion of Wire Rods and Sheets

Takaaki MINAMIDA*¹, Kuniyasu ARAGA*²

*¹ Wire Rod & Bar Products Marketing & Technical Service Department, Iron & Steel Business

*² Sheet Products Marketing & Technical Service Department, Iron & Steel Business

Japanese automakers and parts manufacturers are expanding their production outside Japan, increasing the need for local procurement. To respond to this need, Kobe Steel's wire rod and sheet business has established production plants for steel and intermediate products outside Japan to enable the supplying of products with quality equivalent to that of products supplied in Japan. This paper describes Kobe Steel's approach to expanding its global business, focusing on special-steel wire rods and high-tensile sheet products.

Introduction

Although Japanese automakers have reached a peak of automotive production in Japan, they are steadily increasing production abroad.¹⁾ (Fig. 1) For a very long time, there have been many Japanese companies expanding outside Japan, and there is a growing need for local procurement of steel and semi-finished products from these companies. In particular, parts for Japanese automakers are required to have high functionality and quality with little variation, and those produced in other countries are required to be of the same quality as the ones made in Japan.

In response to this need, Kobe Steel began business in the U.S. and Thailand in 1990 ahead of other steel companies, following Japanese automakers and parts manufacturers that were expanding outside Japan. The company moved into China in the 2000s and into Mexico in the 2010s and expanded its production capacity at each site to establish a global supply system.

This paper reports on Kobe Steel's global

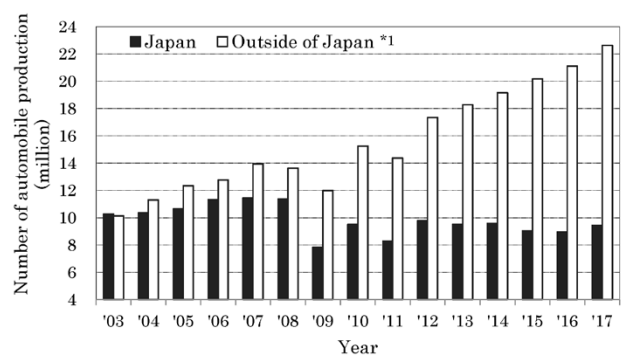


Fig. 1 Trend of automobile production by Japanese automakers (Kobe Steel made this figure on the basis of the database¹⁾ of Marklines Co., Ltd.)

business development in the field of wire rods and steel sheets.

1. Initiative for global supply system

1.1 Wire rods

Highly functional steel (special steel) with a small amount of alloying elements is mainly adapted to wire rods and steel bars used as production materials for automotive parts. Wire rods and steel bars are roughly classified according to shape: i.e., wire rods are wound in coils and steel bars are cut into bars of certain lengths. Kobe Steel carries a variety of special-steel wires outside Japan. Before being shaped into final parts, wire rods are subjected to so-called secondary processing to produce metallographic structures and diameters suitable for fabrication.

Kobe Steel has set up secondary processing sites outside Japan since the mid-1990s and has responded to the requests for local procurement. In addition, the company established a rolling plant for producing base material in Thailand in 2016 and began local production of special-steel wire rods.

1.2 Steel sheets

Steel sheets are mainly used for outer panels (doors, hoods, etc.) and body frames (pillars, members, etc.), among various other auto parts. Outer panels have stringent surface quality requirements, while body frames must be of extremely high strength to protect passengers. The latter, in particular, frequently adopt high-tensile-strength steel (hereinafter referred to as "Hi-Ten") sheets, and the use of Ultra-Hi-Ten (UHSS) with a tensile strength of 780 MPa or greater is also expanding (Fig. 2).²⁻⁵⁾ In recent years, hot stamping steel sheets (PHS)^{6,7)} are also being used frequently.

Kobe Steel has been focusing on the development of Hi-Ten for a long time⁸⁻¹⁰⁾ and has gained a high reputation, being dubbed "Hi-ten Kobe." With its Kakogawa Works as the mother factory, Kobe Steel established joint ventures with local iron and steel manufacturers in the United States and China. In Europe, the company supplies products with the same quality as those supplied in Japan via local technical cooperation partners.

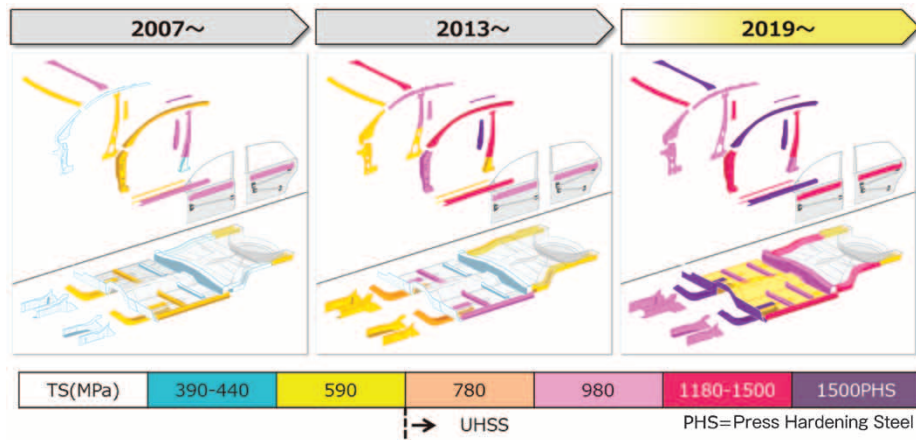


Fig. 2 Application of high tensile strength steel sheet to automotive parts

2. Development of manufacturing sites by regions

In the field of wire rods and sheets, Kobe Steel has sites for manufacturing steel and semi-finished products in major areas of the automotive industry, including North America, Latin America, Europe, Thailand and China (Fig. 3, Table 1, Table 2, and Table 3), thus responding to local procurement requests from customers. This section describes the market trend and development status of Kobe Steel in each region.

2.1 North America

In order to resolve the Automobile Trade Dispute between the U.S. and Japan, many Japanese automakers began local production in the United States in the 1980s. Accompanying the automakers, parts manufacturers also set up factories there, raising the demand for local procurement of materials.

One of the developments of Kobe Steel's manufacturing sites in the field of wire rod was the establishment of Grand Blanc Processing L.L.C. (hereinafter referred to as "GBP") near Detroit, Michigan, in the U.S. in the mid-1990s. Being a secondary processing site of wire rod, GBP produces cold heading wires (hereinafter referred to as "CH wires") and wires for the rolling bodies of bearings (hereinafter referred to as "bearing wires").

In the field of steel sheets, the PRO-TEC Coating Company was established in Leipsic, Ohio, USA, in 1990, with a 50:50 investment by the United States Steel Corporation, the largest iron and steel manufacturer in North America, and Kobe Steel (Fig. 4). In 1993, a hot-dip galvanizing line (hereinafter referred to as "CGL") began production, and in 1998, the second CGL was put into operation, achieving a production capacity of 1 million short tons per

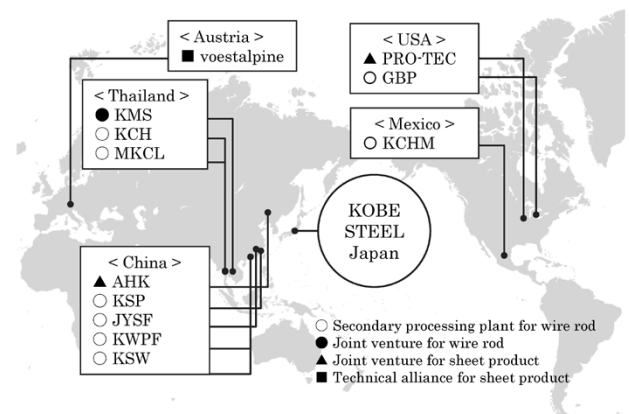


Fig. 3 Locations of steel mills and secondary processing plants for wire rod

Table 1 Steel production mills and their outlines

Company name	Kobelco Millcon Steel Co., Ltd.	Kobelco Angang Auto Steel Co., Ltd.	Pro-Tec Coating Company
Main Product	Wire rod	Cold-rolled High Strength Steel Sheet	Cold-rolled, Galvanized and Galvannealed High Strength Steel Sheet
Place	Rayong, Thailand	Liaoning, China	Leipsic, USA
Tie-up year	2016	2014	1990
Equity participation	50%	49%	50%
Main facilities	Wire rod rolling	CAL	CGL, CAL

year. Over 95% of the production is related to automobiles, and high-value-added products such as outer panels are mainly produced in addition to the Hi-Ten of 590 MPa or higher. In 2013, a continuous annealing line (hereinafter referred to as "CAL") was put into operation to supply cold-rolled Hi-Ten, enabling the supply of both plated and cold-rolled products. Ultra-Hi-Tens, up to 1,500 MPa class for cold-rolled, and up to 980 MPa class for plated, are being mass produced, and the company supplies high quality Ultra-Hi-Ten mainly to Japanese automakers and the Big Three automakers (Detroit 3) in the United States.

In order to meet automaker's demand for Hi-Tens with even higher strength and higher workability,

Table 2 Secondary processing companies for wire rods in USA, Mexico and Thailand

Company name	Grand Blanc Processing L.L.C. GBP	Kobelco CH Wire Mexicana, S.A DE. C.V. KCHM	Kobe CH Wire (Thailand) Co., Ltd. KCH	Mahajak Kyodo Co., Ltd. MKCL
Place	Michigan, USA	Guanajuato, Mexico	Bangkok, Thailand	Bangkok, Thailand
Production	CH & Bearing wire	CH wire	CH wire	Cold drawn bar
Establishment	1995	2014	1997	1996
Equity participation	20%	10%	30%	27.5%

Table 3 Secondary processing companies for wire rods in China

Company name	Kobelco Spring Wire (Foshan) Co., Ltd. KSW	Kobe Special Steel Wire Products (Pinghu) Co., Ltd. KSP	Jiangyin Sugita Fasten Spring Wire Co., Ltd. JYSF	Kobe Wire Products (Foshan) Co., Ltd. KWPF
Place	Foshan, Thailand	Pinghu, Thailand	Jiangyin, China	Jiangyin, China
Production	Valve spring wire	CH & Bearing wire	Suspension spring wire	Cold drawn bar & CH wire
Establishment	2012	2007	2005	2004
Equity participation	50%	47%	60%	60%

in September 2017 the company announced the construction of a third CGL with state-of-the-art heat treatment and cooling functions. Construction is in progress for its inauguration in July 2019. After completion, it will become a steel sheets factory with a total production capacity of 2 million short tons/year.

2.2 Latin America

The expansion of Japanese companies has become significant in Mexico, where the automotive industry has formed a major industrial cluster in recent years. In response, Kobe Steel established Kobelco CH Wire Mexicana, S.A. de C.V., a secondary processing site for wire rods, in Guanajuato, located in central Mexico, and has been producing CH wires since 2016.

2.3 Europe

Europe is still disseminating a lot of the latest and cutting-edge technologies, mainly from Germany, the country where automobiles originated. Japanese automakers have made a full-scale entry into Europe and have been there since the late 1980s.

In January 2002, Kobe Steel signed a "comprehensive alliance agreement for automotive steel sheets" with an Austrian iron and steel maker, voestalpine Stahl GmbH (hereinafter called "voest"). This agreement has established a global supply system of Hi-Ten materials for Japanese automakers



Fig. 4 PRO-TEC Coating Company



Fig. 5 Kobelco Millcon Steel

through mutual transfer and joint research on technologies and know-how related to Hi-Ten. In September 2008, Kobe Steel formed a comprehensive alliance with voestalpine Krams GmbH, the roll forming division of the voest group, on the roll forming technology of Ultra-Hi-Ten. It responds to a wide range of automakers' needs by offering not only materials but also production technologies for

auto parts.

2.4 Thailand

Thailand's automotive industry has continued to develop since the entry of Japanese automakers in the 1960s, building the foundation for the automotive industry in Southeast Asia.

In the field of wire rods, Kobe Steel established, in the late 1990s, Kobe CH Wire (Thailand) Co., Ltd., a production site of CH wires, and Mahajak Kyodo Co., Ltd., which produces various bright bars used in, among other things, hot coiled springs for suspension application, and thus contributed to the expansion of the automotive industry in this country.

In June 2015, Kobe Steel signed an MOU with Thailand's Millcon Steel Public Company Limited on the establishment of a joint venture for rolling and selling wire rods in Thailand. On the basis of this, the two companies worked together to establish Kobelco Millcon Steel Co., Ltd., the ninth wire rod rolling plant of Kobe Steel, in February 2016 (Fig. 5). The newly established company started rolling special-steel wire rods at the end of May 2017 and began supplying these wire rods to Japanese automobile related customers, which are currently the major supply destinations.

2.5 China

The automotive production in China was approximately 500,000 units in the 1990s, has expanded rapidly since 2000, and reached a volume close to 30 million units in 2016. From the 1980s to the mid-1990s, it was mainly U.S. and European automakers that entered the market, followed by Japanese automakers, and production has been fully in progress since 2000.

Kobe Steel has established four sites for the secondary processing of wire rods since 2004. Kobe Wire Products (Foshan) Co., Ltd., and Kobelco Spring Wire (Foshan) Co., Ltd., were established in Guangzhou, where there is a major base for Japanese automakers. In addition, Jiangyin Sugita Fasten Spring Wire Co., Ltd., and Kobe Special Steel Wire Products (Pinghu) Co., Ltd., were established near Shanghai, another location with many parts manufacturers. These sites have established a system in China's major automotive production areas for producing and supplying materials to be processed into safety-critical parts, such as CH wires, bearing wires, bright bars for suspension springs, and wires for engine valve springs.

In the field of steel sheets, Kobelco Angang

Auto Steel Co., Ltd., was established in August 2014 as a joint venture with Angang Steel Co., Ltd., a subsidiary of Anshan Iron and Steel Group Co., Ltd., for the purpose of manufacturing and selling cold-rolled Hi-Tens for automobiles. In April 2016, a CAL with an annual production capacity of 600,000 tonnes began operation, enabling the local production of high-value-additive cold-rolled Ultra-Hi-Ten products, and Ultra-Hi-Tens up to 980MPa class are being mass produced. It is planned to produce high-strength, high-workability Ultra-Hi-Ten and expand supply to the U.S., European, and Chinese automakers, as well as to Japanese automakers.

Conclusions

In order to cope with the need for local procurement of high-grade steel materials associated with the development of Japanese automakers abroad, global development has been promoted sequentially in the fields of both wire rods and steel sheets. Through these efforts, global steel supply systems have been established, involving Japan, the United States, Mexico, Thailand, and China for special steel wire rods, and involving Japan, the United States, Europe, and China for Hi-Ten steel sheets.

It is believed that the need for Japanese quality will grow further in the future not only to expand automotive production, but also to resolve environmental and collision-safety issues. Kobe Steel will strive to maintain its position as the best partner for automakers by continuing to meet these high demands.

References

- 1) MarkLines Inc. MarkLines Automotive Industry Portal. https://www.marklines.com/ja/vehicle_production/search, (reference on 2018-10-30)
- 2) Y. Futamura et al. *R&D Kobe Steel Engineering Reports*. 2011, Vol.61, No.2, pp.41-44.
- 3) Y. Utsumi et al. *R&D Kobe Steel Engineering Reports*. 2017, Vol.66, No.2, pp.3-7.
- 4) M. Ikeda et al. *R&D Kobe Steel Engineering Reports*. 2017, Vol.66, No.2, pp.8-11.
- 5) T. Murata et al. *R&D Kobe Steel Engineering Reports*. 2017, Vol.66, No.2, pp.17-20.
- 6) S. Hamamoto et al. *R&D Kobe Steel Engineering Reports*. 2011, Vol.61, No.2, pp.45-48.
- 7) S. Hamamoto et al. *R&D Kobe Steel Engineering Reports*. 2017, Vol.66, No.2, pp.12-16.
- 8) T. Kashima et al. *R&D Kobe Steel Engineering Reports*. 1992, Vol.42, No.1, pp.16-19.
- 9) Y. Tanaka et al. *R&D Kobe Steel Engineering Reports*. 1992, Vol.42, No.1, pp.20-23.
- 10) J. Iwanani et al. *R&D Kobe Steel Engineering Reports*. 1997, Vol.47, No.2, pp.42-45.

Global Marketing Strategies for Automotive Aluminum Sheet, Extrusion and Forged Suspension Businesses

Dr. Yasuo TAKAKI*¹, Shogo SAKAMOTO*², Takashi OKA*³, Narikazu HASHIMOTO*³

*¹ Aluminum Flat Rolled Products Sales Department for Automotive, Aluminum & Copper Business

*² Daian Works, Aluminum & Copper Business

*³ Aluminum Extrusion & Fabrication Plant, Chfu Works, Aluminum & Copper Business

The need to reduce the weight of automobiles has been increasing year by year due to fuel efficiency regulations responding to environmental issues. Since the 1980s, there has been a gradual increase in the use of aluminum sheets for automotive body panels, aluminum extrusions for bumper reinforcements and door beams, and aluminum forgings for suspension parts. Aluminum has now become an indispensable automotive material. Kobe Steel has been developing business outside Japan by utilizing the material technology, production technology, and application technology for automotive parts; these technologies have been cultivated in response to the requirements of Japanese automakers. This article outlines the technological developments in each type of business, the development of production plants outside Japan, and the company's efforts to globally supply products of the same quality as those supplied in Japan.

Introduction

Regulations and assessments for the safety of automobiles have been strengthened, increasing the weight of safety members and the number of electrical components. On the other hand, fuel efficiency regulations for automobiles are becoming increasingly stringent year by year. **Fig. 1** shows the current status and future targets of fuel efficiency regulations from 2015 to 2030 in Japan, Europe, China and the United States.¹⁾

With this background, automotive weight reduction and electrification have become inevitable issues, creating a new application field for aluminum

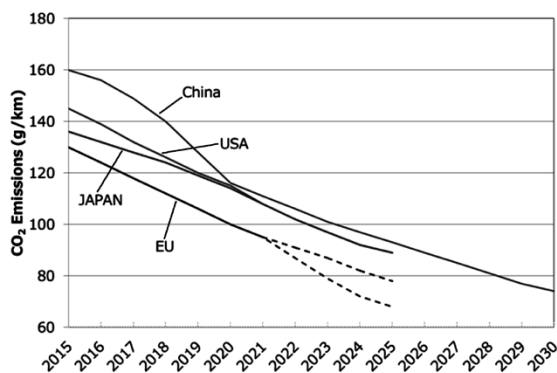


Fig. 1 Trends in strengthening of fuel efficiency and CO₂ criteria for passenger cars in Japan, Europe, China and the U.S.¹⁾ (Fuel efficiency criteria converted to the amount of CO₂)

alloys, which have specific gravities approximately 1/3 that of steel. Kobe Steel has been expanding this field first in Japan and is promoting expansion to other countries.

This paper outlines the global business expansion of aluminum sheets, extruded material, and forged suspensions being promoted by Kobe Steel.

1. Global expansion of automotive aluminum sheets

1.1 Development of automotive aluminum sheets and application to automotive bodies

In Japan, the application of aluminum sheets to automotive body panels began in 1985 and was widely adopted by automakers in the first half of the 1990s (**Fig. 2**).²⁾ During this period, effort was put into developing original Japanese alloys, and the 5000 series alloys, which possessed excellent formability and suppressed the generation of Lüders bands, were first put into practical use. In the mid-1990s, the use of aluminum panels declined for a time due to the slump in the Japanese economy, but during that period, there was no letup in the development of aluminum alloys for automotive bodies. In particular, the development of the 6000 series alloys was promoted because of their excellent bake-hardenability, i.e., their capacity for being age-hardened by the heat during the paint baking of automotive bodies.^{3),4)} These 6000 series alloys became, and continue to be, the mainstream in the 2000s, when aluminum is being used full-scale in mass-produced cars.

During these years, the control on CO₂ emissions and fuel consumption became increasingly stringent in Europe and the United States, where the application of aluminum sheets to automotive bodies is progressing faster than in Japan. Accordingly, aluminum alloys for automotive bodies, such as the 6111 and 6022 alloys in North America and 6016 and 6014 alloys in Europe, were standardized. In addition, special efforts have been put into the development of application technologies involved in the use of aluminum sheets in automotive bodies, such as forming, joining, and painting.

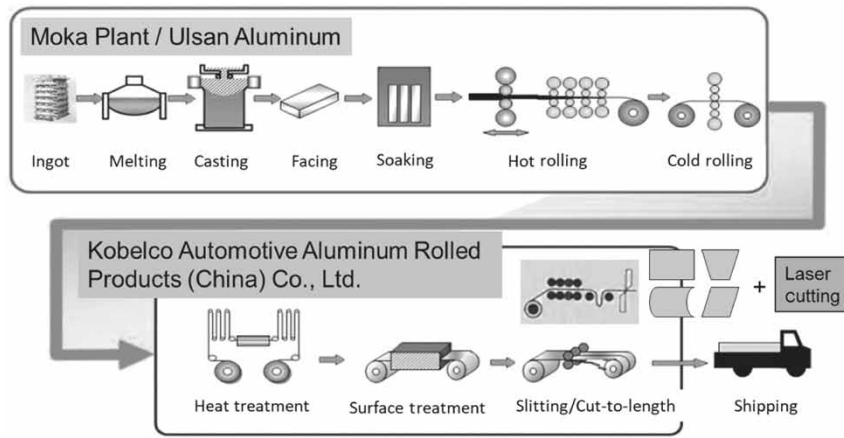


Fig. 3 Supply scheme of automotive aluminum sheet to China by Kobe steel group

2003. This was followed by exporting to China in 2008 and to North America and Australia in 2013. During the peak period, the products were supplied to six countries, and customers outside Japan accounted for the larger portion of Kobe Steel's automotive aluminum sheets. In realizing this global supply, the above-mentioned partnerships with Alcoa and Hydro helped effectively to grasp the demand early and respond to the specifications of each user. Other important points include the achievements in mass production in Japan and technology that is not limited to aluminum sheet material but extends to the application of aluminum sheets to automotive bodies.

The demand for automotive aluminum sheets continues to expand worldwide. Especially in China, now the world's largest automobile producer, it is anticipated that automotive exhaust gas regulations and fuel economy regulations will be strengthened due to environmental problems, and the demand for aluminum is expected to increase with a view to reducing the weight of automotive bodies.

Against this backdrop, Kobe Steel established Kobelco Automotive Aluminum Rolled Products (China) Co., Ltd. (hereinafter referred to as "KARP") in Tianjin, China, in 2014 and began producing automotive aluminum sheets there. KARP owns various types of equipment for the continuous heat treatment processing of cold rolled coils, the subsequent surface treatment process, and finishing processes such as slitting and shearing, and can supply aluminum panel material with the same high quality as that available in Japan. In the new scheme, Kobe Steel's Moka Plant supplies cold-rolled coils (intermediate products) to KARP, where they are heat-treated and surface-treated to be shipped as product coils. These product coils had previously been exported from Moka Plant, which has been switched to the new scheme. Combined with the

parallel development of new customers, production is growing steadily. In 2017, a joint venture company, Ulsan Aluminum, Ltd., was established with Novellis Korea Limited in Korea to produce cold-rolled coils in Korea and supply them to KARP in China and Moka Plant in Japan. (Fig. 3).

In response to the future demand for automotive aluminum sheets, the demand being expected to grow further in China and in Japan, a stable supply of high quality aluminum sheets is secured by the expanded supply capacity; i.e., the upstream process at the 2 sites of Moka Plant and Ulsan Aluminum, and the downstream process at 2 sites, Moka Plant and KARP.

2. Application trends and global development of aluminum extrusions to auto parts

2.1 Trend in application of aluminum extrusions to auto parts

Aluminum extrusions have been increasingly applied since the 1960s as small cross-sectional extrusions for engine heat exchanger tubes, multi-hole profiles, etc. In the 1980s, aluminum alloys began to be applied to body structures, and extruded strips and hollow extrusions were used. In addition, they have been applied to ABS housing and collision safety members since the 1990s. In addition to lightness, aluminum extrusions can be formed into profiles with complex cross-sectional shapes having varying wall thickness distributions, which is difficult with steel, offering an effective means of reducing automotive weight.

Kobe Steel has been focusing on collision safety members such as bumper reinforcements and door beams, which have been steadily and increasingly adopted. In the future, further growth is expected in the demand for aluminum used in automotive frame members and other parts that are required to

be lighter for vehicle electrification.

2.2 Development status of aluminum extrusion alloys for automobiles

For weight reduction, aluminum extrusion alloys themselves are also required to be stronger. In Japan, the use of aluminum for bumpers began in the 1990s with a 6000 series alloy of 230 MPa proof-stress grade. Since then, the adoption of a 7000 series alloy with a proof stress exceeding 300 MPa has been in progress. To achieve further weight reduction, there has recently been a demand for 7000 series alloys with even higher strength.

High strength 7000 series alloys, however, have the problem of high susceptibility to stress corrosion cracking (hereinafter referred to as "SCC"). Hence, Kobe Steel has developed a 7000 series alloy, "7K55," that balances the trade-off characteristics of strength and SCC resistance.⁷⁾ This alloy began to be produced for Japanese manufacturers as a bumper material, and its future production at a plant outside Japan is being considered.

The demand for the weight reduction of aluminum extrusions continues, and there still is a strong need for the higher strength of the 7000 series alloys. Kobe Steel is continuing development, pursuing a balance between strength and SCC resistance.

2.3 Future development and global supply capability of automotive aluminum extrusions

Kobe Steel's extrusion business has been developed mainly by supplying aluminum extrusions to automakers in Japan. Recently, however, there have been an increasing number of cases where local production is required due to global development of the same model, multi-site production, and trade tariffs. Supply capacity in North America is often required, and Kobelco Aluminum Products & Extrusions Inc. was established with a capital of 24 million dollars in Bowling Green, Kentucky, as a manufacturing site integrating the steps from melting to processing. The first phase construction started with a processing line having a planned production capacity of 500 tonnes/month.

The plan is to begin doing business first with Japanese automakers and then with North American automakers in the future.

2.4 Business development in North America

In North America, high tensile strength steel

is mainly used as the material for automobiles ranging from compact/medium-sized cars to large-sized cars. There is, however, a forecast that the adoption of aluminum will increase in response to the above-mentioned world-wide strengthening in fuel efficiency regulations. Aluminum extrusions in North America are mainly made of 6000 series alloys, and the main targets are collision safety members that require high strength.

Kobe Steel will focus on bumpers and door beams, on which the company has accumulated know-how in Japan, and make proposals on 7000 series alloy extrusions, Kobe Steel's specialty, in North America. For future targets, it is expected that the demand for materials will increase for lockers and side sills, which are structural parts of automobiles.

3. Forged aluminum suspension business

3.1 Overview of business development for forged aluminum suspensions

The use of aluminum forgings for suspension parts began in the late 1980s. Initially, they were mainly used in sports cars to improve motion performance. In recent years, they are increasingly being used in a wide range of vehicles in response to fuel and exhaust gas regulations, which have become even more stringent to address global warming, and to suppress the increase in vehicle mass due to the addition of safety equipment, among other considerations.

Kobe Steel started producing forged aluminum suspension parts in Japan in 1988. Since then, the company has responded to the growing demand while increasing its equipment capacity and improving productivity. Japanese automakers, on the other hand, have transferred their manufacturing sites to other countries and are seeking local supplies of materials with the same quality as those available in Japan. In response to such demands, Kobe Steel established manufacturing sites in North America in 2005 and in China in 2012.

3.2 Features of forged aluminum suspension parts

An example of suspension members is shown in Fig. 4.⁸⁾ Suspensions are important security components, connecting automotive bodies and tires; they correspond to the legs of human bodies. These parts require high strength along with high reliability, and greatly affect motion performance and ride quality. From the latter viewpoint, it is important to balance the so-called "sprung mass,"

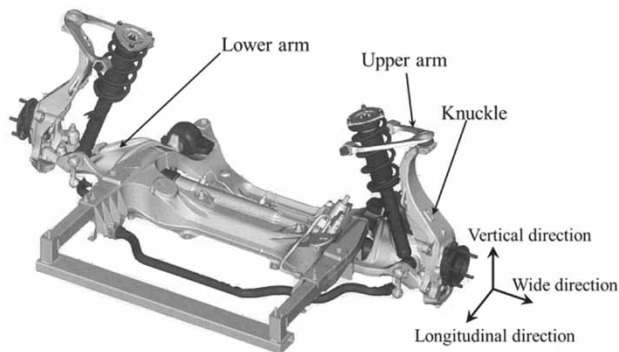


Fig. 4 Example of suspension members (front suspension structure of double wishbone type)⁸⁾

including the mass of a body and frame, and "unsprung mass," including the mass of the tires and suspension arms. For mere weight reduction, lowering the weight of the body, which makes up most of the automotive weight, has the greatest effect; however, there is a concern that the mere reduction of the body weight may result in an improper mass balance and deterioration of the ride quality. For this reason, in order to maintain auto performance, the weight reduction of the suspension, an unsprung component, is also necessary to lowering the weight of an automobile.

Given this backdrop, suspension members are being changed from conventional cast iron or press-formed sheet steel to aluminum alloys. Applicable aluminum products include forged products, cast products, press-formed sheet products, and aluminum extruded products. Aluminum forgings, having strength greater than that of aluminum castings, can achieve more pronounced weight reduction. In addition, because they have degrees of shape freedom higher than those of press-formed products, Kobe Steel believes that forged aluminum products are the best fit for suspension members.

3.3 Features of Kobe Steel's technology

Kobe Steel, anticipating the expanded use of forged aluminum suspension, started production in Japan in 1988, and continued to improve the product after introducing dedicated equipment in the early 1990s. Kobe Steel's production lines have a casting line for producing billets, the stock material for forging, adjacent to the aluminum forging line. Thus, the company has established an integrated production system for forged aluminum products from forging stock to finished forgings, which offers the greatest advantage. A schematic diagram of this integrated production system is shown in Fig. 5.⁹⁾ The integrated production system has realized cost reduction by the complete recycling of forging burrs, reduction of lead time by decreased

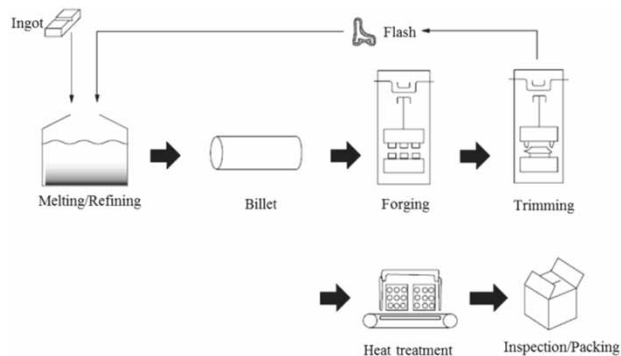


Fig. 5 Integrated production system for forged suspension of aluminum alloy in Kobe Steel⁹⁾

material transportation, and unified management including quality and production, thus enabling highly efficient production.

Other major advantages of Kobe Steel include its design technology for proposing lighter shapes and development technology for providing materials with higher strength.

3.4 Business development outside Japan

As the number of automobiles sold in Japan has peaked, Japanese automakers have moved their production sites outside Japan. Also, since forged aluminum products are increasingly adopted for global platform vehicles produced and sold in multiple countries/regions, the local procurement of forged aluminum suspension parts has become increasingly desirable.

Against this backdrop, and to meet the worldwide demand for forged aluminum products, Kobe Steel has developed technologies for further sales expansion and, in 2005, began production in North America and China to establish a system for supplying suspension parts of the same quality on a global scale. The history of technology development and global expansion is shown in Fig. 6.¹⁰⁾ Kobe Steel's past business development can be divided into the following three phases:

- I. Establishment of technology in Japan (1988-)

Establishing an integrated production system to efficiently produce forged aluminum suspension parts and a system for proposing shapes suitable for weight reduction to expand sales.
- II. Technological evolution and expansion in North America (2005-)

For the purpose of increasing orders outside Japan, further development of design technology for weight reduction, development of high strength alloys, and establishment of technology for producing stable quality to achieve the same quality abroad as that

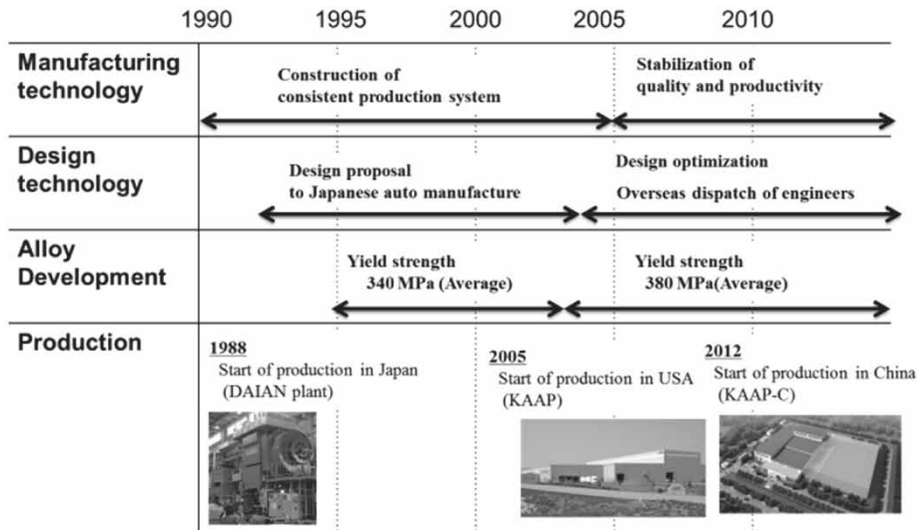


Fig. 6 History of technology development and global expansion of forged suspension of aluminum alloy in Kobe Steel¹⁰⁾

Table 1 Annual production capacity of each plant

Plant	Annual production capacity (pcs/y)
Daian (Japan)	4,000,000
KAAP (USA)	7,000,000
KAAP-C (China)	2,000,000
Ttotal	13,000,000

achieved in Japan

III. Expansion into China and response to global vehicles (2012-)

Expansion of sales in China and to globally-produced vehicles based on stable production utilizing the knowledge of global plant establishment acquired through the North American plant

In particular, in Phase II, which was the first global expansion, automation technologies were developed to enable stable production even by local workers with little experience. As a result, it became possible to stably produce products of the same quality as those made in Japan. These technologies were also exploited when entering China in Phase III.

Since then, the facilities have been expanded along with the increasing demand. **Table 1** shows the actual production capacity at each site. The total production capacity has reached 13 million parts a year at the three sites in Japan, the U.S., and China. In North America, where the sales ratio of large vehicles is relatively high, there is a strong demand for weight reduction, and thus aluminum forgings are prevailing faster. As a result of intensive facility expansion, the plant currently has a capacity of 7 million parts per year, accounting for 53% of the total capacity. Kobe Steel will continue to consider increasing capacity as demand increases.

Conclusions

This paper has explained Kobe Steel's business development in the fields of aluminum sheets, extrusions, forged suspensions in the global market of automobiles, where significant expansion is expected in the future. Among automotive aluminum materials, these three products have different technology trends and market characteristics, and business development will proceed in accordance with the situation. In these businesses, Kobe Steel will strive to focus on ensuring quality first and be worthy of the customers' trust.

References

- 1) T. Tomioka et al. Nikkei automotive. 2016. 3, p.43.
- 2) Japan Aluminium Association Automotive Committee. "Major Japanese Vehicles Adopting Aluminum Body Panels (Hoods)" 2009-03-11, <https://www.aluminum.or.jp/jidosya/japanese/03/03-020304/03-02Localindex.htm>, (Reference on 2018-12-15)
- 3) T. Sakurai et al. J. Jpn. Inst. Light Met. Proceedings of the 87th Conference. 1994, p.185.
- 4) Y. Takaki et al. R&D Kobe Steel Engineering Reports. 1997, Vol.47, No.2, pp.6-8.
- 5) O. Engler et al. Materials Science Forum 877. 2016, pp.231-236.
- 6) C.D. Marioara et al. Proceedings of the 16th International Conference on Aluminum Alloys. 2018.
- 7) T. Shikama et al. R&D Kobe Steel Engineering Reports. 2017, Vol.66, No.2, pp.90-93.
- 8) Y. Inagaki et al. R&D Kobe Steel Engineering Reports. 2009, Vol.59, No.2, pp.22-26.
- 9) A. Fukuda et al. R&D Kobe Steel Engineering Reports. 2007, Vol.57, No.2, pp.61-64.
- 10) H. Nakamura et al. R&D Kobe Steel Engineering Reports. 2017, Vol.66, No.2, pp.99-102.

Global Expansion of Copper Rolled Product Business for Automotive Terminals and Connectors

Yosuke MIWA*1

*1 Copper Rolled Products Plant, Chofu Works, Aluminum & Copper Business (currently Kobelco Reserch Institute, Inc.)

It has been 40 years since Kobe Steel's copper rolled product business first specialized in rolled-copper products for electrical and electronics applications, and a quarter century has passed since the company began actively developing business outside Japan. Five years ago, the company established a trilateral system for supplying rolled-copper products, the system consisting of three sites, one in Asia, another in North America and yet another in Europe. This paper reviews the history of the company's global business development up to date, analyzes the current issues on the basis of comparison with competing non-Japanese manufacturers of wrought copper and copper alloy products and describes the global business strategies, demand, and technical trends in the future. In developing rolled-copper products for electrical and electronics applications, including copper alloys for automotive terminals, it is believed to be important to follow the trends of automobiles, which are expected to be reborn as new mobility, and to acquire a high level of ability in responding quickly to rapidly changing user needs.

Introduction

Kobe Steel's copper rolled product business is about to reach 40 years since it first specialized in rolled-copper products for electrical and electric equipment, including copper alloys for automotive terminals. Also, approximately a quarter of a century has passed since the company began actively expanding outside Japan, in addition to the Japanese market. In this milestone year, this paper reviews the history of global development related to rolled-copper products for electrical and electronic applications such as copper alloys for automotive terminals and copper alloys for semiconductor lead frames. Also described is the outline of the strategy for global business development in the future.

1. Overview of global business development

1.1 Business development in Asia

The aluminum & copper business unit established Singapore Kobe PTE. LTD., the oldest site outside Japan for rolled-copper product business, in Singapore in 1976.

It originally started as a factory making copper pipes for hot-water supply and air conditioning,

and, in the 1990s, was quickly switched to supplying copper alloys for terminals and connectors, as well as manufacturing semiconductor lead frames, in anticipation of increasing demand for automotive terminals and semiconductors. The company began supplying copper alloys for electronic parts.

Later, in order to respond to the demand for automotive terminals and semiconductor lead frames, which were increasing rapidly in the Asia, Kobe Steel established slitting centers in Thailand and China to build a material supply system in the areas closer to customers. These centers are notable for the fact that each not only functions as a site for manufacturing products with slit widths, but also has the technical service function of operating as a sales site close to customers.

In Thailand, the slitter business began in 2001 when Kobe Electronics Material (Thailand) Co., Ltd. was established and, in China, the business began in 2005 when Suzhou Kobe Copper Technology, Co., Ltd. was established. The combined throughput capacity of both the companies has expanded to approximately 2,000 tonnes/month, which accounts for approximately 40% of the capacity of the copper-rolling plant of Kobe Steel's Chofu Works.

1.2 Business development in Europe and US

Direct export of rolled-copper products from Kobe Steel to Europe or to North America is very disadvantageous in terms of cost and delivery. Hence, a local supply system has been established by entrusting the production of Kobe Steel's original alloys to European manufacturers of wrought copper and copper alloy (hereinafter referred to as "wrought copper").

The business began with licensing KFC[®] Note 1) and KLF[®] Note 2)-5 to Trefimetaux, a French wrought copper manufacturer, in 1986. Trefimetaux was later merged into KME, and this license has now been dissolved.

In the early 1990s, the trade frictions between Japan and the U.S. intensified with the emergence of "Buy Americanism." In response to this trend,

Note 1) KFC is a trademark of Kobe Steel registered in the USA.

Note 2) KLF is a trademark of Kobe Steel registered in the USA.

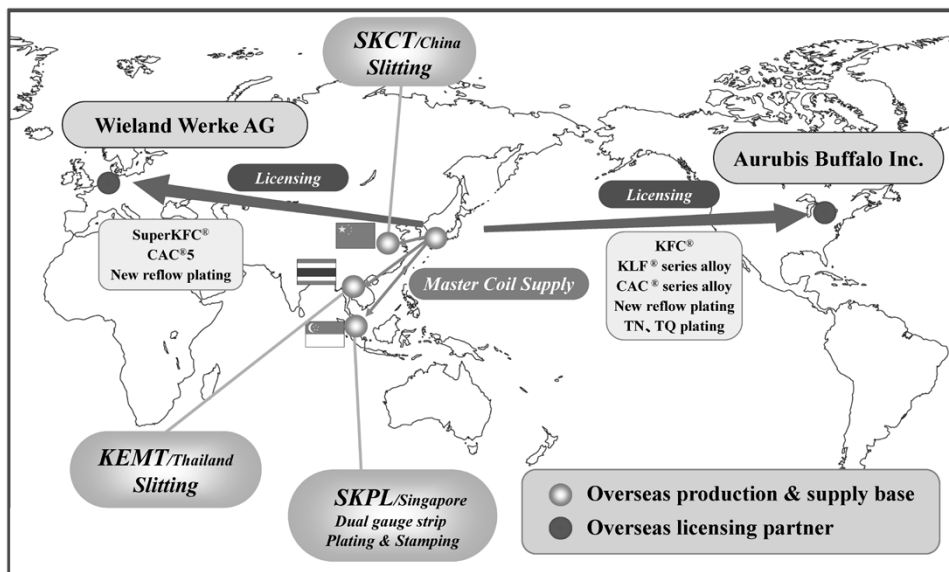


Fig. 1 Global supply system of copper rolled products

Japanese automakers switched their policy from exporting from Japan to producing in the U.S. Then, following automakers, the manufacturers of automotive harnesses, terminals, and connectors also shifted their production to North America. As a result, there was also a strong demand for local supply of rolled-copper products.

Hence, the copper sheet business unit began searching for licensees in North America in 1992 to establish a licensed supply system. There were, however, problems, such as the fact that no agreement was reached with any leading U.S. wrought copper manufacturers, while no small-and-medium-sized manufacturers had enough technology and equipment to produce Kobe Steel's products, including KFC® and KLF®-5.

The licensing in North America began to progress in 1995 when a major Japanese customer made a match between Kobe Steel and Outokumpu American Brass (hereinafter referred to as "OAB"). There also was a difficulty in certifying the change of the license at the time of product transfer to OAB's Buffalo Factory following the closure of its Kenosha Factory in 1998. This significantly delayed the acquisition of customer's certification after the license agreement was signed.

There were many twists and turns, such as dispatching Japanese experts to resolve this issue, and it took until 2001 before both bare material and tin-plated products were produced. After that, the capital of OAB was transferred to Luvata and then to Aurubis, but still, a favorable relationship continues with Kobe Steel.

The menu of licensed products has been expanded and new plating technology, such as new reflowed plating, has been provided. As a result, the

production volume has grown to over 500 tonnes/month, equivalent to 10% of the capacity of Kobe Steel's copper rolling plant. It has been decided that the products will be supplied to several major Japanese and American customers in the future, and further scale up is expected.

1.3 Establishment of trilateral supply system

The preceding sections have described the establishment of the supply system in Asia and North America. On the other hand, supply in Europe was stagnant due to the merger of Trefimetaux. However, major harness makers and terminal/connector manufacturers eagerly desired trilateral material supply in Europe, Asia, and North America, and licensees in Europe were continuously sought.

Although not having to do with the rolled-copper products, there was a joint venture relationship between Wieland-Werke AG and the copper pipe business of Kobe Steel in the 2000s. As a result of aiming to build a relationship extended from the alliance in the copper pipe business, Kobe Steel signed a license agreement with Wieland on strategic products, namely SuperKFC®^{Note 3)} and CAC®^{Note 4)} 5, and new reflowed plating, which paved the way to supplying to Europe.

Beginning in 2009, the supply system was gradually established, and in 2014, the establishment of the trilateral supply system, the final target, was completed. Fig. 1 shows the global supply system,

Note 3) SuperKFC is a trademark of Kobe Steel registered in the USA.

Note 4) CAC is a trademark of Kobe Steel registered in the USA.

then established, of Kobe Steel's rolled-copper products. The global supply system of rolled-copper products for automotive terminals and connectors was materialized at this time, meeting customers' demands.

2. Comparison with wrought copper manufacturers of the world

2.1 Features of wrought copper manufacturers in U.S. and Europe

High performance rolled-copper products used for automotive terminals and connectors have been produced by the world's leading modern wrought copper manufacturers. Most of them exist in Europe, the United States, and Japan, but U.S. and European wrought copper manufacturers have followed a transition different from that of Japanese manufacturers, including Kobe Steel. Especially after the EU integration, U.S. and European wrought copper manufacturers have been strengthening corporate foundations in accordance with trade liberalization in the region and pursuing equipment systems that earn by volume by seeking efficient operation and economies of scale through corporate integration. The end result is that Europe in the 1990s had more than 40 wrought copper manufacturers with a production volume of 10,000 to 20,000 tonnes/year, but in 2010, after the EU integration, they were consolidated into a few giant companies with production capacities of over 100,000 tonnes/year. Representative wrought copper manufacturers include: the KME group, having

sites in Germany, France, Italy, the UK, Spain, etc.; Wieland-Werke AG, also having sites in Germany and UK and Austria; and Aurubis AG, having sites in Finland, the Netherlands, Sweden, Belgium, etc. U.S. manufacturers have also been integrated around Olin Brass.

These giant companies have also expanded into Asia, competing with Kobe Steel in rolled-copper products for automotive terminals & connectors and rolled-copper products for semiconductor lead frames.¹⁾

2.2 Features of Chinese wrought copper manufacturers

Since the late 2000s, Chinese wrought copper manufacturers have been rapidly expanding their scale of business. Like European and U.S. wrought copper manufacturers, they are pursuing the economies of scale through expansion, and their technology and equipment have been acquired from European manufacturers. Several companies are rapidly growing, including Chinalco Copper, a copper business division of Aluminum Corporation of China Ltd. (CHALCO).²⁾

3. Kobe Steel's global strategy

Kobe Steel has a history of developing many high-performance copper alloys that meet customers' needs. Fig. 2 shows the development history of Kobe Steel's rolled-copper products. The company has specialized in automobile and electronics fields and developed, among other

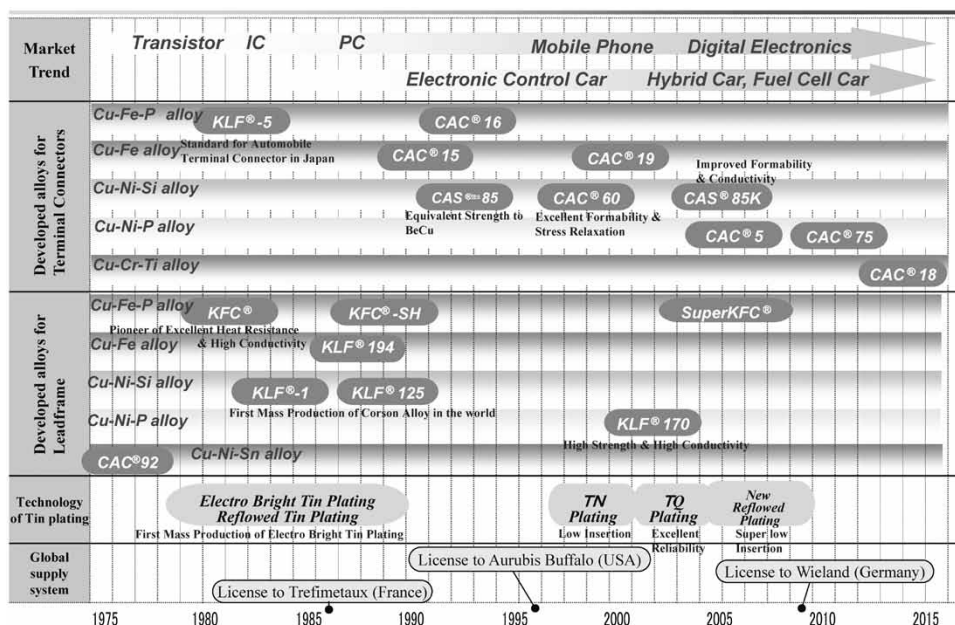


Fig. 2 History of development of rolled copper products

products, copper alloys for automotive terminals, tin plating technology, and copper alloys for semiconductor lead frames. Starting with KFC[®], developed in the 1980s, the KLF[®] series, CAC[®] series, low insertion tin plating, and other new alloys and new products were released into the world market in the 1990s and 2000s. Since 2000, these newly developed alloys have accounted for more than 75% of the company's production. Considering that the ratio of new alloys does not exceed 40% for other wrought copper manufacturers such as European, American, Chinese, Korean, and including Japanese manufacturers, Kobe Steel can be regarded as a very unique company. Hence, in order to supply niche products on a global scale, Kobe Steel signed a license agreement with two giant companies, Aurubis and Wieland, as mentioned in the previous section. Kobe Steel has formed a global alliance that can be called a technology league by entrusting the production of newly developed original copper alloys.

Meanwhile, Kobe Steel has responded to customers' demands in the automobile and electronics fields, as mentioned above. In other words, the company has gained high evaluation outside Japan by supplying the market with copper alloys and tin plating, which can be called special materials with superior functions, as well as rolled-copper products with high level surface quality. Kobe Steel's strategy is to work with customers to supply highly functional rolled-copper products that cannot be developed or supplied by non-Japanese manufacturers, which is particularly in tune with the global development of Japanese automakers and semiconductor manufacturers, and the superiority of this strategy has been demonstrated even outside Japan.

Kobe Steel's superiority has been recognized, especially in the field of automobiles, but now that automakers themselves are integrating their business through cross-border technical collaboration and M&A, it is considered to be becoming necessary to review the business model followed up until now.

So far, Kobe Steel has supplied new/improved products to the market through technical exchanges with Japanese parts manufacturers. As the market for Japanese parts manufacturers and automakers has expanded, Kobe Steel's rolled-copper products have spread worldwide, and hitherto, this has been the company's business style.

Now, one hundred years after the birth of the automobile, a tremendous change is about to take place, and the above approach may not be in line with the prediction that a new mobility society will prevail worldwide. On the other hand, however,

it is considered not appropriate for Kobe Steel to change its approach to "pursuing the economies of scale," as is sought by the wrought copper manufacturers in Europe, the U.S., and China. It will be difficult for these wrought copper manufacturers, which have grown so big, to deal with the situation where automakers are involved in mergers and alliances every year. Giant wrought copper manufacturers may not have the agility to deal with technical exchanges and development at the speed required by customers such as automakers and parts manufacturers.

The future path that Kobe Steel should seek is to acquire a high technological competence capable of communicating equally with automakers, while automakers are required to respond to global changes in the following three points: namely (1) response to diversification of the power train, which is being promoted as a countermeasure to environmental problems; (2) response to automobile intelligence, IoT, and automated driving; and (3) response to changing consumer needs, from owning automobiles to renting.

Thirty years ago, when KFC[®] and KLF[®]-5 were developed, Kobe Steel was able to make direct proposals by developing copper alloys with the required characteristics found through interactions with automakers, the final customers for rolled-copper products. Since the bursting of the bubble, however, the conduit with automakers has become narrower, limiting the technical exchanges to those with Japanese manufacturers of terminals/connectors and harnesses, who are the direct customers. Hence, Kobe Steel believes in the future strategy of establishing a high technological competence enabling strong interaction with automakers and the making of proposal-based improvements.

It is not enough to interact only with Japanese parts manufacturers and automakers. It is also important to create an environment that allows interactions with non-Japanese parts manufacturers and automakers. In such cases, product groups that have not become de facto standard, such as Kobe Steel's CAC[®] series alloys, may become obstacles. Outside Japan, even copper alloys are often commoditized, and the standard alloys that are not in the menu of Kobe Steel's rolled-copper products should be added to the menu.

Conclusions

Kobe Steel estimates that, in Japan, its share of the copper alloys for automotive terminals and connectors exceeds 30%. The market where sales

are expected to grow in the future is the market outside Japan. Hence, it is important to develop a global supply system as well as to acquire the high technological competence and proposal power described above. It is also necessary to expand the Asian sites and increase their market share in response to the increasing demand in the Asia region, which is a direct market for Kobe Steel. Therefore, Kobe Steel is striving to expand the spread of KOBELCO brand rolled-copper products by constructing a system for increasing sales volume in emerging countries such as China, Vietnam, and Indonesia, where large growth can be expected.

References

- 1) Japan Copper and Brass Association. Technological strategy roadmap for wrought copper and copper alloy products 2016. pp.12-13.
- 2) Y. Ohyama. Current Status and Prospect of Chinese Copper Industry (Part 2). Metal Economics Research Institute, Japan, 2017, pp.72-116.

Technical Trends in Aluminum Alloy Sheets for Automotive Body Panels

Yosuke OTA*¹, Dr. Tetsuya MASUDA*¹, Shinpei KIMURA*¹

*¹ Aluminum Sheets & Coils Research Department, Moka Plant, Aluminum & Copper Business

Aluminum alloy sheets are increasingly being used for automotive bodies to reduce their weights and are required to have excellent mechanical properties, joining performance and corrosion resistance. For outer panels, Kobe Steel has been working to improve the performance of 6000 series (Al-Mg-Si) alloys in bake hardenability, formability, and surface quality after stamping. For inner panels and structural members, the application of Ti/Zr surface treatment is being promoted to meet the requirements for the durability of adhesive bonding, which are mainly adopted by non-Japanese automakers. This paper introduces developments in the application of aluminum alloy sheets to automotive bodies and developments for overcoming technological issues.

Introduction

The typical characteristics of aluminum alloys include, in addition to low specific gravity, good corrosion resistance, ease of recycling, high electrical conductivity, good thermal conductivity, and non-magnetic properties. With these advantages, aluminum is being used in various applications as industrial goods and parts.

Meanwhile the weight reduction of automotive bodies has been a challenge in reducing CO₂ emissions, increasing the cruising distance of electrical vehicles, and coping with the increasing weight due to the addition of safety equipment,¹⁾ and the replacement of steel sheet, which has been mainly used so far, with the lightweight material is being studied. Under such circumstances, aluminum alloy sheets, in particular, has been used for various parts of vehicles, including outer panels and structural members, since the 1980s, and the demand for aluminum alloys is expected to increase further in the field of transportation equipment.²⁾

In order to maximize the benefits of body weight reduction by the use of aluminum alloy, it is considered necessary to propose not just material substitution, but also comprehensive technology combining the design of structural parts and the material technology to realize it.

This paper introduces the status of the use of aluminum alloy sheets in automobile bodies and the progress being made at Kobe Steel to overcome technological issues.

1. Status of aluminum alloy sheet use in automotive bodies

In North America and Europe, aluminum alloy sheets were rapidly adopted from 2000 to 2002, and are now applied to mass-produced models. In addition, to cope with weight reduction and strengthened collision safety regulations, the use of high strength steel sheets and aluminum alloy sheets is being studied to find the most suitable placement in the body-in-white for each material.³⁾

In Japan, in 1985, aluminum alloy hoods were applied for the first time to the Mazda RX-7®, and in the first half of the 1990s, the use of aluminum outer panels progressed mainly in sports cars and luxury cars. In recent years, they have been adopted for mass-produced vehicles, and the number of applicable parts such as trunk lids, back doors, and roofs has also increased. In China, which boasts the world's top automotive production volume, there is a growing need for the weight reduction of vehicles against the background of strengthened fuel efficiency regulations.

The Kobe Steel Group is expanding the production capacity to meet the demand for aluminum alloys in the transportation segment, which continues to grow significantly in Asia, including Japan and China. (For details, see the article on this issue, pp.5-10.)

The materials for automotive panels have various performance requirements, such as bondability and corrosion resistance, as well as mechanical properties. Therefore, Kobe Steel has developed materials with optimized chemical compositions and production conditions in accordance with the applied parts. The chemical compositions and required characteristics of typical aluminum alloy sheets for automotive panels are shown in **Table 1** and **Table 2**, respectively. The 5000 series alloy with a high Mg content has excellent formability and is used for various parts exemplified by inner panels. Outer panels are required to have excellent bake hardenability^{Note 1)}, press formability and surface quality after stamping. Taking into account the balance of these required characteristics, 6000 series (Al-Mg-Si series) alloys containing Si higher than

Note 1) Age hardenability in heat treatment at relatively low temperature and for a short time

Table 1 Chemical compositions of aluminum alloys for automotive body panel

Alloy	(mass%)						
	Si	Fe	Cu	Mn	Mg	Cr	Al
AA6014	0.30-0.6	<0.35	<0.25	0.05-0.20	0.40-0.8	<0.20	Bal.
AA6016	1.0-1.5	<0.50	<0.20	<0.20	0.25-0.60	<0.10	Bal.
AA6022	0.8-1.5	0.05-0.20	0.01-0.11	0.02-0.10	0.45-0.70	<0.10	Bal.
AA6111	0.6-1.1	<0.40	0.50-0.9	0.10-0.45	0.50-1.0	<0.10	Bal.
AA5022	<0.25	<0.40	0.20-0.50	<0.20	3.5-4.9	<0.10	Bal.
AA5052	<0.25	<0.40	<0.10	<0.10	2.2-2.8	0.15-0.35	Bal.
AA5754	<0.40	<0.40	<0.10	<0.50	2.6-3.6	<0.30	Bal.
AA5182	<0.20	<0.35	<0.15	0.20-0.50	4.0-5.0	<0.10	Bal.

Table 2 Properties required for automotive aluminum body panel

Applications	Properties
Outer	Yield strength after paint bake
	Surface qualities after stamping (Roping/S-S mark free)
	Formability
	Hemming property
	Anti-filiform corrosion property
Inner	Deep drawing performance
	Joining property
	Adhesion property

the stoichiometric composition are the ones most often used. It is mainly non-Japanese automakers that require durability after adhesive application for inner panels and structural members.

2. Required characteristics of aluminum alloys for automotive bodies and development status at Kobe Steel

2.1 Bake hardenability

For outer panel material, lower strength is required, with a view to ensuring shape accuracy after stamping with suppressed spring back. On the other hand, the final products are required to have high strength in order to maintain the dent resistance^{Note 2)} with reduced thickness. Hence, 6000 series alloy sheets are mainly used because of their gaining strength during the heat treatment of paint baking in the automotive production process. The age hardenability during paint baking at a relatively low temperature for a short time is called bake hardenability. As improvement measures, pre-aging⁴⁾ and a reversion process⁵⁾ have been proposed. These heat treatment processes are performed in order to control the nanoscale material structure formed by Mg and Si, which are the main additive elements in 6000 series alloys.

Kobe Steel is working to develop a new process for the further improvement of the bake hardenability of 6000 series alloys,⁶⁾ to optimize the

Note 2) Resistance to being dented when hit by pebbles, etc.

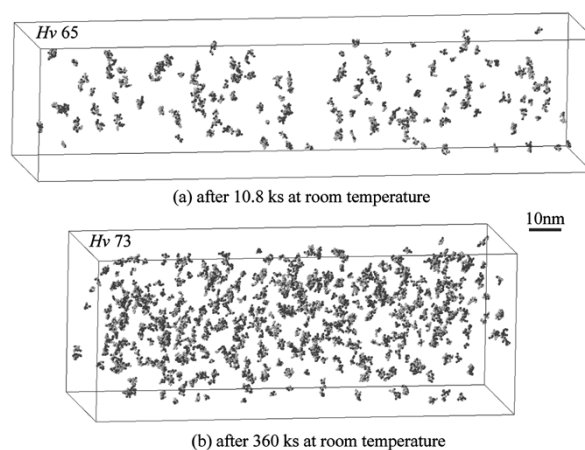


Fig. 1 3D distribution maps of Mg and Si atoms aggregated in Al-Mg-Si alloy and Vickers hardness⁸⁾

chemical compositions and production conditions,⁷⁾ and furthermore, to establish a microstructural analysis technology for clarifying the mechanism. Fig. 1 shows 3D distribution maps of Mg and Si atoms aggregated in a 6000 series alloy along with the results of hardness measurement.⁸⁾ The three-dimensional distribution in the figure was obtained by a fine region analysis apparatus that can three-dimensionally image the atomic arrangement inside the material. As is shown in Fig. 1, the hardness, and the number of atomic aggregations, including Mg and Si, with diameters of several nanometers, have increased with the increasing holding time at the room temperature. In other words, it has been clarified that this very small change in structure is responsible for the change in hardness that takes place during holding at the ambient temperature.

2.2 Formability

In general, the formability of 6000 series alloy sheets at the room temperature is regarded as inferior to that of mild steel sheets. For improvement, Kobe Steel is trying to raise the forming limit by developing press technology suitable for aluminum alloy sheets and is also developing materials with excellent formability. In such efforts, it has been found that a newly developed material with an optimized amount of additive elements such as Mg, Si, and Cu and produced under optimized conditions shows excellent elongation and work hardening characteristics. As the mechanism of this phenomenon, the dislocation growth during tensile deformation and kinetic recovery behavior have been clarified.⁹⁾

These efforts to improve the formability of aluminum alloy sheets are believed to enable complex-shape parts to be made of aluminum, improving the merchantability of vehicles with realized vehicle design needs and to contribute to the reduction of the total cost with a decreased parts count.

2.3 Improvement of surface quality after stamping

In 6000 series alloy sheets, a parallel concave-convex pattern called roping may appear in the rolling direction on the sheet surface after stamping (Fig. 2). For the sake of vehicle appearance, roping must be suppressed even in the high strain region, as the shape of the stamping parts has become more complex in recent years.

Kobe Steel conducted deformation analysis using crystal plasticity theory on the basis of the actual texture information for 6000 series sheets and investigated in detail the deformation behavior of the sheet cross-section shape associated with tensile deformation. As a result, the roping is considered to be partially attributable to bending deformation caused by inhomogeneous stress distribution in the sheet cross-section, in which specific crystal orientations such as Goss orientation and Cube orientation are distributed un-uniformly.¹⁰⁾ On the basis of these analysis results, a production process has been established to further improve the uniformity of the crystal orientation distribution, and materials have been developed that can suppress roping even in the parts with complex shapes.

The conventional method of evaluating roping involves applying prescribed tensile deformation, applying stone grinding and/or painting, and visually evaluating the level of concaveness/

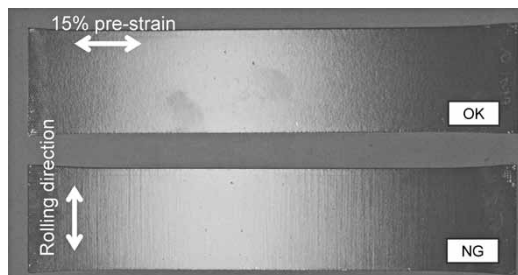


Fig. 2 Appearance roping test piece (15% pre-strain, after spray coating)

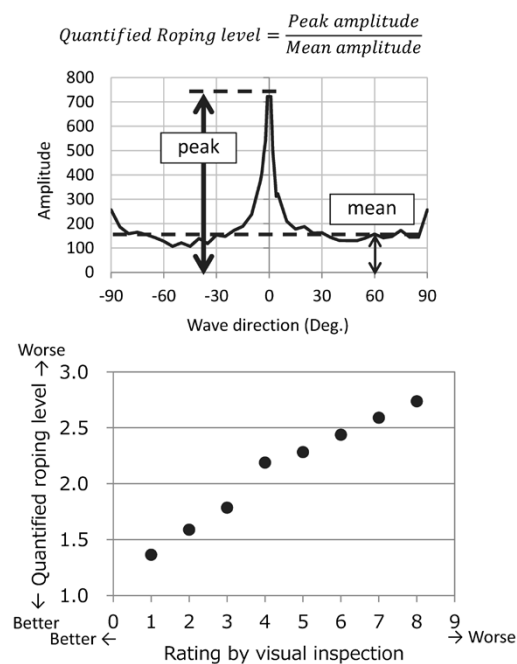


Fig. 3 Relationship between quantified roping level and rating by visual inspection

convexness that appears; thus the problem with this method is that it depends on the skill of workers. It was against this backdrop that Kobe Steel developed a method of quantifying the degree of roping by performing frequency analysis on the three-dimensional shape measured on the deformed sheet surface and separating and analyzing the in-plane wavelength.¹¹⁾ Fig. 3 shows the relationship between the roping index value, which is the ratio of the intensity of the wavelength component in the rolling direction to the average intensity of the wavelength component in all directions, and the conventional visual evaluation results. An excellent correlation has been recognized between the two, and it is considered that the new method of quantitatively evaluating roping can replace the conventional method and improve the efficiency of material development.

2.4 Adhesive durability

In Japan, aluminum alloy sheets for automobile

panels are generally shipped out as materials that have been subjected to pickling, or other procedures to remove the oxide film formed during the heat treatment, so as to improve paintability, adhesion properties, and weldability.¹²⁾ On the other hand, outside Japan, surface treatment may be applied to improve durability when adhesive is applied. This is to prevent the adhesive from peeling off at the interface under the influence of the harsh market environment to which adhesive joints are assumed to be exposed, so as to ensure the reliability of adhesive properties.¹³⁾ It is known that proactive use of adhesives improves rigidity, collision safety, noise suppression, vibration characteristics (NVH properties), and the like. In Europe, adhesives are being used frequently for such purposes.¹³⁾

Specific surface treatments include Ti/Zr treatment applied in Europe and Alcoa 951 treatment applied at the material stage in North America.¹³⁾ Of these, Ti/Zr treatment is a technology widely used by non-Japanese automakers, mainly in Germany. In the process as shown in Fig. 4, an oxide film of Ti and Zr is formed on the deoxidized surface of aluminum alloy.¹⁴⁾

Fig. 5 shows examples of fractured bond surfaces after a shear tensile test performed following the evaluation of adhesive durability (using epoxy adhesive; 3,000 hours of salt spray).¹⁵⁾ The surface with pickling-only shows a metallic luster caused by interfacial fracture, whereas the Ti/Zr-treated material has no metallic luster, exhibiting cohesive failure. Fig. 6 shows the results of a study on the influence of the cohesive failure ratio on Ti/Zr film mass, wherein the Ti/Zr film mass is defined as the total amount of Ti and Zr metal components on the Ti/Zr-treated material surface.¹⁵⁾ The cohesive failure

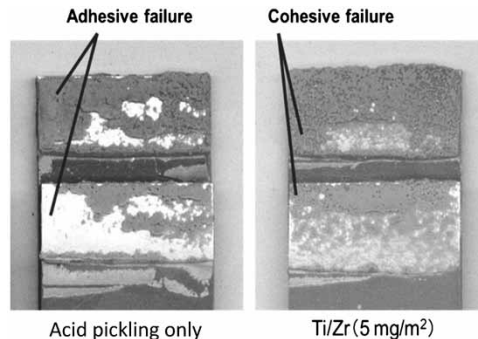


Fig. 5 Appearance of samples for adhesive durability test (Lap shear test)

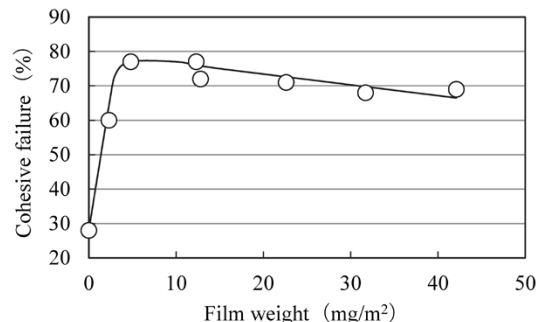


Fig. 6 Relationship between cohesive failure ratio and film weight

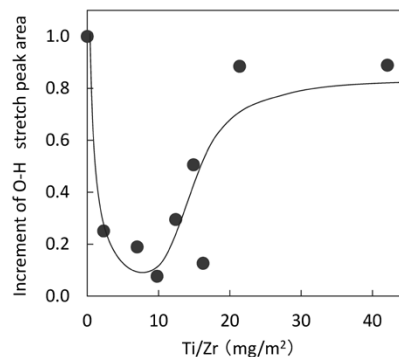


Fig. 7 Hydration variation with Ti/Zr film weight

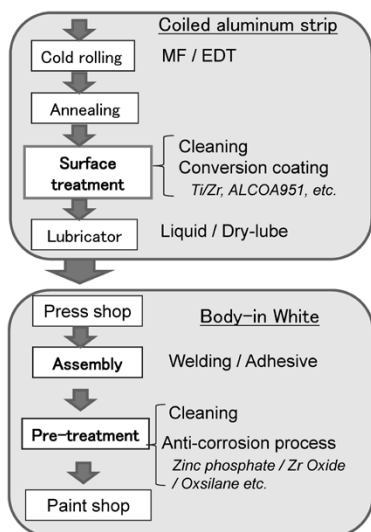


Fig. 4 Manufacturing process of aluminum sheet for automobiles (surface related technology)

ratio is about 30% for the pickling-only material, and the cohesive failure ratio improves as the amount of Ti/Zr film increases, reaching a maximum at 5 to 10 mg/m². The cohesive failure ratio decreases as the Ti/Zr film mass increases further. This is considered to be due to the fact that, as the film mass increases, fracture occurs easily inside the Ti/Zr film.¹³⁾

The interfacial fracture when an adhesive is applied has been attributed to the hydration of the material surface.¹³⁾ Fig. 7 shows the effect of film mass, in the pickling-only material and in the Ti / Zr-treated material, on the amount of hydration, wherein the hydration amount of the pickling-only material is regarded as 1. Here, the hydration amounts of pickling-only material and Ti/Zr-treated material were determined by Fourier transform infrared spectrometer (FT-IR) analysis on the surface before and after holding in a humid environment

(50°C, 95% RH, 24 hours) and by calculating the increase in the area of the peak of the OH stretching vibration observed near 3,400 cm⁻¹. These results confirm that the amount of hydration is suppressed by the increased film mass. It should be noted, however, that it tends to increase again when the film mass increases further.¹⁵⁾ This behavior corresponds to the evaluation results for adhesive durability.

The Ti/Zr-treated materials have been confirmed to exhibit conversion treatability and weldability characteristics equivalent to those of pickling-only materials.^{14), 15)}

Conclusions

In recent years, the business environment surrounding automobiles has changed significantly. Along with technological innovation, new vehicle structures and parts are expected to be developed, and the role of aluminum alloy sheets as lightweight structural materials is expected to become increasingly important. In order to meet these needs, Kobe Steel is conducting research and development of aluminum sheet materials, and for that purpose, strong partnerships with customers have become more vital than ever before. The company strives to play a major role in reducing the weight of automobiles and protecting the global environment by promoting comprehensive R&D combining material development, component structure proposals for exploiting the characteristics of materials, and dissimilar materials joining technology for aluminum and high-strength steel sheets.

References

- 1) H. Sakagami et al. Journal of the Society of Automotive Engineers of Japan. 2016, Vol.70, No.8, p.42
- 2) T. Inaba. *R&D Kobe Steel Engineering Reports*. 2002, Vol.52, No.3, p.79
- 3) J Naito et al. Journal of the Society of Automotive Engineers of Japan. 2018, Vol.72, No.11, p.17.
- 4) T. Sakurai et al. Proceedings of the 87th Autumn Meeting, Jpn. Inst. Light Met. 1994, p.185.
- 5) T. Sakurai et al. Proceedings of the 91st Autumn Meeting, Jpn. Inst. Light Met. 1996, p.175.
- 6) T. Masuda et al. J. Jpn. Inst. Light Met. 2010, Vol.60, No.4, p.183.
- 7) Y. Takaki et al. J. Jpn. Inst. Light Met. 2013, Vol.63, No.7, p.245.
- 8) Y. Aruga et al. *R&D Kobe Steel Engineering Reports*. 2017, Vol.66, No.2, p.42.
- 9) Y. Koshino et al. J. Jpn. Inst. Light Met. 2018, Vol.68, No.4, p.201.
- 10) H. Konishi et al. *R&D Kobe Steel Engineering Reports*. 2012, Vol.62, No.2, p.39.
- 11) T. Ichikawa. *R&D Kobe Steel Engineering Reports*. 2017, Vol.66, No.2, p.86.
- 12) H. Ishii. J. Surf. Finish. Soc. Jpn. 1997, Vol.48, No.10, p.691.
- 13) EAA Aluminium Automotive Manual-Joining 9. Adhesive bonding. http://c.ymcdn.com/sites/www.aec.org/resource/resmgr/PDFs/9-Adhesive-Bonding_2015.pdf, (Referred on 2018-11-21).
- 14) Y. Ota et al. *R&D Kobe Steel Engineering Reports*. 2017, Vol.66, No.2, p.82.
- 15) T. Kojima et al. Journal of light metal welding. 2016, Vol.54, No.8, p.293.

Technical Trends in Copper Alloys and Plating for Automotive Terminals

Hiroshi SAKAMOTO*1

*1 Copper Rolled Products Plant, Chofu Works, Aluminum & Copper Business

Copper alloys and tin-plated strips are widely used for automobile terminals. These terminals are being downsized, requiring their copper alloy materials to have higher strength and excellent stress relaxation resistance. The tin plating is now required to have high fretting corrosion resistance, in addition to a low friction coefficient and low contact resistance. This paper describes the technical trends in automobile terminals and the properties of newly developed copper alloys and tin plating, as well as future trends in technical development.

Introduction

Lately, in the field of automobiles, electric vehicles have been spreading rapidly, viewed from the environmental aspect, in addition to vehicles equipped with higher level self-driving technology and cars that can be connected to external communication networks. With such trends, the number of electronic components mounted in an automobile has increased remarkably, and the number of electrical wiring and connectors connecting them continues to increase. Along with this, electrical wiring has become finer, and the terminals that constitute connectors have become smaller. Also, their materials have been made thinner, and higher strength has been demanded.

In addition, the number of electronic components mounted in high-temperature environments such as engine rooms has increased, and there has been a demand for heat resistant copper alloys with excellent stress relaxation resistance.

In general, automotive terminals with surface treatment such as tin plating have difficulty in ensuring contact reliability, due to downsizing, and have a major issue in dealing with the slight sliding

abrasion phenomenon caused by vibrations and impact.

Kobe Steel has been developing high-performance copper alloys and surface treatments to meet such technical demands for automotive terminal materials. This paper describes the copper alloys for automotive terminals, the technology required for surface treatment, and their development status, as well as future performance requirements.

1. Copper alloys for automotive terminals

Fig. 1 schematically shows the cross-sectional view of a typical automotive terminal and the characteristics required for its material. A terminal consists of a female terminal and a male tab. The most important function of a terminal is to maintain the contact pressure of the spring of the female terminal (hereinafter referred to as "contact pressure") and keep the contact resistance of the contact point stable and low.

For this reason, a high proof stress is required for the copper alloy so that the stress does not exceed the elastic limit even when the spring is greatly bent, so as to be suitable for and tolerant of a high load. In addition, sufficiently high electrical conductivity is required to allow the passage of an electric current. Furthermore, stress relaxation resistance is important in maintaining the contact pressure to press the male tab without losing the spring function even in high-temperature environments such as engine rooms. Moreover, in order to form a terminal of a box shape, the material must also have excellent bendability.

Fig. 2 shows the relationship between the proof

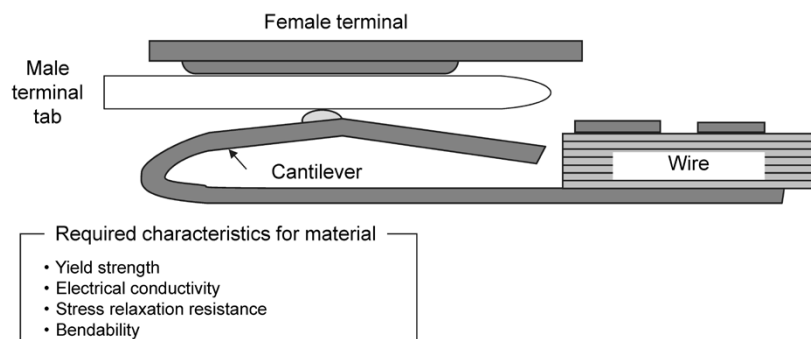


Fig. 1 Cross section of terminal and characteristics required for material

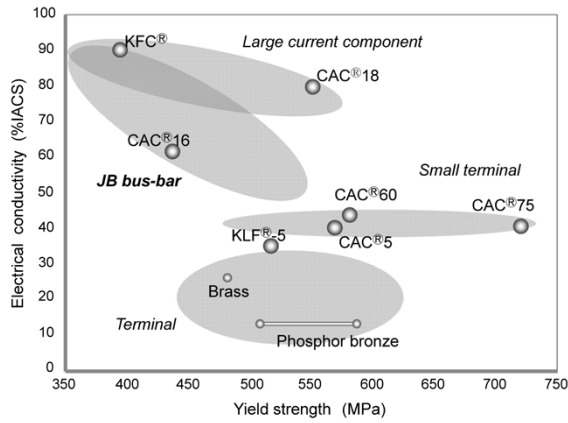


Fig. 2 Relationship between yield strength and electrical conductivity of copper alloys for terminals

stress^{Note 1)} and electrical conductivity of Kobe Steel's copper alloys for automotive terminals. In general, proof stress and electrical conductivity are in a trade-off relationship, and elements added to increase the strength (proof stress) of copper decrease its electrical conductivity. Broadly speaking, copper alloys with emphasis on conductivity are used for power system parts such as junction blocks (JBs) that carry large currents. On the other hand, copper alloys that emphasize strength are often used for small female terminals.

Brass and phosphor bronze, which are general-purpose copper alloys with an electrical conductivity of less than 30% IACS, are used widely in accordance with the required performance.

1.1 Copper alloys for small automotive terminals

Table 1 shows the mechanical properties and conductivities of copper alloys for small automotive terminals. Fig. 3 shows the stress relaxation characteristics of these copper alloys at 160°C.¹⁾ In general, small terminals carry a small current, and copper alloys with a conductivity of 30-50% IACS are used, while copper alloys having low stress relaxation ratios are used in high temperature environments.

KLF^{Note 2)-5}, which has long been used for small automotive terminals, is a copper alloy based on KFC^{Note 3)} (Cu-0.1Fe-0.03P) and contains 2% tin in the solid solution for emphasizing strength. The new model alloy of this KLF-5 is CAC^{Note 4) 5}. CAC 5 is a copper alloy containing a smaller amount of tin compared with that of KLF-5, and also contains nickel and phosphorus to exert the dislocation

Note 1) In the case of copper alloys, which exhibit no clear yield points, the stress at which the material undergoes an amount of plastic strain equal to 0.2 percent is used as the proof stress.

Table 1 Typical mechanical properties and electrical conductivity of copper alloys for small terminals

Alloy	Nominal composition (mass%)	Temper	0.2% Yield strength (MPa)	Elongation (%)	Electrical conductivity (%IACS)
KLF [®] 5	Cu-0.1Fe-0.03P-2Sn	H	530	12	35
CAC [®] 5	Cu-0.8Ni-0.07P-1.2Sn	EH/SP	570	12	40
CAC [®] 60	Cu-1.8Ni-0.4Si-1.1Zn-0.1Sn-0.01Mg	H	580	16	44
CAC [®] 75	Cu-2.5Ni-0.55Si-0.2Sn-1.0Zn	H	730	10	40

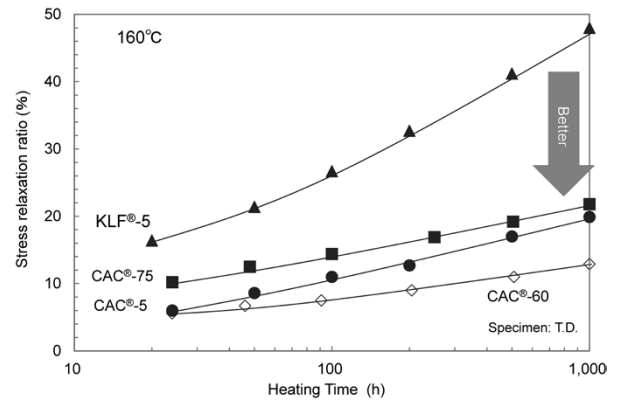


Fig. 3 Change of stress relaxation ratio at 160°C heating (initial load: 0.2% yield strength × 80%)

anchoring action of these solid solution elements. Its stress relaxation resistance has been improved to a level comparable to those of Cu-Ni-Si alloys.²⁾ This alloy is increasingly being used thanks to its simple manufacturing process and easy-to-process characteristics compared with Cu-Ni-Si alloys.

CAC60 and CAC75, on the other hand, are copper alloys that utilize the precipitation phenomenon of Ni and Si during aging to ensure strength, and each has both high conductivity and excellent stress relaxation resistance.

CAC60 is capable of W-bending with $R/t=0.0$ (the ratio of bending radius R to thickness t , called the "critical bending ratio") in both the good way (bending axis perpendicular to rolling direction) and bad way (bending axis parallel to rolling direction), and has an advantage of a high degree of freedom for designing terminals. One of the reasons for excellent bending workability is that the amount of Sn or Mg, element inhibiting bendability in Cu-Ni-Si alloys, is kept to the minimum amount necessary to improve stress-relaxation resistance. This made it possible to achieve both excellent bending workability and stress-relaxation resistance.³⁾

CAC75 has further increased proof stress by the enhanced amount of Ni and Si compared with CAC60. It can be box-formed thanks to its W-bending of $R/t=0.5$ in both the good way and bad way.

Note 2) KLF is a registered trademark of Kobe Steel.

Note 3) KFC is a registered trademark of Kobe Steel.

Note 4) CAC is a registered trademark of Kobe Steel.

Automotive terminals are expected to be further miniaturized in the future, and the materials will be made thinner. In order to ensure important spring reliability, it will be necessary to achieve a proof stress exceeding 1,000 MPa. In addition, the punch-ability and bending workability required for fine processing are also important, and there are high hurdles for material development. However, since the electric current applied is small, it is highly possible that a material with a brass level conductivity of less than 30% IACS could be used.

1.2 Copper alloys for power system parts

Table 2 shows the mechanical properties and electrical conductivity of copper alloys for power system parts. **Fig. 4** shows their stress relaxation characteristics at 180°C. KFC has a conductivity of 90% IACS and is widely used for medium-to-high current applications. This alloy, however, has a low stress relaxation resistance and is not suitable for a fitting-type terminal relying on spring connection.

CAC16, on the other hand, was developed by adding a small amount of Sn and Mg to KFC to impart stress relaxation resistance. This alloy is widely used in junction blocks with tuning-fork-type terminals. Its conductivity, however, is 60% IACS and is lower than that of KFC.

Hence, CAC18 was developed with a conductivity and stress relaxation resistance that represent an improvement over those of CAC16. CAC18 is a Cu-Cr-Ti alloy and ensures high strength

Table 2 Typical mechanical properties and electrical conductivity of copper alloys for power line

Alloy	Nominal composition (mass%)	Temper	0.2% yield strength (MPa)	Elongation (%)	Electrical conductivity (%IACS)
KFC®	Cu-0.1Fe-0.03P	H	390	7	90
CAC®16	Cu-0.1Fe-0.03P-0.4Zn-0.2Mg-0.2Sn	H	430	10	61
CAC®18	Cu-0.3Cr-0.05Ti-0.02Si	H	550	12	80

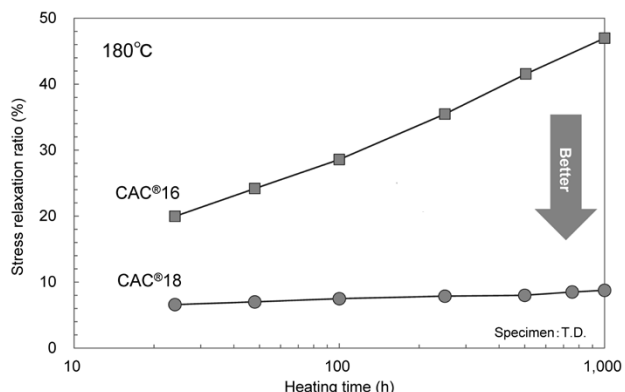


Fig. 4 Change of stress relaxation ratio at 180°C heating (initial load: 0.2%yield strength×80%)

and conductivity by the precipitation strengthening of Cr-based precipitates and solid solution strengthening of Ti. In a large-current circuit, the contact temperature may rise to approximately 180°C due to instantaneous overcurrent. As shown in Fig. 4, CAC18 has a small change in the stress relaxation ratio even after 1,000 hours at 180°C. Stress relaxation is a phenomenon in which dislocations are moved by a thermal activation process, and excellent stress relaxation resistance is realized by suppressing the movement of the dislocations by adding a small amount of active metal element.⁴⁾ CAC18 has a composition in the range of CDA18070, which has a proven record in the EU and US and is a global alloy available from multiple companies. With the backing of this experience, its market is expected to grow.

In the future, the market of electric vehicles will expand, requiring higher power density. Hence, it is anticipated that materials that can handle higher voltage and higher current will be needed, and a new material in a range of higher conductivity and strength must be found.

2. Tin plating for automotive terminals

2.1 Types of Kobe Steel tin plating

The cross-sectional structure of a tin-plated copper alloy mass-produced at Kobe Steel is schematically shown in Fig. 5.⁵⁾ The term "reflow," as used in "reflowed tin plating," means remelting, and the term "reflowed tin plating" indicates that heat is applied after electrodeposition plating to remelt the electrodeposited tin. During remelting, a layer of intermetallic compound consisting of tin and copper is formed by the interdiffusion

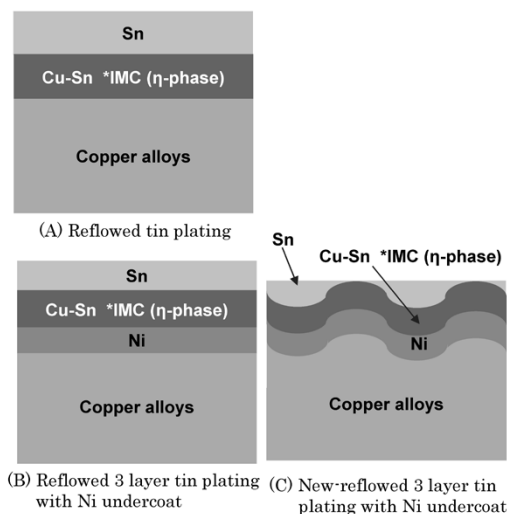


Fig. 5 Schematic image of cross-section of tin plated copper alloys
*IMC: intermetallic compound layer of Sn and Cu

between the Cu base material and tin layer (Fig. 5 (A)). The reflowed 3-layer tin plating with nickel undercoat consists of three layers: a nickel layer, an intermetallic compound layer of tin and copper, and a tin layer (Fig. 5 (B)). The new reflowed plating layer is deposited on an uneven surface of a copper alloy base, and consists of a nickel layer, an intermetallic compound layer of tin and copper, and a surface layer that is a mixture of tin and intermetallic compound layers (Fig. 5 (C)).

2.2 Friction coefficient

As automotive components become increasingly electrified and more sophisticated, an increasing number of circuits and connectors are being used per unit. In addition, as the number of electrodes per connector increases, a greater insertion force is required for fitting the connector.

The increasing insertion force deteriorates the workability of assembly and thus must be decreased. The insertion force of a terminal is determined by the friction coefficient of the material surface and the contact pressure of the terminal. In the case of friction between two tin-plated surfaces, adhesion friction becomes the main component, and the friction coefficient μ is expressed by Equation (1):⁶⁾

$$\mu = F/W = As/Ap = s/p \dots\dots\dots (1)$$

wherein F : friction force, W : load in the normal direction of the sheet, A : contact area, s : shear strength of the adhesion part, p : plastic flow pressure=material hardness.

Equation (1) indicates that the friction coefficient can be reduced by increasing the plastic flow pressure. The plastic flow pressure is the pressure that plastically deforms all the bulk close to the surface near the contact when the contact pressure is increased and corresponds to the hardness of the material. Therefore, one way of reducing the friction coefficient is to harden the plating, and another is to make the plating thin enough so that the hard base material exerts its effect, which increases the apparent hardness.

Fig. 6 is a schematic diagram of the friction coefficient measurement apparatus, and **Fig. 7** shows the friction coefficients of the tin-plated materials. The reflowed 3-layer tin plating with nickel undercoat has a thinner tin layer and is more easily affected by the hard base material, which increases the apparent hardness and reduces the friction coefficient. The new reflowed plating has a surface layer consisting of a mixture of tin and intermetallic compound layers. which makes adhesion less likely to occur. Such adhesion is more

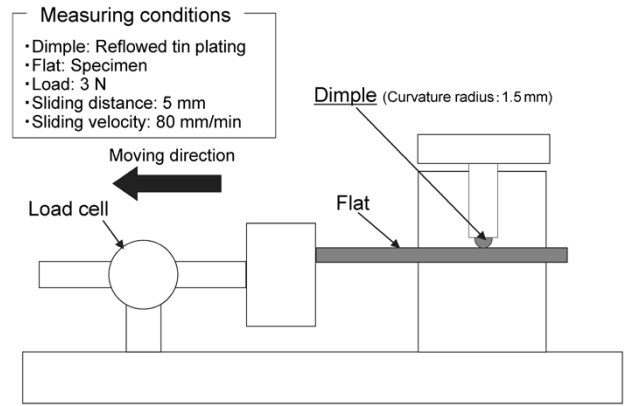


Fig. 6 Schematic diagram of apparatus for measuring friction coefficient

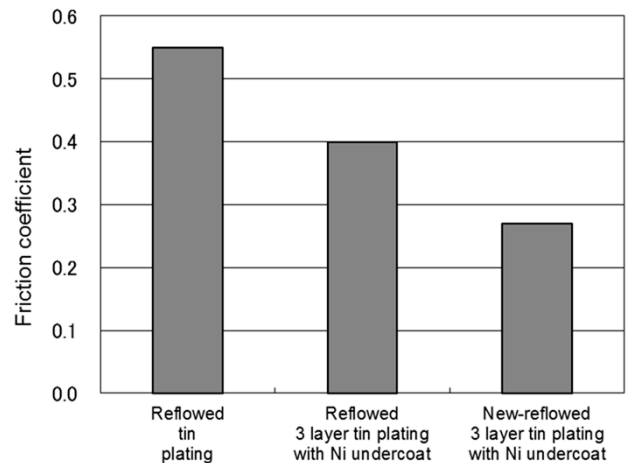


Fig. 7 Comparison of friction coefficients

likely to occur in the friction between tin and tin, while the intermetallic compound of tin and copper suppresses the adhesion friction of tin. As a result, the friction coefficient is greatly reduced to about half that of reflowed tin plating.

2.3 Contact resistance characteristics

In order to secure space inside a vehicle, many electrical components that require low contact resistance at temperatures as high as 150 to 160°C are being installed in the engine room. **Fig. 8** shows the change in contact resistance at the holding temperature of 160°C. **Fig. 9** shows the cross-sectional observation results after heating at 160°C for 120 hours. The electrical resistivity of the base metal, plating layer, and oxide film are shown in **Table 3**.⁷⁾⁻⁹⁾

As mentioned earlier, the reflowed tin plating layer consists of two layers: a tin layer on the surface and a Cu_6Sn_5 layer (η phase) of copper and tin below it. The cross-sectional observation after 120 hours of heating shows that the tin layer has disappeared, and a Cu_3Sn layer (ϵ phase) has been

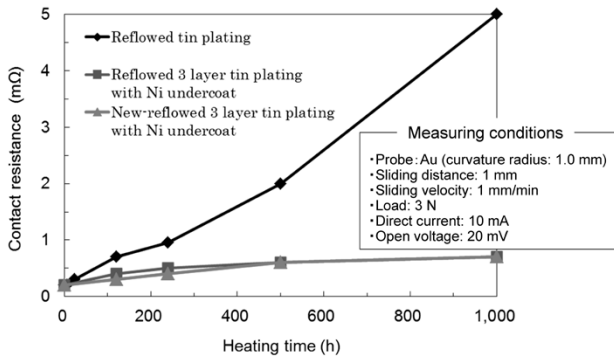


Fig. 8 Change of contact resistance during heating at 160°C

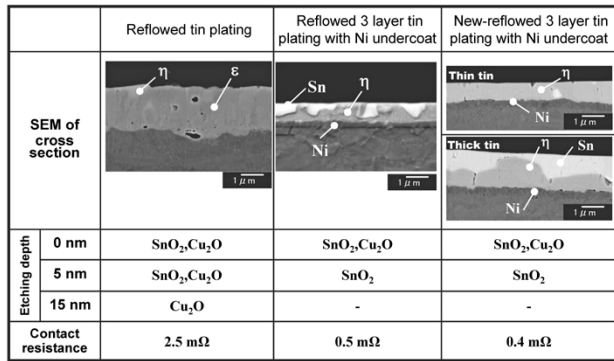


Fig. 9 SEM of cross section after 160°C × 120 h, and relationship between composition of oxide film and contact resistance

Table 3 Electrical resistivity

	Ω·m		Ω·m
Cu	1.7 × 10 ⁻⁸	Cu ₂ O	10 ⁶ ~10 ⁷
Sn	12.6 × 10 ⁻⁸	CuO	1~10
Cu ₆ Sn ₅	12.5 × 10 ⁻⁸	SnO ₂	4 × 10 ⁻⁴
Cu ₃ Sn	20.5 × 10 ⁻⁸	NiO	10 ¹¹

formed, while a slight amount of the Cu₆Sn₅ layer (η phase) remains. This is because the copper of the base material has diffused while being held at a high temperature, and the tin layer has generated a Cu₆Sn₅ layer (η phase), while the diffusion further progressed to generate a copper-rich Cu₃Sn layer (ϵ phase).

Qualitative analysis detected Cu₂O at the surface and at a depth of 15 nm. Since the electrical resistivity of Cu₂O is so great, it is considered to increase the contact resistance. On the other hand, the electrical resistivity of tin oxide, SnO₂, is much lower than that of Cu₂O and has little effect on contact resistance.

The reflowed 3-layer plating and new reflowed plating, both with a Ni undercoat, exhibit only a small increase in contact resistance after the heating. In these, the nickel undercoat acts as a barrier against the diffusion of copper into the tin layer,

preventing the copper-rich Cu₃Sn layer (ϵ phase) from forming and causing the tin layer and the Cu₆Sn₅ layer (η phase) to remain. Observations were conducted on thin and thick portions in the new reflowed plating, and neither one showed any Cu₃Sn layer (ϵ phase). In any type of the plating, Cu₂O exists only at the outermost surface as a very thin film, not extending in the depth direction, and is considered to have kept the low contact resistance.¹⁰⁾

2.4 Fretting corrosion characteristics

Fretting corrosion is a phenomenon in which an electrical contact, being worn due to sliding caused by vibration or thermal cycling, generates abrasion particles, which are oxidized, increasing the contact resistance.

As the terminals are downsized, the need for reduced insertion force has increased due to the decreasing contact pressure and increasing number of contacts, raising the susceptibility to fretting corrosion. As a result, the contacts have become more prone to shift due to vibration and impact, as well as to thermal expansion and contraction caused by the heat generated during energization. These problems, which hitherto have caused no trouble, have made fretting corrosion an increasingly important issue.

Fig.10 schematically shows the fretting corrosion test. Fig.11 shows the change in contact resistance with sliding cycles. Once fretting corrosion occurs, wear particles are generated by sliding. Some part of the wear particles is discharged outside; however, most of what remains is deposited on the contact surface. These wear particles accumulate and oxidize, increasing the contact resistance (the 1st peak in Fig.11). Subsequently, once the intermetallic compound layer is worn out, the discharge amount becomes greater than the amount of wear particles generated, decreasing the amount of the wear particles deposited on the contact and reducing the contact resistance. Further sliding increases wear and exposes the copper alloy base material, which ultimately increases the contact resistance due to the wear and oxidation of the base material.¹¹⁾

As shown in Fig.11, the 1st peak height decreases in the order of reflowed tin plating, reflowed 3-layer tin plating with nickel undercoat, and new reflowed plating. The 1st peak is attributable to the deposition and oxidation of the wear particles of tin, and to prevent the contact resistance from increasing, the generation and deposition of wear particles should be suppressed. To that end, it is necessary to suppress the wear of the tin plating, or to increase the contact pressure to promote discharge.

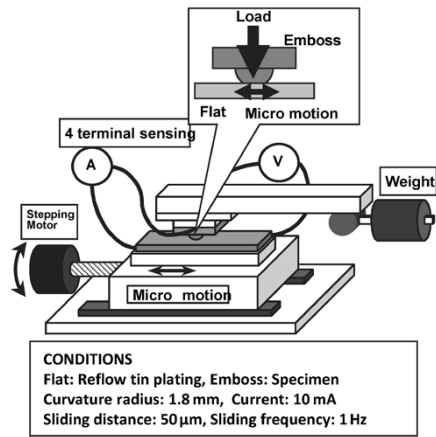


Fig.10 Schematic diagram of fretting corrosion test

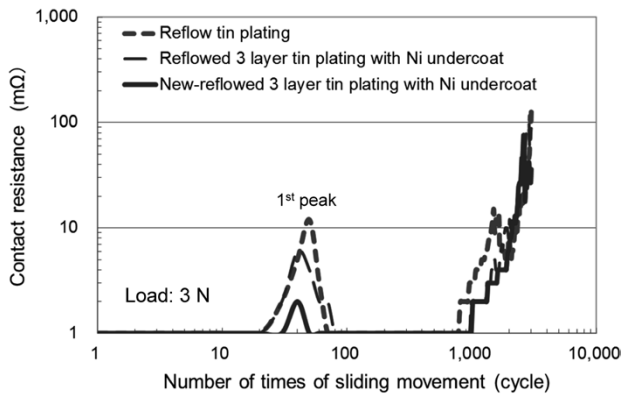


Fig.11 Relationship between contact resistance and number of times of sliding movement at 3 N of load

The reflowed 3-layer tin plating with nickel undercoat is thinner than the reflowed tin plating and is more resistant to being ground. As a result, it generates a smaller amount of wear particles and exhibits a lower peak value. On the other hand, the new reflowed plating has a tin layer and a hard intermetallic compound layer mixed on the surface, making the plating less likely to be abraded. Furthermore, the combination of different materials (tin layer and intermetallic compound) makes adhesion of the contact points unlikely to occur. This is considered to be responsible for the smaller amount of wear particles generated and lower peak value.

It is anticipated that terminals will be further downsized and have more electrodes, decreasing the contact pressure from 3 N to 2 N or to 1 N, requiring a fretting corrosion resistance at the lower contact pressure. In general, tin plating becomes difficult to use as the contact pressure drops. Gold plating may be used; however, gold plating is expensive and is not widely applicable to automotive terminals.

Figs.12 and 13 show the fretting corrosion characteristics for the contact pressures of 2 N and 1 N, respectively. In the case of reflowed tin plating,

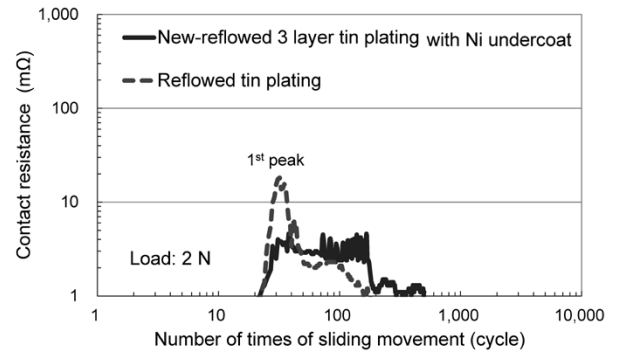


Fig.12 Relationship between contact resistance and number of times of sliding movement at 2 N of load

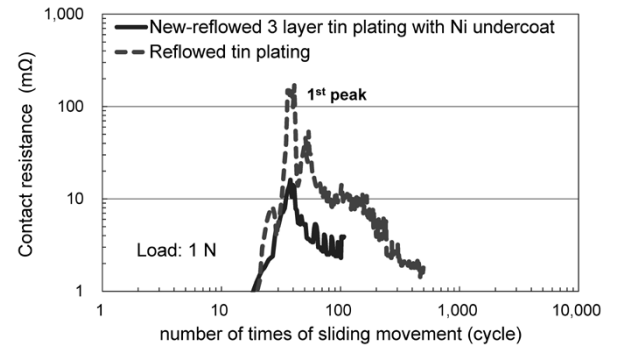


Fig.13 Relationship between contact resistance and number of times of sliding movement at 1 N of load

the 1st peak increases remarkably when the contact pressure is reduced to less than 3 N, and exceeds 100 mΩ at 1 N. The new reflowed plating, on the other hand, exhibits a peak that is less than 10 mΩ at 2 N and slightly higher than 10 mΩ at 1 N. These peaks are lower than the ones for reflowed plating. This is considered to be greatly attributable to the fact that, as described above, this plating is more resistant to abrasion and adhesion of the contacts is less likely to occur.

Kobe Steel will continue to develop tin plating that can ensure contact reliability even at a low contact pressure by further improving the plating.

Conclusions

Automobiles will continue to undergo functional upgrading and to be provided with more advanced electrical equipment. A greater number of cars will be electrically powered. Meanwhile, copper alloys for automotive terminals have a number of challenges to address: e.g., to increase strength and improve stress-relaxation resistance and conductivity, while ensuring the electrical reliability of contacts. Kobe Steel will strive to develop materials while considering more urgent needs for the future and aiming for higher performance and reliability. The company also intends to strengthen its proposal ability not only for material technology,

but also for the best matching in combination with surface processing technology.

References

- 1) K. Nomura. *R&D Kobe Steel Engineering Reports*. 2015, Vol.65, No.2, pp.33-42.
- 2) K. Nomura. *R&D Kobe Steel Engineering Reports*. 2012, Vol.62, No.2, pp.53-58.
- 3) T. Ogura. *R&D Kobe Steel Engineering Reports*. 1998, Vol.48, No.3, pp.13-16.
- 4) Y. Sumino. *R&D Kobe Steel Engineering Reports*. 2017, Vol.66, No.2, pp.103-106.
- 5) T. Hara et al. *R&D Kobe Steel Engineering Reports*. 2004, Vol.54, No.1, pp.9-12.
- 6) M. Muraki. *Tribology*. Nikkan Kogyo Shimbun,LTD., 2007, pp.39-41.
- 7) W. J. Reichenecker. *Tin and its Uses*. 1981, No.130, pp.14-16.
- 8) W. J. Reichenecker. *Welding Journal*. 1980, Vol.59, No.10, pp.308-310.
- 9) G. V. Samsonov. *New Oxide Handbook-Physical and Chemical Properties-Second revised edition*, Nisso Tsushinsha, 1979, p.209.
- 10) M. Tsuru. *J. Surf. Finish. Soc. Jpn.* 2016, Vol.67, No.12, pp.59-63.
- 11) M. Tsuru et al. *R&D Kobe Steel Engineering Reports*. 2012, Vol.62, No.2, pp.59-62.

Hot-dip Galvannealed Steel Sheet of 980MPa Grade Having Excellent Deformability in Axial Crush

Michiharu NAKAYA*¹, Shinjiro KANETADA*¹, Michitaka TSUNEZAWA*²

*¹Sheet & Plate Products Development Department, Research & Development Laboratory, Iron & Steel Business

*²Sheet Products Marketing & Technical Service Department, Iron & Steel Business

Automotive parts that play the roles of energy absorbers must not fracture upon collision. It has been reported that the cracking behavior of a hat-shaped column during an axial crush test correlates with the bending properties of its material and that the conventional hot-dip galvannealed (GA) dual-phase (DP) steel sheets of 980MPa grade have insufficient performance. The newly developed GA 980MPa grade steel sheet with a homogeneous microstructure shows no cracking at a bending angle that would have caused cracking in conventional DP steel sheets, preventing crack propagation in the thickness direction. In order to evaluate the axial crush performance of a part made of the newly developed steel sheet, hat-shaped columns with two different cross-sectional geometries were examined by drop weight impact testing. For both geometries, the newly developed steel exhibited cracks with smaller lengths and higher energy absorption compared with conventional steel.

Introduction

The application of high-strength steel sheets is accelerating in order to reduce the weight of automobiles and improve fuel economy and crashworthiness.¹⁾ The same applies to galvannealed (hereinafter referred to as GA) steel sheets used for underbody parts that require corrosion resistance, and steel sheets with high strength and excellent formability have been developed.^{2), 3)} There are a wide variety of parts to be strengthened, and for the parts around the cabin, materials that can keep the deformation as small as possible are being studied with a view to passenger protection in the event of a collision. In the meantime, materials suitable for members that absorb impact energy by deformation, such as parts in the front and rear of a vehicle, are being studied.⁴⁾ Furthermore, studies are being conducted on steel sheets used for energy-absorbing members. Such steel sheets are required to exhibit no large cracks caused by crushing deformation, as well as to have press formability and weldability. According to these studies, cracks appearing during crushing deformation are highly correlated with indices related to local deformation such as bendability and hole expansibility (index: λ value).⁴⁾⁻⁷⁾

Currently, major 980MPa grade GA steel sheets

are dual phase (hereinafter referred to as DP) steel sheets consisting of ferrite and martensite.⁷⁾ These steel sheets are prone to cracking due to strain concentration at the microstructure boundary and are considered to have limits when it comes to improving bendability and hole expansibility. Thus they are not necessarily suitable for energy-absorbing members. Meanwhile, cold-rolled steel sheets have been developed that, unlike DP steel sheets, have improved hole expansibility and bendability by using a composite structure containing no ferrite.^{9), 10)} Since energy-absorbing members often require corrosion resistance, practical application using GA steel sheets is desired.

Hence, Kobe Steel has developed a 980MPa grade GA steel sheet with a performance suitable for energy-absorbing members. This paper reports the evaluation results of the mechanical properties, bendability and axial crushing properties of the newly developed steel sheet.

1. Characteristics of samples

1.1 Tensile properties and hole expandability

All of the samples were galvannealed steel sheets with a thickness of 1.6 mm. The coating mass was in the range of 45 to 65 g/mm², and the iron concentration in the plating layer was in the range of 7 to 15%. **Table 1** shows the mechanical properties, and **Fig. 1** shows the microstructures.

Table 1 Mechanical properties of sample steels

Sample	Thickness (mm)	YP/YS (MPa)	TS (MPa)	EL (%)	λ (%)
A	1.6	659	1,059	15	17
B	1.6	882	1,004	14	86

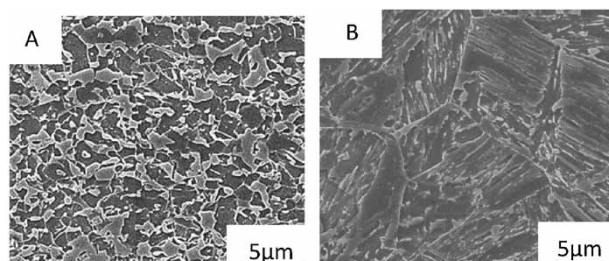


Fig. 1 Typical microstructures of A) DP steel
B) Developed steel

Sample A is DP steel consisting of ferrite and martensite structure. It has low YS characteristics, with λ being slightly less than 20%. Its chemical compositions include C and Mn with the addition of Cr, Mo, etc.

Sample B has a homogeneous microstructure with almost no excessively hard structure, nor soft ferrite; either of these could become a crack initiation point. It is characterized by a high YS and a high hole expandability value compared with Sample A. Its chemical composition includes a decreased amount of C so as to reduce hard structures and hardenability-improving elements to suppress the formation of ferrite.

1.2 Bendability

1.2.1 Bending test method

It has been reported that there is a correlation between cracking behavior and bendability in the axial crush test.^{5), 6)} The German Automobile Manufacturers Association (Verband der Automobilindustrie (VDA)) standard stipulates VDA2380-100 (hereinafter referred to as the "VDA bending test") for evaluating the cracking behavior during member crushing.

In the VDA bending test, a sample placed on a pair of support rolls is bent with a sharp punch (Fig. 2). From the punch load and stroke measured during the test, the bending load-angle diagram (Fig. 3) is created. Since the decrease in load after the maximum load corresponds to crack occurrence, the bending angle at the maximum load (α_{Fmax}) indicates the bending crack limit. In addition, the post uniform slope (PUS), the slope of the straight line connecting the maximum load and the inflection point during the load drop,⁶⁾ is obtained. This slope is related to the propagation of cracks in the sheet thickness direction, and the smaller the slope, the more difficult it is for the cracks to propagate.

Also conducted were a 90° V bending test based

on a general bendability evaluation method. In this test, each test piece is placed on a V-block and bent with a 90° punch having a tip radius of R in the range of 0 to 2.5 mm (0.5 mm pitch). The value R/t was obtained by dividing the minimum bending radius, the smallest radius that caused no cracking, by the sheet thickness, and using that as an index. For both the VDA bending and 90° V-bending, the bending ridge line was made parallel to the rolling direction.

1.2.2 Bending test results

Fig. 4 shows the bending angle vs. load diagram of the VDA bending test and the cross-sectional observation results of a few sample bending angles. Sample A reached the maximum load at a bending angle of 60°, and cracks propagated to half of the sheet thickness in cross-sectional observation at a bending angle of 67°. Sample B, on the other hand, did not crack even at a bending angle of 80°, and

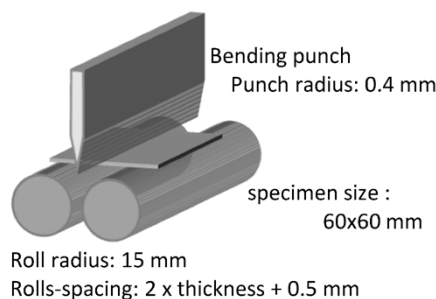


Fig. 2 Set up for VDA bending test

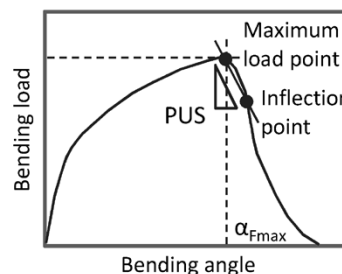


Fig. 3 Bending load-angle curve

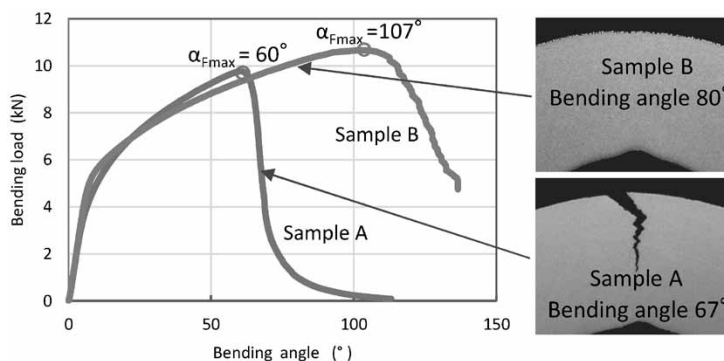


Fig. 4 Bending load-angle curves and cross-sectional observations of samples with bending angles indicated by arrows

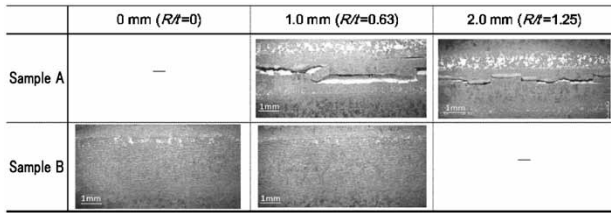


Fig. 5 Appearance of ridge surface after V-bending test

Table 2 Results of bending test

	VDA bending angle (°)	Post uniform slope (MPa)	R/t
Sample A	107	138	1.56
Sample B	60	34	0

the maximum load reached 107°. In the subsequent load reduction process, Sample B showed a slope (PUS) smaller than that of Sample A, and no crack was observed to propagate in the sheet thickness direction.

Fig. 5 shows the observation results of the bending ridge line after the 90° V-bending test. Sample A cracked even for punch $R = 2$ mm, whereas sample B exhibited no crack even when punch $R = 0$ mm.

Table 2 summarizes the results of the above VDA bending test and 90° V-bending test. Sample B shows a favorable value for any index compared with Sample A.

2. Axial crushing characteristics of hat-shaped members

2.1 Test method

The above samples were used to prepare, by bending, two types of columns with hat-shaped cross-sections (type 1 and type 2) (Fig. 6). The column length (perpendicular to the paper surface) was 200 mm, and a backing plate of 590MPa grade cold-rolled high tensile steel (thickness: 1.4 mm) was spot-welded to the column at a spot spacing of 30 mm. On the top and bottom of each column, a steel plate (SS400) with a thickness of 10 mm was arc-welded all around.

A drop weight tester was used for the axial crushing deformation. Each column was fixed to the pedestal on the load cell, and a weight of 190 kg was dropped so that the collision speed was 60 km/h. The weight was stopped at 80 mm after contacting the top of each sample. Two tests were performed for each column and each cross-sectional shape.

In order to quantitatively evaluate the degree of cracking in each sample, crack lengths were measured. The cracks subjected to the measurement were those penetrating the plate thickness. The

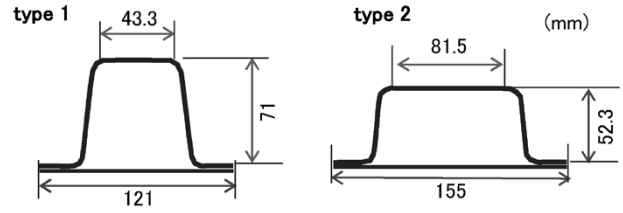


Fig. 6 Cross-sectional geometries of hat-shaped columns

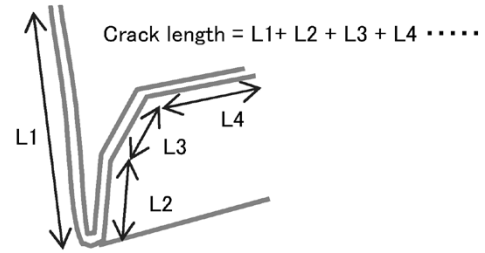


Fig. 7 Method of measuring crack length

fracture surface caused by the axial crushing deformation was identified by visual observation of the outer appearances and half-cut cross-sections of the columns. Next, each fracture surface was divided such that the surface was approximated by straight lines, and the length of each line was measured. The total of these lengths was taken as the fracture surface length (Fig. 7). Although there are two fracture surfaces for one crack, only one of the two fracture surfaces was taken here to avoid duplication, and the fracture surface length was used as the crack length.

2.2 Test results

Fig. 8 shows the absorbed energy vs. displacement curves of the drop weight test. In the case of the type 1 shape, the absorbed energy at the deformation of 80 mm was 8.8 kJ and 9.6 kJ for Sample A, whereas it was 9.7 kJ and 10.1 kJ for Sample B. In the case of type 2, the results were 9.5 kJ and 9.7 kJ for Sample A, and 10.1 kJ and 10.9 kJ for Sample B. For both shapes, Sample B showed higher values.

Fig. 9 include photographs of the appearance of the columns after axial crush. In the columns of Sample A, the ridgeline part was bent at the initial stage of compression to initiate cracks, and the cracks were observed to have propagated along the ridgeline (Fig. 9a)), or to have occurred at the bent part after buckling. (Fig. 9b)). On the other hand, Sample B (Fig. 9c, d)) exhibits no such large cracks. Fig.10 shows the total length of cracks generated during the drop weight tests for each column. Sample A has a large total crack length that may exceed 450 mm at the maximum. On the other hand, that for Sample B was 127 mm at the maximum, and it was found that cracking was suppressed even

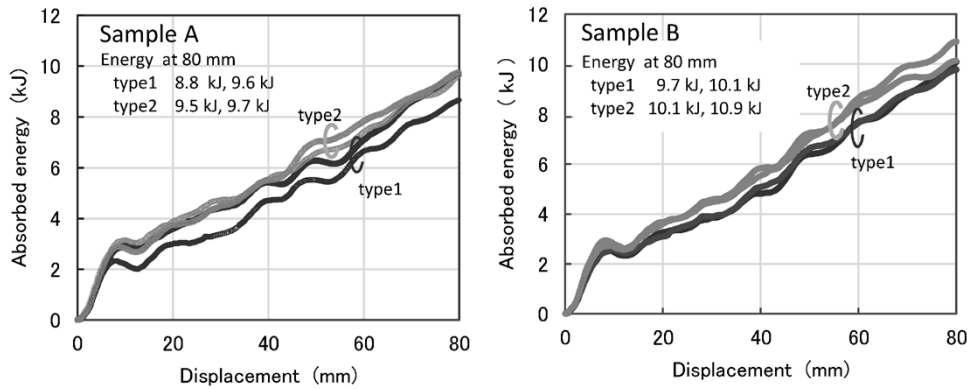


Fig. 8 Absorbed energy vs. displacement curves

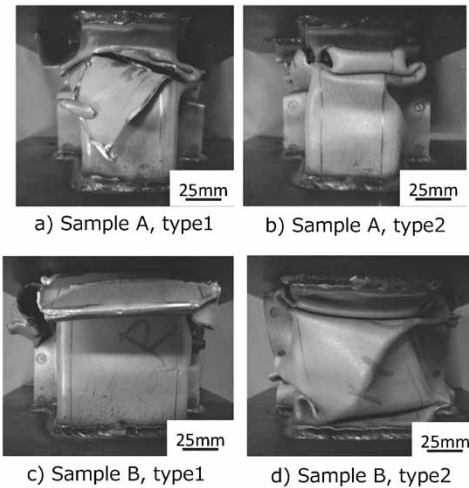


Fig. 9 Appearance of hat-shaped columns after axial crush

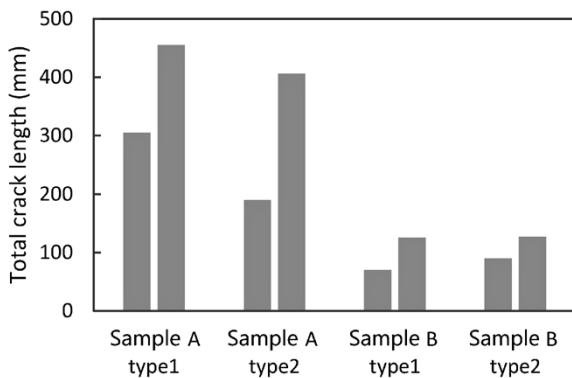


Fig.10 Total crack length in crushed hat-shaped columns

in axial crushing deformation as in the case of the bending test and hole expansion test.

As shown in Fig. 4 (bending angle vs. load diagram), the bending load decreased upon crack occurrence during bending deformation. Even in the case of axial crushing, the deformation load of the entire part may be reduced when cracks occur. A conceivable reason why the absorbed energy of Sample B was higher than that of Sample A is that the decrease in its deformation load due to such

cracking was suppressed, in addition to the high YS of Sample B.

Conclusions

This paper has reported the evaluation results for the mechanical property, bendability, and axial crushing characteristics of GA980MPa grade galvanized steel sheet with homogenous microstructure. This steel sheet exhibited bendability and hole expandability superior to those of the conventional DP steel sheet and was confirmed to suppress the generation of cracks in axial crushing deformation. The newly developed steel sheet is expected to be used widely in the future thanks to its excellent bending workability and stretch flange workability, as well as its advantage in crushing deformation upon collision.

References

- 1) World Auto Steel of World Steel Association Japan Committee. Super Steel, "Advanced High-Ten." Bungeishunju Ltd, 2009, p.10.
- 2) Y. Futamura et al. *R&D Kobe Steel Engineering Reports*. 2011, Vol.61, No.2, p.41.
- 3) M. Ikeda et al. *R&D Kobe Steel Engineering Reports*. 2017, Vol.66, No.2, p.8.
- 4) H. Maki et al. *IJAE*. 2017, Vol.48, No.66, p.1347.
- 5) P. Larour et al. International Deep Drawing Group, IDDRG International Conference 2010. Graz, Austria, 2010, 0531/06-02.
- 6) J. Naito et al. *R&D Kobe Steel Engineering Reports*. 2017, Vol.66, No.2, p.69.
- 7) S. Chinzei et al. *R&D Kobe Steel Engineering Reports*. 2017, Vol.66, No.2, p.76.
- 8) World Auto Steel of World Steel Association Japan Committee. Super Steel, "Advanced High-Ten." Bungeishunju Ltd, 2009, p.18.
- 9) M. Miura et al. *R&D Kobe Steel Engineering Reports*. 2009, Vol.57, No.2, p.15.
- 10) M. Nakaya et al. *R&D Kobe Steel Engineering Reports*. 2009, Vol.59, No.1, p.49.

Multi-material Automotive Bodies and Dissimilar Joining Technology to Realize Multi-material

Dr. Junya NAITO*¹, Dr. Reiichi SUZUKI*¹

*¹ Automotive Solution Center, Technical Development Group

This paper introduces multi-material car body designs using ultra-high strength steel and aluminum alloy to realize an estimated weight reduction of 12 to 33% from the base body composed of conventional steel. Also included is an explanation of the dissimilar joining necessary for realizing multi-material car bodies as well as a dissimilar joining technology uniquely developed by Kobe Steel.

Introduction

As a measure for protecting the global environment, fuel efficiency regulations aimed at reducing CO₂ emissions are being increasingly strengthened in each country. In addition, the levels of fuel efficiency, environmental performance, motion performance, and safety performance required for automobiles are becoming increasingly higher every day. In addition to improving the efficiency of ICEV^{Note 1)}, there is a rapid movement toward electrification as seen in HEV, PHEV^{Note 1)}, EV^{Note 1)}, and FCV^{Note 1)}. These electric vehicles are additionally equipped with heavy objects such as batteries and hydrogen tanks, and considering the movement performance and collision performance, it is said that the demand for weight reduction of the entire vehicle remains the same regardless of the type of powertrain.^{1), 2)}

In recent years, aluminum has come to be used extensively for luxury cars. Examples include panels such as bonnet and trunk lids, as well as hang-on parts such as bumpers and door impact beams. To cope with weight reduction and strengthened collision safety regulations, high-strength steel sheets have come to be used for the body frames of popular cars, and multi-material including aluminum alloys combined with high-strength steel sheets has begun to be used for luxury cars and large vehicles. In the EU and U.S., some luxury cars have begun to adopt magnesium alloys, as well as resins such as CFRP, in addition to high strength steel sheet and aluminum alloys to further reduce their body weight.

In order to realize a multi-material structure,

design and evaluation technologies are essential to maximize the effect of weight reduction by effectively combining materials with different physical properties. Furthermore, it is important to develop technologies such as dissimilar metal joining, which enables low-cost, high-strength joining of difficult-to-join materials such as high-strength steel sheets and aluminum alloys.

This paper focuses on multi-material bodies made of high-strength steel sheets and aluminum alloys, which are the current mainstream, and introduces the results of trial calculations of car body weights when the ratio of high-strength steel sheets and aluminum alloy is changed. Also introduced are existing dissimilar metal joining technologies to realize multi-material bodies and an example of low-cost dissimilar metal joining technology being developed by Kobe Steel.

1. Trial calculation of weight reduction effect of body frame based on steel-aluminum

In the EU and U.S., lightweight projects have preliminarily calculated the weight reduction effect of multi-material bodies.^{3), 4)} There are, however, few publicly known cases where the relationship between the ratio of the applied materials and the weight reduction effect has been estimated for a given vehicle body. This section introduces examples of light weight designs with a changing ratio of steel and aluminum alloy for a given vehicle body, in which the effects of weight reduction and reduced number of parts are estimated.

An E-segment SUV was used as the base for weight reduction design. **Fig. 1** shows the main specifications of the vehicle, design requirements, body-in-white, and material compositions. The base car body is all made of steel, using approximately 40% high-tensile steel with a tensile strength of 590 MPa, and approximately 12.5% ultra-high tensile steel with a tensile strength of 780 MPa or higher. In order to examine the weight reduction from the base body, four cases were designed under different policies. Case 1 fully exploits ultra-high tensile steel, which is less expensive than non-ferrous materials, Cases 2 and 3 aim at reducing weight by combining steel and aluminum alloys, while aiming to reduce the number of parts by applying

Note 1) ICEV, Internal Combustion Engine Vehicle; HEV, Hybrid Electric Vehicle; PHEV, Plug-in Hybrid Electric Vehicle; EV, Electric Vehicle; FCV, Fuel Cell Vehicle

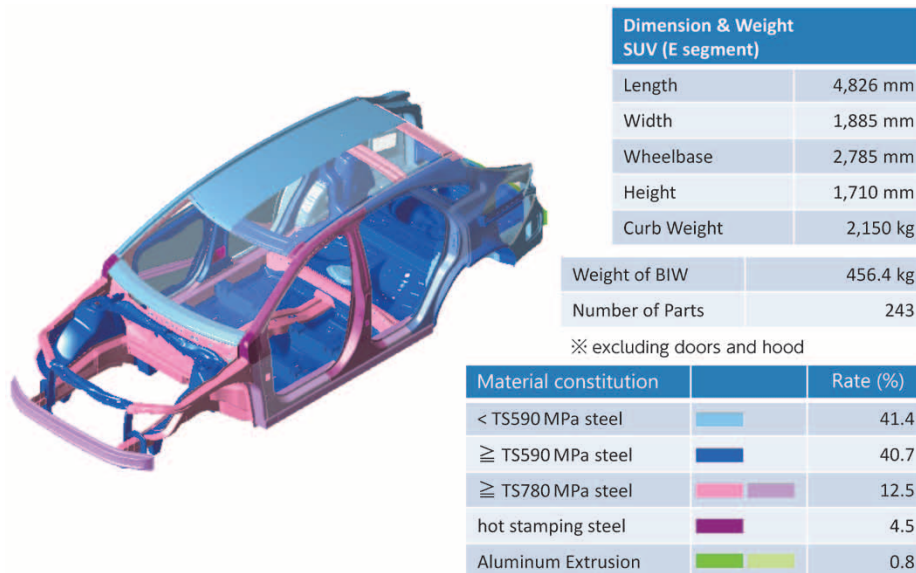


Fig. 1 Body-in-white, main specifications, and material constitution of base vehicle

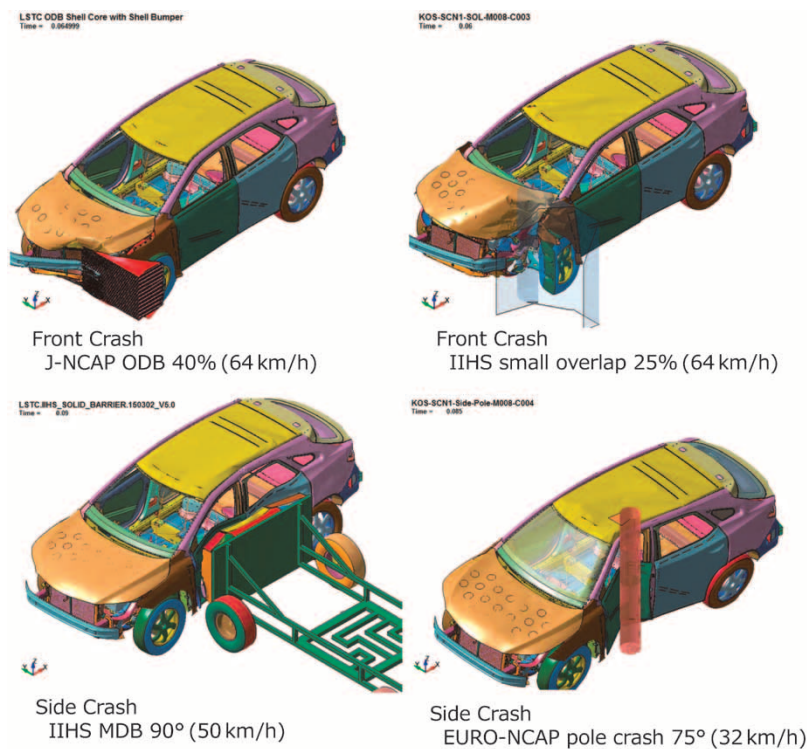


Fig. 2 Deformation of vehicle in typical cases of crash simulation

aluminum extrusions and die castings, and in Case 4, high-strength steel is applied only to the parts with severe collision requirements while making the best use of aluminum alloy.

The requirements for vehicle design are: (a) the amount of deformation at each part, evaluated by collision analysis, is to be evaluated as "Good" on the basis of the main collision criteria; and (b) the torsional stiffness and bending stiffness of the entire vehicle, evaluated by dynamic stiffness, are to be 50 Hz and 40 Hz or higher, respectively. Fig. 2 shows

the deformation of a vehicle body based on the crush simulation of typical collision cases.

Fig. 3 shows the calculated results of weight reduction, with the vertical axis representing the weight of the body-in-white and the horizontal axis representing the rough cost. The costs are based on relative comparisons that take into account the difference in material cost per weight of steel and aluminum alloy, as well as the cost reduction effect of machining and joining processes with the reduced number of parts. Table 1 shows the weight ratio

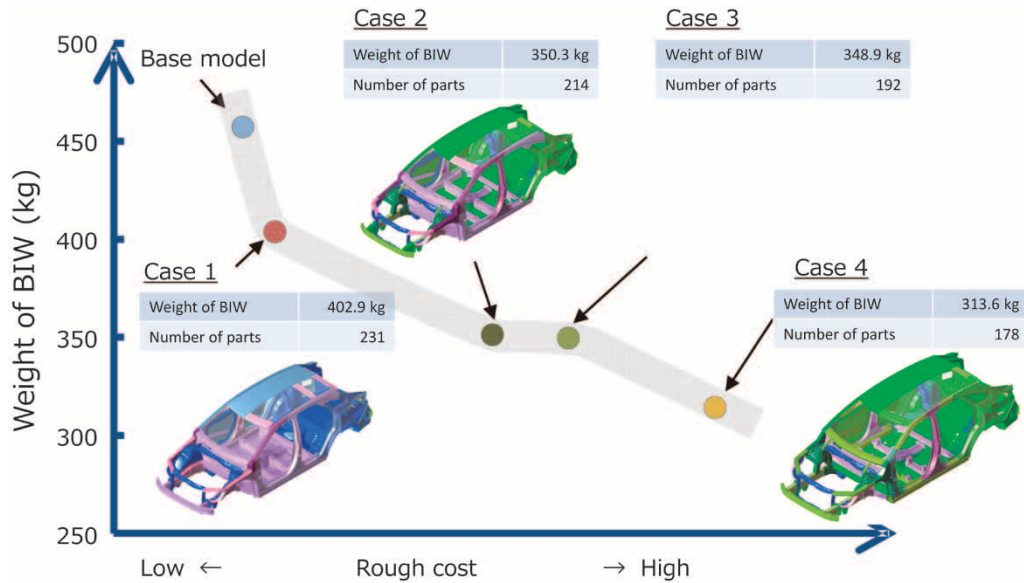


Fig. 3 Results of light weight design

Table 1 Material constitution ratio of each weight reduction case

Case 1			Case 3		
Material constitution		Rate (%)	Material constitution		Rate (%)
< TS590 MPa steel		24.1	Steel		61.4
≥ TS590 MPa steel		32.9	Al Extrusion		4.8
≥ TS780 MPa steel		38.3	Al sheet		26.2
Hot stamping steel		3.8	Cast Al		7.6
Al Extrusion		0.9			
Case 2			Case 4		
Material constitution		Rate (%)	Material constitution		Rate (%)
Steel		50.1	Steel		27.5
Al Extrusion		12.0	Al Extrusion		20.5
Al sheet		30.1	Al sheet		37.6
Cast Al		7.8	Cast Al		14.4

of steel and aluminum alloy used when sorted by steel strength class and the type of aluminum alloy. According to Kobe Steel's calculations, Case 1 results in a 12% (53.5 kg) weight reduction by the full exploitation of ultra-high-tensile material, Cases 2 and 3 result in a 22 to 24% (106.1 to 107.5 kg) weight reduction by the use of multi-materials, and Case 4 results in a 33% (142.8 kg) weight reduction by the proactive use of aluminum alloy. It should be noted, however, that an increase in cost associated with weight reduction is inevitable, as shown in Fig. 3. It is anticipated that not only the material cost, but also processing costs such as pressing and joining will increase.

Some of the materials used in this study are under development. It is necessary to make such efforts to put new materials into practical use for further reduced weight and lower costs. In addition, it is considered to be effective, for the sake

of suppressing the cost, to reduce the number of parts by integrating parts by aluminum die-casting or extrusion, or to omit reinforcing members by increasing the strength of the steel. Developing technology for minimizing the capital investment in dissimilar material joining, which is a major issue for multi-materials, is also considered to be effective.

2. Existing dissimilar metal joining and low-cost dissimilar material joining technology

2.1 Issues in dissimilar metal joining and joining methods actually in use

Steel-to-steel joining is mostly accomplished by welding. Although there are differences between the resistance spot welding used for bodies-in-white and the arc welding used for the chassis, both mechanisms involve melting the base materials at

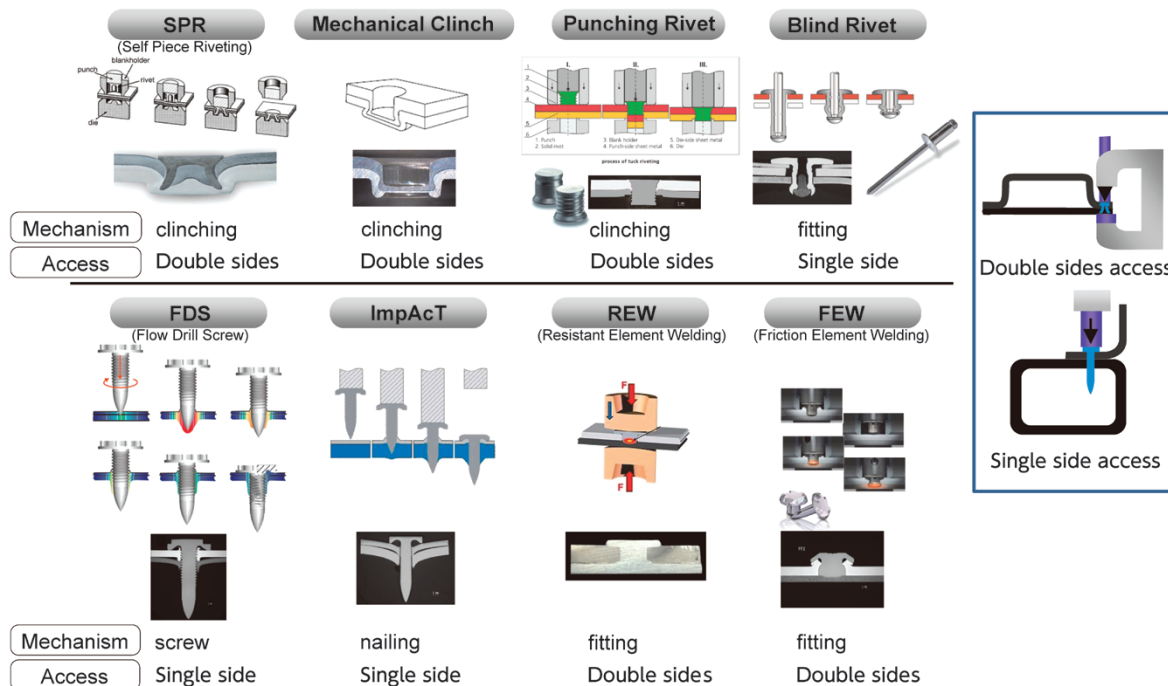


Fig. 4 Practically applied methods of joining dissimilar metals for car body structure

high temperatures to form metal bonds. However, weld joining between steel and aluminum alloy is impossible due to the formation of extremely brittle intermetallic compounds.

Hence, instead of melting and mixing the two metals, mechanical joining methods are mainly used for dissimilar metal joining, in which geometrical constraint or friction is used as a joining force. Fig. 4 illustrates major methods of dissimilar metal joining for automobiles. To give just a simple explanation here, self-pierce riveting (SPR), which is the most popular clinching mechanism, involves more than 2,000 piercing points per vehicle. There also are some cars, each of which has more than 700 penetration points of a flow drill screw (FDS) mechanism.

2.2 Trends in adhesives

Another problem in joining dissimilar materials is electrolytic corrosion (galvanic corrosion). When different metals come into contact with each other, a local battery is formed, and one of the metals is selectively corroded. In the case of steel and aluminum alloys, the latter corrode. A practical way to prevent electrolytic corrosion is to keep moisture away from the joint surface. Most of the practical mechanical joining methods described above produce point joints and therefore lack the watertight seal function. The formation of a local battery can be prevented by applying an adhesive to the interface or surface in advance and then

performing mechanical joining. This hybrid joining method is the de facto method of dissimilar metal joining taking into account the electric corrosion. In addition, since the adhesive forms a surface joint, it exhibits not only the above-mentioned sealing function but also high shear strength. On the other hand, there are many points to be considered, such as the quality control of the application state, as well as the deterioration of adhesive strength after exposure at low temperatures or for a long period of time. Despite this, the importance of adhesives has increased with the development of multi-material structures involving resins, and their use has increased.

2.3 Dissimilar material joining method for high strength steel and aluminum alloy^{5), 6)}

As described in the previous section, aluminum alloys are more frequently being used with proactive application of high-strength steel sheets, which are relatively inexpensive and have a weight reduction effect, requiring dissimilar metal joining between high-strength steel sheets and aluminum alloy. However, the conventional mechanical joining method, in which a steel sheet is plastically deformed or penetrated, is becoming difficult as the strength of the steel sheet increases. On the other hand, although the adhesive can be applied to high-strength steel sheets, there is a disadvantage in that the cross tension strength (CTS) in the direction

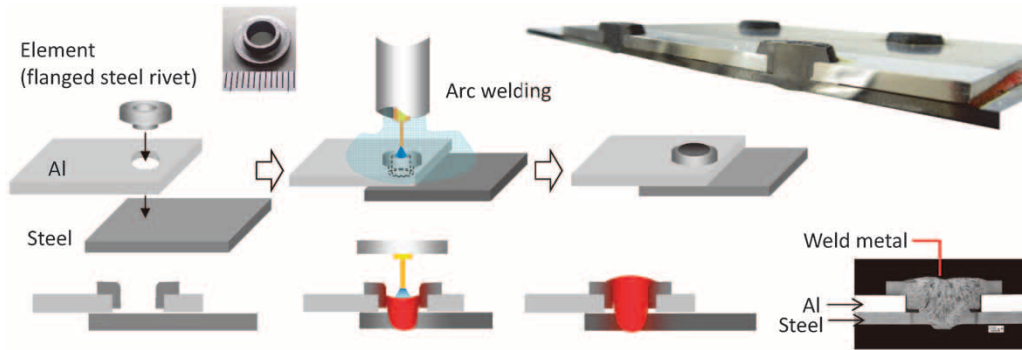


Fig. 5 Basic mechanism of EASW ⁷⁾

perpendicular to the shear strength is low, and the joint strength with adhesive alone is likely to be insufficient.

Hence, Kobe Steel uniquely developed "element arc spot welding (hereinafter referred to as "EASW")," a dissimilar metal joining method that enables the strong joining of high-strength steel sheets and aluminum alloys.⁷⁾ This mechanism is shown in Fig. 5. A hollow steel element (rivet) is inserted into an aluminum alloy sheet, and a steel welding wire is supplied to the hollow portion of the element by gas shielded arc welding and is casted. As a result, the steel element and the lower steel sheet are firmly welded together, while the aluminum alloy sheet is sandwiched between them to achieve fastening. Since the method requires no plastic deformation of the steel sheet, it is possible to join high-strength steel sheets involving hot stamping. Fig. 6 compares the shear strength (TSS) and cross tensile strength (CTS) of conventional dissimilar material joining and EASW. It can be seen that EASW exhibits both TSS and CTS higher than those of the conventional joining methods. The features of EASW are as follows:

- (1) Higher joining strength, irrespective of shearing or cross tensile, compared with the conventional dissimilar material joining methods (Fig. 6);
- (2) No need to sandwich the base material from both its sides, allowing joining from one side and increasing the application range.
- (3) Enabling the joining of a three-layer structure such as aluminum/steel/steel; and
- (4) Simple and applicable to repairs.

In order to realize EASW on the actual production lines of automobiles, a robot system was jointly developed with FANUC, including necessary devices for automatically detecting the position of elements, inserting them, and automatically performing arc welding. Its prototype has been released lately (Fig. 7). Currently, its development for practical use is underway.

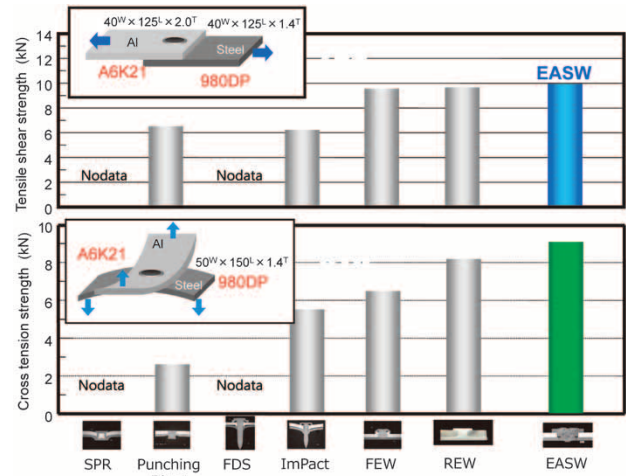


Fig. 6 Joining strength of EASW

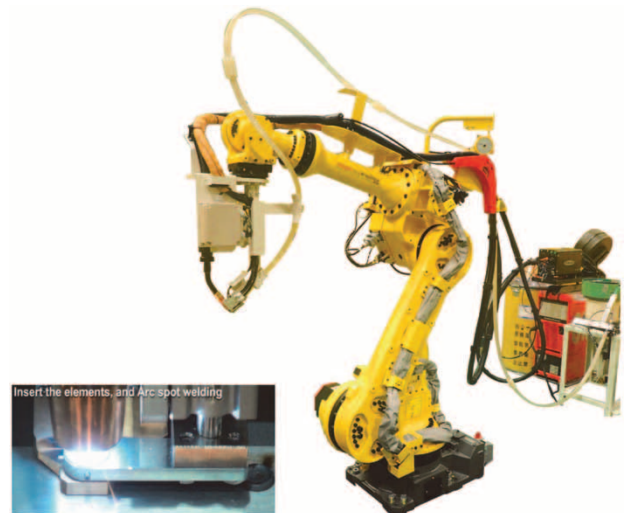


Fig. 7 Prototype robot system for EASW (right) and appearance of joining (left)

Conclusions

Continuous efforts are necessary to reduce the weight of automotive bodies in consideration of CO₂ emission and collision safety regulations; and the trend toward multi-materials, as a measure for weight reduction, is inevitable. The practical

application of multi-material bodies has already progressed in the EU and U.S. In Japan, each company is increasing efforts toward realizing this application.

Since the automobile industry is a key industry that can be said to represent national power, it is expected that there will be greater efforts than ever before, including industry-government-academia collaboration and cooperation among different industries and supply chains. Kobe Steel will also continue to contribute its efforts toward reducing automotive weight.

References

- 1) M. Maeda et al. Knowledge creation and integration. April, 2017, pp.46-63.
- 2) H. Sakagami et al. Journal of the Society of Automotive Engineers of Japan. 2016, Vol.70, No.8, pp.42-44.
- 3) Jens Meschke. ALIVE Final publishable summary report. Nov. 2016.
- 4) Tim Skrzek et al. Multi-Material Lightweight Vehicles. June 2015.
- 5) R. Suzuki. Welding technology. January 2017. pp.64-72.
- 6) R. Suzuki et al. International Institute of Welding. July 2018, Doc.XII-2390-18.
- 7) L. CHEN et al. *R&D Kobe Steel Engineering Reports*. 2018, Vol.67, No.1, pp.104-110.

Outline of Steel Production System

Tsutomu HAMADA*1

*1 Business Planning Section, Kakogawa Works, Iron & Steel Business

While taking place of upgrading such as consolidations and mergers in order to increase competitiveness in the steel industry, Kobe Steel aims to enhance competitiveness through the high added value of technology, products and services, and further differentiation by constructing unique business models. In order to provide competitive technologies and products, in 2017 Kobe Steel completed a new hot metal pretreatment plant at its Kakogawa Works and in order to enhance cost competitiveness, decided and implemented the consolidation of upstream (ironmaking and steelmaking) processes of Kobe Works with Kakogawa Works. After consolidation, Kakogawa Works has been transformed into the cost-competitive steelworks that manufactures a wide variety of steel products, such as steel sheets, thick plates and wire rods. Kobe Works could significantly improve the quality and cost competitiveness of special steel wire rods and bars using billets manufactured by Kakogawa's equipment introduced the latest technology, without reducing steel production. In the global supply system for products, Kobe Steel has established a three-pole supply system in Japan, US and China for special steel wire rods (steel wire) and high formable advanced high tensile strength steel sheet.

Introduction

Kobe Steel's iron and steel business has contributed to the development of society and industry by promoting "MONODZUKURI" (the art of design and manufacturing) in a wide range of fields and providing excellent products and technologies. The Iron and Steel Business comprises business units of iron and steel products, steel castings, titanium products and steel powders and is thoroughly strengthening the "Monodzukuri power" with an eye to improving quality, productivity, and cost competitiveness. Kobe Steel is also strengthening the global expansion of distinctive products and technologies and its response to the demand fields where future growth is anticipated, such as the field of transportation equipment represented by automobiles.

This paper describes a iron and steel production system capable of supplying highly efficient and high-quality products, which has been renewed by consolidating the upper processes at Kakogawa Works, as well as its global supply system of distinctive iron and steel products, in addition to

recent capital investment in the application of state-of-the-art technology.

1. History of Kobe Steel's Iron and Steel Business

Kobe Steel's products at the time of the company's establishment in 1905 began with castings including anvils, anchors, and the wheels of coal mining vehicles. In 1924, the No. 1 wire rod mill was made available for operation in the Wakinohama area of Kobe, and high carbon steel wire material began to be produced domestically in Japan. Subsequently, new wire rod mills were added to expand the production volume in response to the increasing domestic demand. In 1959, the operation of Kobe Steel's first blast furnace began in the Nadahama area of Kobe; thus, Kobe Works was inaugurated as an integrated iron mill. In addition, the company undertook the construction of Kakogawa Works; and, following the completion of the steel plate plant in 1968, the No.1 blast furnace was blown-in in 1970. The main plants for steelmaking, hot rolling, cold rolling and wire rods were completed one after another, leading to the inauguration of Kakogawa Works, the second integrated iron mill. As a result, Kobe Steel was able to add steel plates and steel sheets to its menu, in addition to steel wire rod and bar.¹⁾

Today, the company produces about 6 million tonnes/year of steel products at Kobe Works and Kakogawa Works and has developed multiple processing bases in North America, China and Asia to provide various steel products to customers inside and outside of Japan.

2. Steel manufacturing bases and merchandise category mix

Kobe Steel currently produces steel wire rods and bar products at Kobe Works, and steel wire rod products in addition to steel sheets and steel plates at Kakogawa Works.

Steel wire rods and bar products are mainly special steel for automobiles. The company ships a wide range of products, including steel wire rods for springs used especially for automotive engines and suspension parts,^{2), 3)} steel bars for crank shafts and gears, and cold heading quality (CHQ) steel wire rods used for fasteners such as bolts and nuts, with

a focus on automotive manufacturers in Japan, but also in North America, Europe, China and Asia.

Steel sheets are mostly used in automobiles and home electronics and as building materials. In particular, the company is focusing on the development and production of high-tensile-strength (Hi-Ten) steel sheets, which have the world's highest level of strength and excellent workability,⁴⁾⁻⁶⁾ to respond to societal needs, particularly those for the weight reduction of automobiles and reduction of the environmental burden through automotive fuel efficiency improvement. As for steel plate products, used mainly in the fields of buildings, bridges and ships, the company is developing new products that meet customer needs for high strength steel with excellent weldability, among others.

3. Capital investment for strengthening competitiveness of steel business

3.1 New molten iron treatment plant at Kakogawa Works

Molten iron treatment is an indispensable process for producing high-quality steel that requires a high degree of cleanliness. Kakogawa Works has a new molten iron treatment plant (Fig. 1) that was put into operation in 2014, and established a system including two dephosphorization furnaces and two desulfurization apparatuses in 2017. Conventionally, the dephosphorization process had been performed in torpedo cars; however, the newly introduced dephosphorization furnace improved the dephosphorization ratio by approximately 50% and increased the crude steel production capacity. In addition, the introduction of desulfurization and dephosphorization technology with the highest



Fig. 1 New plant for molten iron treatment

efficiency in the industry has resulted in significant cost improvement. The new operation has increased the production capacity of products that require high cleanliness, such as special steel wire rods, high-tensile-strength steel sheets and steel plates for energy related applications.

3.2 Consolidation of upstream processes at Kakogawa Works

In view of the mid-to-long term business environment, both domestically and abroad, the environment surrounding the iron and steel business is becoming tough due to the decreased demand in Japan and an increased supply due to the expansion of iron & steel works outside Japan. The cost competitiveness of Kobe Works was inferior to that of Kakogawa Works due to structural factors, including the lack of in-house pretreatment facilities, such as coke plants and sintering plants, and its small production scale. Therefore, in 2017, the upstream process equipment (blast furnace to continuous casters, and some bloom mills) at Kobe Works was shut down and these processes were consolidated at Kakogawa Works. As mentioned in the preface of this issue, the upstream process utilization rate and steel quality were improved by addressing the process-specific issues through this consolidation. Moreover, the production cost has been improved, and a system has been established for reliable delivery on the dates desired by customers.

Conventionally, Kakogawa Works has been a large steelworks for producing large lot products of steel sheets and steel plates. However, as a result of the above-mentioned consolidation, special steel products such as steel wire rods and bars, which are produced in small lots and large variety, can be produced in large quantities with high quality at low cost. As such, Kakogawa Works was renewed and has become a steelworks that is unprecedented, both domestically and abroad.

3.3 Renovation of Kakogawa Works No. 3 blast furnace

The shutdown of the upstream process equipment at Kobe Works, including the blast furnace, and its consolidation into Kakogawa Works would make Kakogawa Works the only supply base for raw iron. For this reason, the No. 3 blast furnace of Kakogawa Works was renovated in 2016, prior to the consolidation. The renovation work adopted the continuous use of the steel outer shell of the blast furnace body, which was a first for any large

blast furnace in Japan. The renovation was finished in a short construction period of 90 days with the aim of shortening as much as possible the period of reduced crude steel production.

On the other hand, renovation aimed at anti-aging measures alone cannot attain the significance and effect of consolidation. In other words, a higher level and stable operation of the blast furnace is required to meet the responsibility of supplying raw iron. Hence, various sensors were installed in the blast furnace, and an AI system was introduced to support stable operation using the information obtained from the sensors.⁷⁾

4. Steel production system after consolidation

Fig. 2 shows the steel production system in both works after the equipment enhancement described in Section 3. As the blast furnace and steelmaking equipment at Kobe Works was shut down for consolidation, the semi-products produced at Kakogawa Works were supplied to the rolling plants at both Kakogawa Works and Kobe Works. The following is an overview of the advantages of each process in both of the steelworks:

4.1 Kakogawa Works

4.1.1 Raw material pretreatment process

Kakogawa Works has one line each of a sintering plant and pellet plant for pretreating raw materials (iron ore). Sintered ore produced by firing and sizing the raw ore fines in the sintering plant and smaller fines not suitable for the sintering raw material are

mixed to be granulated and fired into ore pellets for use in the blast furnaces. The applicable range of iron ore is expanded in this way to reduce the cost. The sintering plant improves productivity by the appropriate designing of the raw material grain size, and the pellet plant is designed to further reduce cost by adopting a grate-kiln process,⁸⁾ made in-house and one of the world's greatest, for firing.

The reductant coke has been processed by Kansai Coke and Chemicals Company Limited in Kakogawa Works since 1970, and coke gas is supplied together with coke. There are 4 coke furnaces, a total of 248 gates, in operation, which will become a 50-year-old furnace in 2020. For that reason, the renewal of these coke furnaces is being planned.

4.1.2 Ironmaking process

Prior to the consolidation of the upstream processes, Kobe Steel operated three blast furnaces; namely the No. 3 blast furnace of Kobe Works and No. 2 and No. 3 blast furnaces of Kakogawa Works. As mentioned above, the No. 2 blast furnace was renovated in 2007 and the No. 3 blast furnace was renovated in 2016. After the consolidation, these two blast furnaces of Kakogawa Works are currently in full operation discharging molten pig iron.

Kakogawa Works has been purchasing a part of coke from the outside, which has increased the cost. Therefore, with the purpose of reducing the energy costs, technologies are being developed, aiming at operation with a high pulverized coal ratio and low coke ratio.⁹⁾ As a result, operation continues with a high pulverized coal ratio and low coke ratio, which

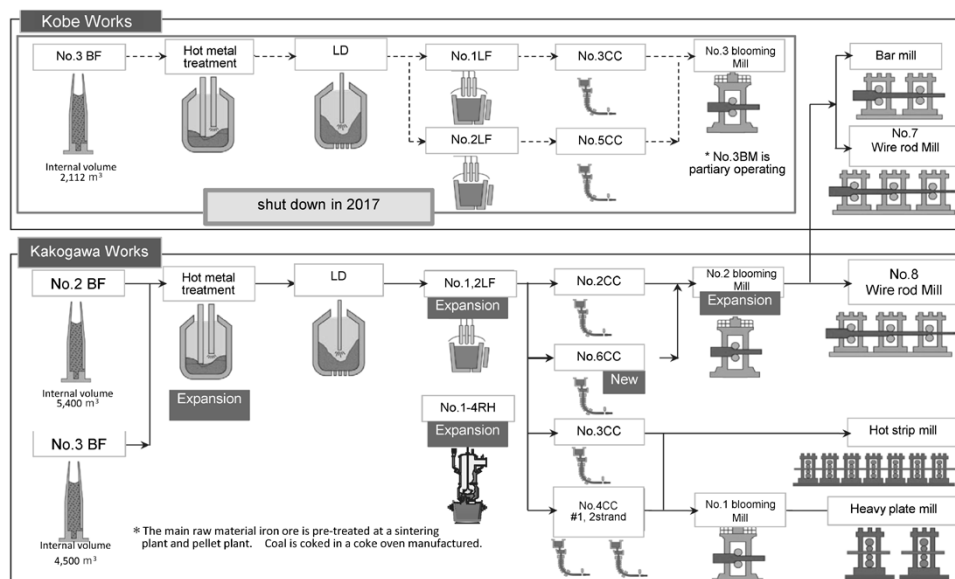


Fig. 2 Steel production system

is top level in Japan.

4.1.3 Steelmaking process

The steelmaking plant of Kakogawa Works features the supplying of crude steel for use in a wide variety of steel sheets, steel plates and wire rods. In other words, molten iron is dephosphorized and desulfurized and processed by three top-blowing converters to create a wide range of steel compositions. After the blowing, the molten steel is subjected to molten steel treatments using a ladle furnace (LF), Ruhrstahl-Heraeus (RH) degassing apparatus and so on, enabling the production of high-quality steel such as inclusion-controlled steel¹⁰⁾⁻¹²⁾ and ultra-clean steel.¹³⁾

After the molten steel treatment, various special steels with high quality and high function are produced by continuous slab casting equipment and continuous bloom casting equipment.

In 2017, Kakogawa Works completed a new molten iron treatment plant equipped with two Kanbara reactor (KR) desulfurization apparatuses and two converter-type dephosphorization furnaces. With this completion of facilities, the molten iron treatment time was significantly shortened, while improving efficiency in the production, among others, of special steel wire rods /steel bars that require a high degree of cleanliness, high-tensile-strength steel plates, and of steel plate for energy related applications.

In addition, the upstream process consolidation accompanied the new installations of continuous casting equipment and molten steel processing equipment incorporating advanced technologies, such as surface quality technology, which have been cultivated over many years at Kobe Works. As a result, Kakogawa Works has established a system for supplying the 150,000 tonnes/month of crude steel required to produce steel wire rods and bars at Kobe Works.

4.1.4 Blooming mill process and logistics for semifinished products

Since the upstream process consolidation, Kakogawa Works has been supplying 130,000 tonnes/month of steel billets, produced at its No. 2 blooming mill plant, to Kobe Works for use in the production of steel wire rods and bars there. The conventional blooming capacity of the No. 2 blooming mill plant was 150,000 tonnes/month. Therefore, production capacity enhancement was carried out in the upstream process consolidation work, such as newly installing a heating furnace



Fig. 3 Rolling mill in No. 2 blooming mill factory at Kakogawa Works

and reinforcing the continuous rolling mill for steel billets (Fig. 3). As a single unit, the blooming mill secured a rolling capacity of 300,000 tonnes per month, which is unparalleled in the world. In addition, two new roll-on/roll-off (RORO) ships were built to deal with the transportation of steel billets from Kakogawa to Kobe, which has increased dramatically from approximately 30,000 tonnes per month to 130,000 tonnes per month. Previously, these steel billets were loaded on the ships by a slinging operation. Now the steel billets are loaded onto pallets to be moved, establishing a transportation system that is safe, efficient and low-cost. These and other efforts have helped maintain a stable supply to the rolling process at Kobe Works. In addition, steel billet yards were constructed at both Kakogawa Works and Kobe Works with a total inventory capacity of 160,000 tonnes. This allows the inventory to be increased, establishing a system to meet the customer's desired delivery date for small quantity, large variety orders, which are unique to special steel.

4.1.5 Steel sheet process

The hot-rolling plant with a nominal monthly capacity of 360,000 tonnes produces hot-rolled products (steel plate) and titanium materials that are shipped after hot rolling. It also supplies the cold-rolling plant with stock materials for, among other things, high-tensile-strength steel sheets for automobiles and highly functional steel sheets for home electronics.^{14), 15)}

In the cold-rolling plant, hot-rolled coils are used as the stock material to be cold-rolled into cold-rolled products (steel sheet) and as stock material for plated steel sheets. A continuous annealing line (CAL), continuous galvanizing line (CGL), and electro galvanizing line (EGL) are used to make a

large assortment of products, including high-tensile-strength steel sheet and highly functional, surface-treated steel sheet.¹⁶⁾

4.1.6 Steel plate process

Steel plates are produced in a steel plate finishing mill (Fig. 4) with a nominal monthly capacity of 140,000 tonnes, and are used in the fields of construction, bridges and shipbuilding. Thermo-mechanical control process (TMCP) technology,¹⁷⁾ based on controlled rolling and accelerated cooling, is used to produce steel with excellent strength and toughness while having favorable welding workability, providing a large assortment of products, including high-heat-input steel^{18), 19)} for building construction and steels for low temperature service in shipbuilding.²⁰⁾ Recent applications include circular steel pipes used in Tokyo Skytree and Roppongi Hills.

4.1.7 Wire rod process

The No. 8 wire rod mill with a nominal monthly capacity of 115,000 tonnes produces steel wire rods, each with a diameter of 5-18 mm. Being a 4-strand mill plant for mass production, the No. 8 wire rod mill is suitable for the mass production of high carbon steel wires, such as tire steel cords and wire ropes, adopting controlled cooling with a Stelmor conveyor after the winding of steel wire rods.

In recent years, with the improvement of the production process, the rolling quantity of highly functional products for automobiles, such as steel wire rods for cold heading and spring steel, has been increased to meet the strong demand from customers. In addition, in response to the recent increase in demand for special steel wire rods for automobiles, a production technology to improve the surface quality has been developed and introduced into this mill, despite its mass production type, which has increased the production volume of the steel wire rods for cold heading that have stringent surface quality requirements.

4.2 Kobe Works

About 70% of the total shipping volume of steel wire rods and bars produced at Kobe Works is highly functional special steel for automotive applications.

4.2.1 Wire rod mill

The No. 7 wire rod mill (Fig. 5) has a nominal

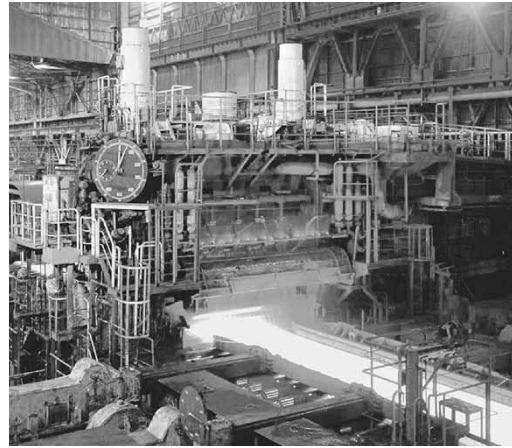


Fig. 4 Finishing mill for steel plate at Kakogawa Works



Fig. 5 Laying head of No. 7 wire rod and bar mill at Kobe Works

monthly capacity of 55,000 tonnes and produces steel wire rods, each with diameters of 5.5 to 22 mm. The finish rolling line has the world's highest level of controlled rolling and controlled cooling capabilities.²¹⁾ The company supplies steel wire rod products with high dimensional accuracy, and they are softened by a thermomechanical control process,²²⁾ which can reduce the cost of auto parts by simplifying the secondary processing.

4.2.2 Steel bar mill

The steel bar mill has a nominal monthly capacity of 68,000 tonnes and produces ϕ 17-108 mm steel bars and large diameter ϕ 17-60 mm steel rods. The finish rolling line has a finish rolling mill capable of rolling with one of the highest product dimension accuracies (± 0.1 mm) in the industry, which meets the needs of many customers. In the steel bar processing plant, steel bars are subjected to non-destructive testing to guarantee the quality of all surfaces and all cross-sections.

Table 1 Processing bases for steel products outside Japan

Category	Company name	Start up	Investment ratio (%)	Business content	Location
Wire Rod and Bar	Grand Blanc Processing, LLC	*2003- 4	20	Manufacture and sales of CHQ wire	Michigan, USA
	Kobe CH Wire (Thailand) Co., Ltd.	1997- 8	30	Ditto	Thailand Bangkok
	Mahajak Kyodo Co., Ltd.	*2002- 5	30	Manufacture and sale of grinding bars	Thailand Bangkok
	Kobelco Millcon Steel Co., Ltd.	2016- 2	50	Rolling and sales of special steels and ordinary steel wire materials	Thailand Rayong Rayong County
	Kobe Wire Products (Foshan) Co., Ltd.	2004-11	60	Manufacture and sale of steel bars and CHQ wires	Foshan, Guangdong, China
	Kobelco Spring Wire (Foshan) Co., Ltd.	2012- 1	50	Manufacture and sale of high-grade spring steel wire	Foshan, Guangdong, China
	Jiangyin Sugita Fasten Spring Wire Co., Ltd.	2005- 8	60	Manufacture and sales of wire for automobile suspension springs	Jiangyin, Jiangsu Province, China
	Kobe Special Steel Wire Products (Pinghu) Co., Ltd.	2007-11	50	Manufacture and sales of CHQ wire and bearing steel wire	Pinghu, Zhejiang Province, China
Sheet	Kobelco CH Wire Mexicana, S.A. de C.V.	2014- 9	10	Manufacture and sales of CHQ wire	Mexico Guanajuato
	PRO-TEC Coating Company	1990- 3	50	Manufacture and sale of hot dipped galvanized steel sheet and cold rolled high tensile steel	Leepsic, Ohio, USA
Other	Kobelco Angang Auto Steel Co., Ltd.	2014- 8	50	Ditto	Anshan City, Liaoning Province, China
	Kobe Steel Asia Pte. Ltd.	1990- 1	100	Steel-related market research and technical services	Singapore

*Date of investment



Fig. 6 Kobelco Millcon Steel in Thailand



Fig. 7 PRO-TEC Coating Company in USA

4.2.3 Secondary processing of steel wire rods and bars

The bases for the secondary processing of steel wire rods and bars are located in-house. These bases provide customers with higher added value by conducting the pickling, heat treatment, and surface lubrication treatment of cold heading steel, bearing steel, spring steel, and the like.

5. Global supply system of special steel wire rods and high-tensile-strength steel sheets

5.1 Wire rod rolling base

In the Asian region centering on Thailand, demand for special-steel wire rods for automobiles is expected to increase in the future. Hence, Kobe Steel established "Kobelco Millcon Steel Co., Ltd. (hereinafter referred to as "KMS", Fig. 6)" in Rayong, Thailand in 2016, and began production in 2017. This is the only Kobe Steel wire rod mill base outside Japan.

5.2 Bases for secondary processing of steel wire rods and bars, and for processing parts

As a secondary processing base for wire-rods in Japan, Shinko Wire Company, Ltd., a group

company of Kobe Steel, manufactures secondary processed products such as high strength springs and wire ropes for buildings and bridges. Shinko Bolt, Ltd. produces high-strength bolts for buildings, civil engineering and bridges, while Nippon Koshuha Steel Co., Ltd. manufactures secondary processed products such as steel wire rods for bearing steel.

Table 1 contains a list of steel processing bases outside Japan. They are located in North America, China, and Southeast Asia for the timely supply of steel wire rods and bars, which are stock materials for the production of automobile parts, among other parts. The main customers are Japanese parts manufacturers that have entered each local market.

In 2016, the company established "Kobelco CH Wire Mexicana, S.A. de C.V. (KCHM)" in Mexico, its 9th base outside Japan, to produce and sell steel wires for cold heading.

5.3 Bases for steel sheets and highly formable high-tensile-strength steel sheets

In North America, the PRO-TEC Coating Company (hereinafter referred to as "PRO-TEC Co." (Fig. 7)), established by a splitting investment of Kobe Steel and United States Steel Corporation, started operations in 1993. This company serves as a production base for thin-gauge steel sheet and

highly formable high-tensile-strength steel sheet and produces hot-dip galvanized thin-gauge steel sheets and cold-rolled high-tensile-strength steel products.

In China, Kobelco Angang Auto Steel Co., Ltd. was established as a joint venture with Angang Steel Co., Ltd. (hereinafter referred to as "Angang Steel"), a subsidiary of Anshan Iron and Steel Group Corporation., in 2015. A continuous annealing line (CAL) with an annual production capacity of 600,000 tonnes was built in Anshan Steelworks, Angang Steel, and inaugurated in 2016 as a production base for cold-rolled high-tensile-strength steel sheet.

With the opening of these bases, Kobe Steel has established a trilateral global production system for high-tensile-strength steel sheets in Japan, the US, and China.

6. Future plans

During the upstream process consolidation, continuous casting equipment and molten iron treatment equipment with advanced technologies were newly installed to improve the quality of special steel wire rods and bars. KMS, which has started rolling special-steel wire rods in Thailand, is currently being evaluated by local Japanese automobile manufacturers with a view to acquiring approval for special steel wire rods. The plan is for it to meet the demand for special-steel wire rods in the ASEAN region as Kobe Steel's No. 9 wire rod mill.

The automobile manufacturers inside and outside Japan are promoting "automotive weight reduction" vigorously, and to meet this demand, there are plans to increase the production capacity of "highly formable, ultra-high-tensile-strength" steel sheets in the US and Japan. In the United States, a third CGL has been added to PRO-TEC Co., and production is scheduled to start in 2019. In Japan, there are plans to equip Kakogawa Works with a manufacturing line for cold-rolled steel sheet and hot-dip galvanized sheet. This line will combine continuous annealing equipment and hot-dip galvanization/alloying equipment and is scheduled to start operation in 2021. Both lines apply state-of-the-art technologies of heat treatment with a cooling function and can produce highly formable ultra-high-tensile-strength steel sheets with industry-leading strength and workability (above 780 MPa or higher). With the addition of China (Kobelco Angang Auto Steel Co., Ltd.), the trilateral supply capacity in Japan, the US and China has been established to supply high-tensile-strength steel sheets with excellent quality to customers, which will contribute to the weight reduction of automobiles and will lead to fuel efficiency

improvements and CO₂ reduction in the future.

Conclusions

In the automotive industry, the source of the greatest demand for iron and steel, there has been an increase in the production volume of environment-friendly vehicles such as electric vehicles and fuel-cell vehicles in order to reduce CO₂ emissions and prevent global warming. Great changes are occurring in response to more stringent fuel efficiency regulations and collision safety regulations, which will further increase the need for "lighter and stronger automotive bodies", and the progress of business globalization will increase the need for local production and supply.

In this environmental change, Kobe Steel, the only manufacturer in the world that has welding consumables and dissimilar material joining technology in addition to iron & steel and aluminum products, believes it is necessary to focus on the following initiatives in order to continue contributing to our customers and society:

- (1) Responding to customers' needs by proposing new products using highly functional, high-performance steel,
- (2) Developing environment-friendly production technology that saves resources and energy, and
- (3) Proposing solutions for improving quality, delivery time, cost, etc.

In order to advance these efforts, it is indispensable to make an accurate response to the customers' needs, which continue to progress and diversify. Furthermore, it is necessary to create a process and technology for stably producing highly functional, high quality steel at the minimum cost. To this end, Kobe Steel is actively engaged in multifaceted development, including advanced AI technology for measuring, predicting and controlling the complex behaviors of molten iron, molten steel materials, and the like in steel production, as well as the further use of evaluation technologies.

References

- 1) Centennial Anniversary Executive Committee. 100 Years of Kobe Steel pp.42-103.
- 2) N. Yoshihara. *R&D Kobe Steel Engineering Reports*. 2011, Vol.61, No.1, pp.39-42.
- 3) T. Maruo et al. *R&D Kobe Steel Engineering Reports*. 2011, Vol.61, No.1, pp.43-46.
- 4) M. Nakaya et al. *R&D Kobe Steel Engineering Reports*. 2009, Vol.59, No.1, pp.46-49.
- 5) T. Murata et al. *R&D Kobe Steel Engineering Reports*. 2017, Vol.66, No.2, pp.17-20.
- 6) Y. Utsumi et al. *R&D Kobe Steel Engineering Reports*. 2017,

- Vol.66, No.2, pp.3-7.
- 7) K. Kamo et al. *R&D Kobe Steel Engineering Reports*. 2018, Vol.68, No.2, pp.7-11.
 - 8) S. Yamaguchi et al. *R&D Kobe Steel Engineering Reports*. 2010, Vol.60, No.1, pp.12-21.
 - 9) R. Ito et al. *R&D Kobe Steel Engineering Reports*. 2000, Vol.50, No.3, pp.6-11.
 - 10) S. Kimura et al. *R&D Kobe Steel Engineering Reports*. 2004, Vol.54, No.3, pp.25-28.
 - 11) S. Kimura et al. *iron と steel*. 2002, Vol.88, No.11, p.53.
 - 12) Tomoko SUGIMURA et al. *ISIJ International*, 2011, Vol.51, No.12, p.1982.
 - 13) H. Ohta et al. *R&D Kobe Steel Engineering Reports*. 2011, Vol.61, No.1, pp.98-101.
 - 14) Y. Hirano et al. *R&D Kobe Steel Engineering Reports*. 2011, Vol.61, No.2, pp.80-82.
 - 15) Y. Hirano et al. *R&D Kobe Steel Engineering Reports*. 2009, Vol.59, No.1, pp.50-53.
 - 16) H. Irie et al. *R&D Kobe Steel Engineering Reports*. 2002, Vol.52, No.3, pp.35-38.
 - 17) Y. Omiya et al. *R&D Kobe Steel Engineering Reports*. 2009, Vol.59, No.1, pp.40-45.
 - 18) Y. Kobayashi et al. *R&D Kobe Steel Engineering Reports*. 2008, Vol.58, No.1, pp.47-51.
 - 19) K. Abe et al. *R&D Kobe Steel Engineering Reports*. 2005, Vol.55, No.2, pp.26-29.
 - 20) M. Kaneko et al. *R&D Kobe Steel Engineering Reports*. 2008, Vol.58, No.1, pp.39-41.
 - 21) Y. Ichida et al. *R&D Kobe Steel Engineering Reports*. 2000, Vol.50, No.1, pp.6-11.
 - 22) H. Hata et al. *R&D Kobe Steel Engineering Reports*. 2000, Vol.50, No.1, pp.29-32.

Decreasing Coke Rate under All-Pellet Operation in Kobe No.3 Blast Furnace

Hitoshi TOYOTA*¹, Tomonori MAEDA*², Nayuta MITSUOKA*², Kota TANAKA*³

*¹Ironmaking Development Department, Research & Development Laboratory, Iron & Steel Business

*²Ironmaking Department, Kakogawa Works, Iron & Steel Business

*³Environmental Control & Disaster Prevention Department, Head Office (Corporate Administrative Departments)

Having no coke plant, Kobe Works of Kobe Steel aimed at low coke-ratio operation of its blast furnace process. Furthermore, its sintering plant was closed in 1999, and the process was converted to all-pellet operation in 2001. Afterward, the plant was using self-fluxed dolomite pellets produced at and shipped from Kakogawa Works. Kobe Works was the only site in Japan that adopted and continued all-pellet operation and optimized the complex control of burden distribution in accordance with the high pellet ratio and pulverized coal combustion in accordance with the multi-brand coal types, which it did in the 4th blast furnace (inaugurated in 2007). Furthermore, replacing lump ore with self-fluxed dolomite pellets has improved the meltdown property of iron ore at high temperature. As a result, operation at a low coke rate of 283 kg/tonne was achieved under the severe conditions of a high pellet ratio (80%) and raw materials that were all stored in the yard.

Introduction

Kobe Steel started operation as an integrated iron and steel works in 1959 with the firing of the No.1 blast furnace at Kobe Works. After that, Kobe Works began operating a three-blast furnace system, but in 1983, it shifted to a single blast furnace system consisting of the No. 3 blast furnace only. After experiencing the Great Hanshin-Awaji Earthquake in 1995, Kobe Works carried out blast furnace renovation work in 2007, and the No. 3 blast furnace (hereinafter referred to as the "Kobe No. 3 blast furnace") was put into operation. However, the Kobe No. 3 blast furnace was shut down on October 31, 2017 to consolidate the upstream processes at Kakogawa Works in order to strengthen the profitability of the Iron and Steel Business division. This closed the 59-year history of blast furnace operation at Kobe Works.

In October 2016, one year before the Kobe No. 3 blast furnace was shut down, the technologies cultivated till then were applied together to achieve low coke rate operation at 283 kg/tonne under the harsh conditions of 80% pellet composition and raw materials that had all been stored in the yard. This paper reports on the concept and history of the operation.

Table 1 Comparison of properties between sintered ores and pellets for blast furnace burden

	Advantages	Disadvantages
Sintered ores (Crushed sizing)	High inclination angle High reducibility	Wide size range High reduction degradation
Pellets (Pelletizing)	Low slag rate Low reduction degradation	Low inclination angle Retardation of reduction

1. Features of raw materials used in Kobe No. 3 blast furnace

Kobe Works had no coke oven and purchased coke from outside. It was forced to use coke that was more expensive than that used by other ironworks. For this reason, the blast furnace operation of Kobe Works aimed at low coke-ratio operation. Also, in response to the construction of a power generation plant in the Kobe Works, its sintering plant was closed in 1999, and the process was converted to all-pellet operation (pellet ratio 73%, lump ore 27%) in 2001.¹⁾ **Table 1** compares the properties of sintered ores and pellets. Pellets generally have drawbacks in high-temperature properties compared with sintered ore. Kobe Steel has been producing self-fluxed dolomite pellets with improved quality by adding dolomite at the pellet plant of Kakogawa Works. The Kobe No. 3 blast furnace used these pellets to realize low coke rate operation.

Then, at the Kobe No. 3 blast furnace, Kobe Works optimized the complex control of burden distribution in accordance with the high pellet rate, and pulverized coal combustion in accordance with the multi-brand coal types.²⁾ Furthermore, replacing some parts of lump ore with self-fluxed dolomite pellets³⁾ improved the meltdown property of burden materials at high temperature. These and other efforts enabled all-pellet operation, the only example in Japan, to continue in a stable manner.

2. Concept of decreasing coke rate under all-pellet operation

Fig. 1 shows the concept of reducing the coke rate under all-pellet operation. There are two possible measures to use against the changes in the in-furnace

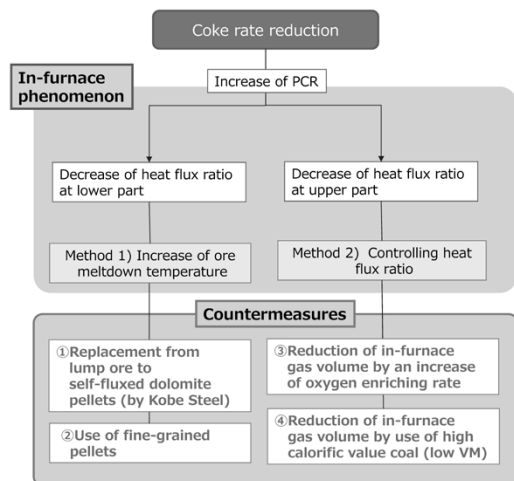


Fig. 1 Concept of coke rate reduction in all-pellet operation

phenomena when the coke rate is decreased: raising the ore melt down temperature and adjusting the heat flow ratio (the heat capacity of falling burden material/the heat capacity of furnace top gas).

Both of the measures were implemented in the low coke rate operation this time, and this section mainly focuses on the measures for raising the ore melt down temperature.

2.1 Effect of internal volume of blast furnace on ore melt down control

In general, the furnace height decreases as the internal volume of the blast furnace decreases. For this reason, the height from tuyeres to the bottom of the furnace bosh also tends to decrease. As a result, when the unreduced ore in the periphery collapses, the possibility of unreduced FeO reaching a tuyere increases, raising the risk of breaking down the tuyere. In particular, the body of a small blast furnace with an internal volume of 3,000 m³ or less has a heat capacity smaller than a large blast furnace body has, and it is more important to control the melt down properties of the peripheral ore at high temperatures. Since the Kobe No. 3 blast furnace was a small blast furnace (inner volume of furnace: 2,112 m³), efforts were made to improve the high temperature melt down properties of the peripheral ore.

2.2 Melt down properties of ore required for an increased amount of injected pulverized coal

To reduce the coke rate, it is necessary to increase the amount of pulverized coal, a substitute reductant, injected from tuyeres. Fig. 2 shows the results of calculating the temperature changes of solid and gas, assuming that the lower part of the

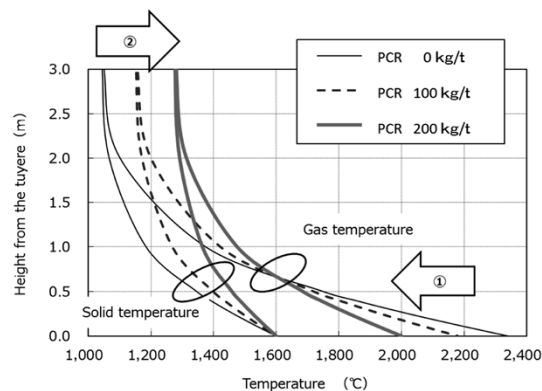


Fig. 2 Changes of solid and gas temperature in lower part of furnace with pulverized coal injection

blast furnace is the field for the heat exchange of the solid and gas that have completed chemical reactions. Even when the gas temperature before a tuyere decreases with the increase of the pulverized coal ratio (① in Fig. 2), and if the molten iron temperature is kept constant, the temperature rises in the lower furnace part (② in Fig. 2). In order to maintain the ventilation of the lower furnace part while raising its temperature, it is considered to be necessary for the pellets to melt down at a higher temperature. Hence, to reduce the coke rate under this all-pellet operation, the lump ore was replaced with self-fluxed dolomite pellets with excellent high-temperature melt down properties to improve the high-temperature melt down characteristics in the periphery.

3. Concept of burden distribution control to decrease coke rate

3.1 Four-batch charging of ore to improve accuracy of burden distribution control and peripheral charging of fine pellets

Fig. 3 shows the configuration of the furnace-top charging device of the Kobe No. 3 blast furnace.⁴⁾ The charging is performed by a bell-less system of two-parallel top hopper type. Fig. 3 (a) shows the movement when the coke is charged in the center, and Fig. 3 (b) shows the movement of the distributing chute when the ore is charged.

Fig. 4 shows the method of controlling burden distribution for low coke rate operation. In 2-batch charging of coke and ore using the bell-less charging device, center coke charging was implemented (Fig. 4 (a)). The following three points are particularly important in all-pellet operation:

- (1) Forming a flat part of coke layer and ore layer in the periphery.
- (2) Smoothing the ratio, $L_o/(L_o + L_c)$ (hereinafter

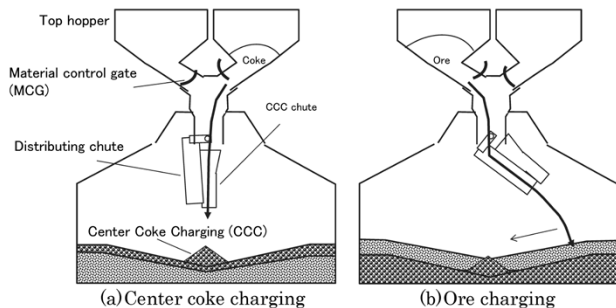


Fig. 3 Furnace-top charging device for Kobe No. 3 blast furnace

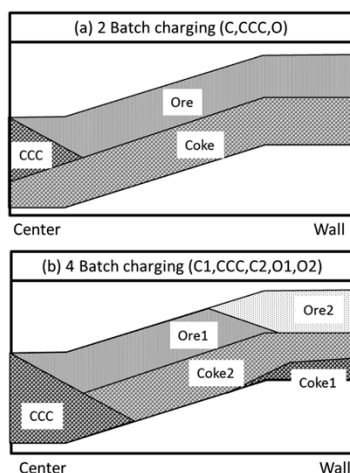


Fig. 4 Scheme of burden distribution control for low coke rate operation

referred to as "layer thickness ratio") of ore layer thickness L_O and ore and coke layer thicknesses $L_O + L_C$ in the radial direction of the furnace throat in the periphery to prevent pellets from flowing in.

- (3) In the parallel two-stage hopper, the circumferential balance must be controlled precisely.

Fig. 5 is a conceptual diagram of burden distribution control in all-pellet operation. This burden distribution control enabled the optimization of the surrounding gas flow while maintaining a strong central gas flow. Furthermore, the gas utilization rate ($\text{CO}_2\% / (\text{CO}\% + \text{CO}_2\%)$, hereinafter referred to as ηCO) of the furnace-top gas was increased, allowing the reductant rate to be decreased.

Fig. 6 shows the change over time in the diameter of coke grains discharged from the furnace top hopper. The coke diameter was determined by image analysis of coke being discharged from an actual machine. Particularly for the center charged coke that forms the deadman coke, the coke grains with large diameters at the end of the discharge were used.

For this all-pellet operation, it was necessary to improve the control accuracy of the burden

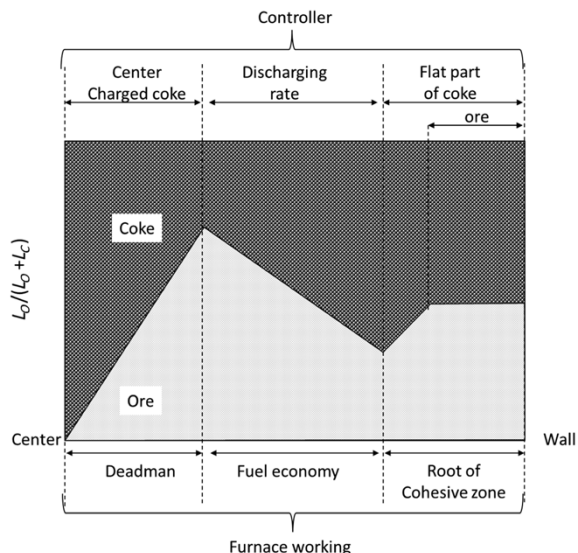


Fig. 5 Concept of burden distribution control for Kobe No. 3 Blast Furnace

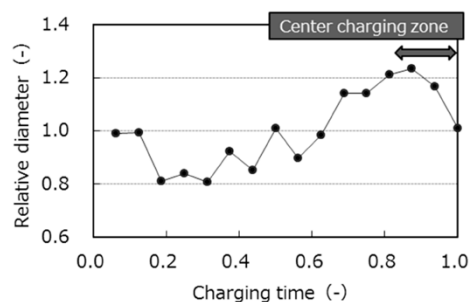


Fig. 6 Change with time of diameter of coke charged from furnacetop hopper

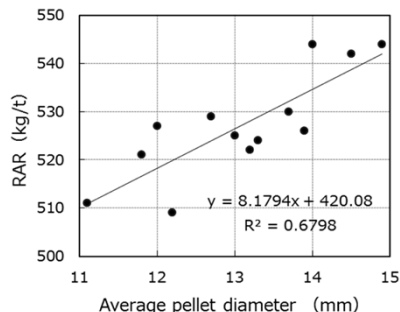


Fig. 7 Influence of average diameter of pellet on reducing agent rate (RAR)

distribution on the side of the ore in order to replace lump ore with self-fluxed dolomite pellets. Hence, the conventional 2-batch charging (pellet 65%) was converted to 4-batch charging⁵⁾ (pellet 80%) (Fig. 4 (b)).

Fig. 7 shows the effect of the average diameter of the pellets on the reducing agent ratio.⁶⁾ It can be seen that the smaller the average diameter of the pellets, the better the reducibility and the lower the reductant rate. In this all-pellet operation, fine pellets with small diameters (3 to 6 mm) and excellent reducibility were mixed (1.8%) at the time of the second batch charging and were selectively charged

into the periphery in order to improve the ore melt down properties in the periphery.

3.2 Relationship between burden distribution in furnace throat and gas flow in lower furnace part

Controlling the shape of the cohesive zone through the airflow resistance distribution in the shaft is of significant importance in the burden distribution in the furnace throat. Meanwhile, from the viewpoint of the function of the lower furnace part, the importance of the burden distribution is that it regulates the amount of inflow in the radial direction of the lower furnace part of coke, which is the only filling structure.

Fig. 8 shows the change in the layer thickness ratio between the conventional 2-batch charging and 4-batch charging. Despite the increased amount of pellet, the distribution of the layer-thickness ratio from the middle to the periphery is smoothed, with almost no change in the layer thickness ratio in the center, which successfully avoided the destabilization of burden distribution due to the increased amount of pellets.

Fig. 9 shows the rate of coke supplied to the lower furnace part, which corresponds to the layer thickness ratio distribution in the furnace throat.⁷⁾ The rate of coke supplied at the lower part of the furnace was the value obtained by subtracting the carbon consumption (solution loss, carburization and metalloid reaction) from the coke rate in the

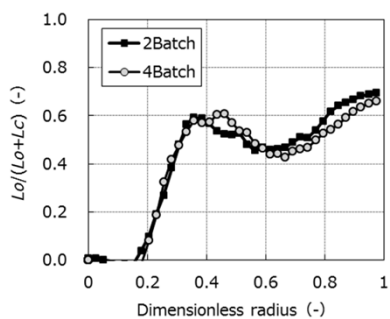


Fig. 8 Distribution of layer thickness ratio in radius at furnace throat

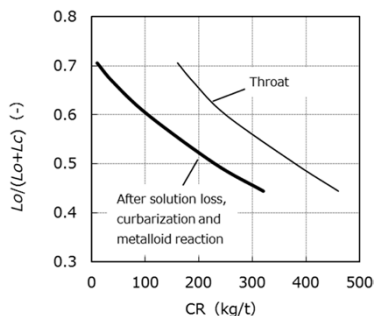


Fig. 9 Coke rate (CR) supplied to the raceway corresponding to layer thickness ratio in radius of furnace throat

diameter direction, which corresponds to the layer thickness ratio distribution in the furnace throat. When the layer thickness ratio exceeds 0.7, the rate of the coke supplied to the lower furnace part becomes almost zero, the coke slit disappears locally, and the gas distribution function decreases. When the layer thickness ratio of the periphery exceeds 0.7 in order to strongly suppress the peripheral gas flow, the heat dissipated from the furnace body increases, and the gas flow tends to become unstable due to the formation of an S-shaped cohesive zone.⁸⁾ Therefore, the burden distribution was adjusted to make the layer thickness ratio 0.7 or less.

In this all-pellet operation, upon replacing lump ore with self-fluxed dolomite pellets, the accuracy of burden distribution control on the side of the ore was improved by the 4-batch charging to prevent the pellets from flowing in. Furthermore, from the change in the η CO distribution in the furnace throat during the low coke rate operation (Fig.10), it can be said that the peripheral η CO was improved by the peripheral charging of fine pellets.

3.3 Effects on raceway of blast condition and rate of coke supplied to lower furnace part

The ratio between the total cross-sectional area of the blast furnace tuyere raceways and the cross-sectional area of the furnace floor at the same height level (hereinafter referred to as "raceway area ratio"⁹⁾) affects the reductant rate of the blast furnace as follows: In short, the increase in the raceway area ratio is due to the increase in blast energy and increases the inflow of gas to the center. This suppresses the peripheral gas flow, decreases the heat dissipated from the furnace body, and decreases the reductant rate. On the other hand, an excessive increase in the raceway area ratio accompanied a decrease in the deadman coke volume, which decreases the heat capacity of the furnace and conversely increases the reductant rate. The Kobe No. 3 blast furnace is a small blast furnace with a relatively large raceway area ratio. It therefore

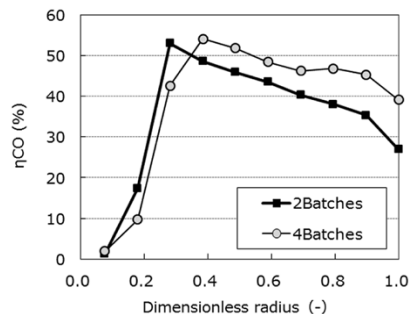


Fig.10 Radial distribution changes of gas utilization ratio at furnace throat in low coke rate operation

Table 2 Changes of raceway area ratio and reducing agent rate

	Before (2016/4)	After (2016/10)	dif.
Productivity (t/d/m ³)	1.92	1.99	+0.07
Blast volume (Nm ³ /min)	2854	2601	-253
Oxygen (Nm ³ /min)	105	160	+55
CR (kg/ t)	315	283	-32
PCR (kg/ t)	198	220	+22
Raceway area ratio	0.514	0.498	-0.016
RAR (kg/ t)	513	503	-10

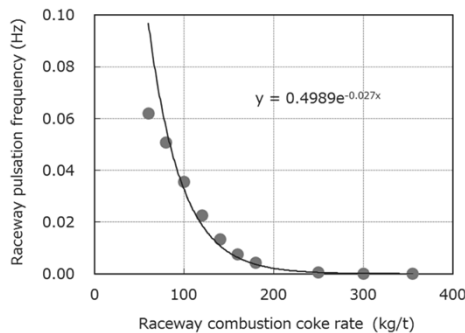


Fig.11 Relationship between combustion coke rate at tuyere and pulsation frequency of raceway

has a margin to decrease the raceway area by high oxygen enrichment, and the pressure loss in the furnace can be decreased as the amount of gas in the furnace decreases. In this low coke rate operation, the raceway area ratio of the Kobe No. 3 blast furnace was decreased from 0.514 (average value in April 2016) to 0.498 (average value in October 2016), resulting in a decrease in the reductant rate from 513 kg/tonne to 503 kg/tonne (Table 2).

Fig.11 shows the relationship between the combustion coke rate at a tuyere and the pulsation frequency¹⁰⁾ of its raceway. An increase in the pulsation frequency of a raceway means that bridging is likely to occur immediately above the tuyere, and the occurrence of bridging increases the risk of tuyere breakage due to the fall of unreduced FeO. In Fig.11, the pulsation frequency of the raceway increases as the combustion coke rate at the tuyere decreases. This is because the amount of coke supplied to the lower furnace part decreases due to the decrease in the combustion coke rate at a tuyere, turning smoothly moving layers into almost stationary layers. In particular, when the combustion coke rate at a tuyere falls below 100 kg/tonne, the pulsation frequency of the raceway increases rapidly. Assuming that the amount of carbon consumed due to solution loss is 90 kg/tonne, the amount due to metalloid reaction is 5 kg/tonne, and the amount due to carburization is 50 kg/tonne, the lower limit of the coke rate charged from the furnace top is calculated to be approximately 245 kg/tonne. This value was used as the guideline for the lower limit in low coke rate operation.

4. Results of low coke rate operation of Kobe No. 3 blast furnace

Fig.12 shows the change in operational data associated with the low coke rate operation. High oxygen enrichment operation (from 2.8% to 4.6%) began in April 2016, and the amount of high calorie coal was increased (from 60% to 100%) along with the increase of pellets (from 65% to 80%) on August 5. On this occasion, a complex control of burden distribution and pulverized coal injection began, decreasing the coke rate from 315 kg/tonne to 283 kg/tonne. It should be noted that the low coke rate operation was not performed from September 19th to October 17th.

In addition, η CO increased with an increasing addition of pellets, and the effect of self-fluxed dolomite pellets with excellent high temperature melt down properties was fully exploited. At the same time, Si in the molten iron was also decreased (from 0.71% to 0.48%).

Fig.13 shows the change in the temperature distribution inside the furnace measured by a descending probe¹¹⁾ during low coke rate operation. Focusing on the 1,200°C line, which corresponds to the upper surface of the softened cohesive zone, the 1,200°C line was kept under control almost at the upper end of the furnace bosh despite a decrease in coke rate (from 315 kg/tonne to 283 kg/tonne). This verifies that the heat flow rate at the lower furnace part is controlled properly by the complex control of the burden distribution and pulverized coal injection. Incidentally, on the basis of the fact that a decrease in hot metal Si (from 0.71% to 0.48%) was observed with the decrease in molten-iron temperature (from 1,507°C to 1,498°C), the decrease in hot metal Si after correcting the molten iron temperature is estimated to be 0.71% to 0.54%.¹²⁾ From this result, it is considered that the increase in self-fluxed dolomite pellets lowered the lower surface level of the cohesive zone (1,450°C) while maintaining the 1,200°C line at the upper end of the furnace bosh.

Table 3 shows the results of low coke rate operation for the Kobe No. 3 blast furnace. In this trial, the coke rate reduction effect (from 315 kg/tonnes to 283 kg/tonnes) brought about by increasing the self-fluxed dolomite pellets was 19 kg/tonnes, and the effects of complex controlling of the oxygen enrichment rate and increasing the amount of high calorie (low VM) coal were 8 kg/tonne and 4 kg/tonne, respectively. Including other considerations, the coke rate was successfully decreased to 32 kg/tonne in total.

Table 4 compares the specifications of blast

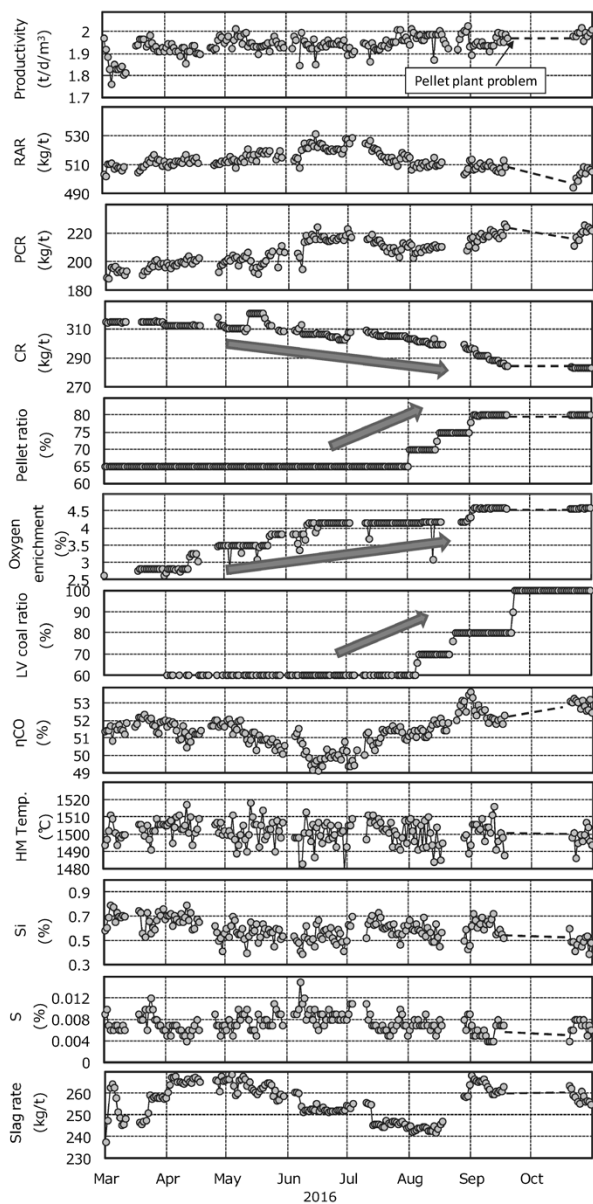


Fig.12 Changes of operation data with low coke rate operation

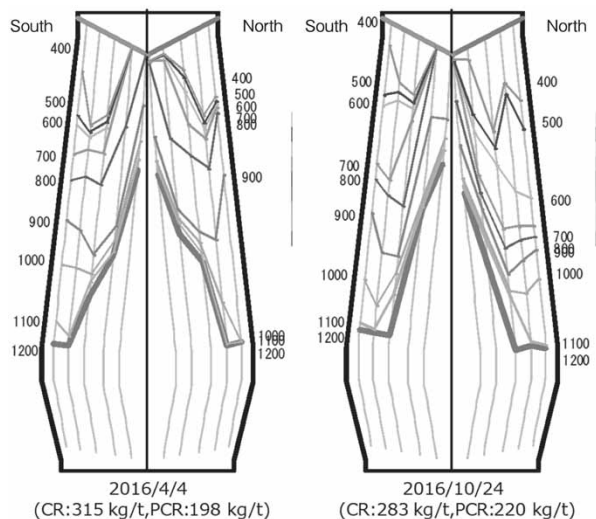


Fig.13 Changes of temperature distribution of blast furnace with low coke rate operation

Table 3 Results of low coke rate operation

	Before (2016/4)	After (2016/10)	dif.	
Productivity (t/d/m ³)	1.92	1.99	+0.07	
RAR (kg/t)	513	503	-10	
CR (kg/t)	315	283	-32	
PCR (kg/t)	198	220	+22	
	Before (2016/4)	After (2016/10)	dif.	ΔCR (kg/t)
Pellet rate (%)	65	80	+15	-19
Oxygen enrichment (%)	2.8	4.6	+1.8	-8
LV coal rate (%)	60	100	+40	-4
Converter slag rate (kg/t)	5	10	+5	-3
Other (-)	-	-	-	2
SUM. (-)	-	-	-	-32

Table 4 Comparison of blast furnaces in low coke rate operation

		2016/4	2016/10	2009/9-10
		Kobe 3BF		IJmuiden 7BF
Inner volume	m ³	2112		-
Working volume	m ³	1863		3775
Productivity	t/d/m ³	1.92	1.99	2.22
Pellet ratio	%	65	80	60
Sinter ratio	%	0	0	40
Lump ore ratio	%	35	20	0
RAR	kg/t	513	503	495
CR	kg/t	315	283	261
PCR	kg/t	198	220	234
Heat flux ratio	-	0.81	0.83	-
O ₂ enrichment	%	2.8	4.6	-
ηCO	%	51.5	52.9	49.4
Slag rate	kg/t	258	257	195

furnaces. Outside Japan, Tata Steel Limited achieved a low coke rate operation of 261 kg/tonne at its IJmuiden 7BF.¹³⁾ It is noteworthy that IJmuiden7BF has realized low slag rate operation despite the operating conditions of the mixed charging of pellet and sintered ore.

On the other hand, the Kobe No. 3 blast furnace has the slag rate almost leveling out (258 kg/tonne to 257 kg/tonne) despite the increase in pellets (from 65% to 80%). This is due to the increase and fluctuation of the gangue (SiO₂, Al₂O₃) rate in the raw material ore of pellets, that is, the deterioration of the iron ore raw material that is occurring in Japan's ironmaking industry.¹⁴⁾ This is also attributable to the low and stable S in molten iron required from the steelmaking process, that is, to achieve high quality steel.

5. Summary of low coke rate operation

In the Kobe No. 3 blast furnace, Japan's only all-pellet operation was continued, lump ore was replaced with self-fluxed dolomite pellets, and the complex control of burden distribution and pulverized coal combustion was optimized. As a result, low coke rate operation at 283 kg/tonnes was achieved under the harsh conditions of 80% pellet composition and all raw materials being stored in a yard. The results are summarized below:

(1) In small blast furnaces, the control of the melt

down properties at high temperatures of the periphery ore is of particular importance. In this all-pellet, low coke rate operation (283 kg/tonne), lump ore was replaced with self-fluxed dolomite pellets, and the upper surface of the softening cohesive zone (1,200 °C line) was successfully controlled almost at the upper end of the furnace bosh. This result is presumably because the heat flow rate at the lower furnace part was properly controlled by the complex control.

- (2) A decrease in hot metal Si (from 0.71% to 0.48%) was observed, indicating that the lower level of the cohesive zone was successfully lowered by increasing the self-fluxed dolomite pellets.
- (3) The increased addition of pellets increased η CO, indicating that the effect of self-fluxed dolomite pellets was fully exploited.

Conclusions

The blast furnace operation at Kobe Works of Kobe Steel closed its long history on October 31, 2017. Meanwhile, after the consolidation of the upstream process equipment into Kakogawa Works of Kobe Steel, stable operation of the two large blast furnaces and low coke rate operation have become even more important.

In the future, the ironmaking industry in Japan

will be required to produce higher quality steel using iron ore with deteriorating quality. Kobe Steel strives to improve the operation of the large blast furnace at Kakogawa Works by effectively utilizing the technologies of burden distribution control in accordance with high pellet composition, and high temperature melt down control of self-fluxed dolomite pellets, as described in this paper.

References

- 1) Y. Matsui et al. ISIJ Int. 2003, Vol.43, No.2, pp.166-174.
- 2) M. Tate. Tetsu-to-Hagane. 1972, Vol.58, No.5, pp.567-577.
- 3) K. Narita et al. Tetsu-to-Hagane. 1976, Vol.62, No.7, pp.885-894.
- 4) T. Matsuo et al. Ironmaking Conf. Proc. Vol.56, Chicago, USA, 1997-4-13/16, ISS, Warrendale, PA, pp.203-204.
- 5) K. Tanaka et al. CAMP-ISIJ. 2017, Vol.30, p.659.
- 6) M. Taguchi et al. Tetsu-to-Hagane. 1973, Vol.59, No.2, pp.A5-A8.
- 7) Y. Matsui et al. CAMP-ISIJ. 2003, Vol.16, pp.764-767.
- 8) K. Shibata et al. 1st ICSTI. 1994 Sendai, 1994-6-14/17, ISIJ, p.553.
- 9) T. Sugisaki et al. Tetsu-to-Hagane. 1979, Vol.65, No.14, pp.2005-2011.
- 10) Y. Matsui et al. ISIJ Int. 2005, Vol.45, No.45, pp.1445-1451.
- 11) I. Kobayashi et al. Tetsu-to-Hagane. 1987, Vol.73, No.15, pp.2092-2099.
- 12) K. Tanaka et al. CAMP-ISIJ. 2016, Vol.29, p.640.
- 13) J. R. H. Stuurwold et al. METEC InSteel Con. Dusseldorf, Germany, 2011-6-28/7-1, pp.1-6.
- 14) M. Naito et al. ISIJ Int. 2015, Vol.55, pp.7-35.

Establishment of Special Steel Production System at Kakogawa Works

-Construction of No.3 Secondary Refining Equipment and No.6 Continuous Caster-

Yasumasa YOSHIDA*1, Hideya OKADA*1, Hiroaki SAKAI*1, Hiroyuki ONODA*2, Dr. Takehiro NAKAOKA*3

*1 Steelmaking Department, Kakogawa Works, Iron & Steel Business

*2 Steelmaking Development Department, Research & Development Laboratory, Iron & Steel Business

*3 Mechanical Engineering Research Laboratory, Technical Development Group

Kobe Steel shut down the operation of the ironmaking and steelmaking process at Kobe Works in October 2017, and in November 2017, this upstream process was consolidated at Kakogawa Works. Prior to this, by January 2017, the Steelmaking Department of Kakogawa Works had established a special-steel production system for wire rods by installing No.3 secondary refining equipment (2LF, 4RH) and a No.6 continuous caster. A challenge in designing the new process was to produce small lots of special steel with high productivity, high yield and high quality at Kakogawa Works, which has a large heat size. In order to solve this problem, cutting edge technologies were introduced in the upstream equipment. This has enabled small-lot production and quality improvement while continuing stable production under the full production system after the consolidation of the upstream process. This paper reports the features of newly installed equipment, the concept of quality design, and the operational status.

Introduction

The Steelmaking Department of Kobe Steel's Kakogawa Works launched a new plant to consolidate the upstream process and worked to establish the manufacturing technology of special steel for wire rods and steel bars that had

been produced at Kobe Works. The department established a technology for adjusting nitrogen during molten steel processing, along with a technology for operating a 5-strand continuous bloom caster, and inaugurated a one-base system for producing crude steel at Kakogawa Works in November 2017, as planned.

This paper describes the features and quality design concepts of No.3 molten steel treating equipment, including a No.4 Ruhrstahl-Heraeus degassing apparatus (4RH) and No.2 vessel furnace (2LF), as well as those of the No.6 continuous caster (6CC), and reports on their operational status after the consolidation of the upstream process.

1. Changes in steel production system

The upstream process consolidation was a structural reform of the steel production system to build a stable revenue base through steps such as reducing the costs of molten iron and steelmaking, as well as expanding the sales of the company's main products. **Fig. 1** shows the changes in the steel production system associated with the consolidation of the upstream process. Kobe Steel shut down the upstream process at Kobe Works, from the blast furnace to the No.3 blooming mill plant, in

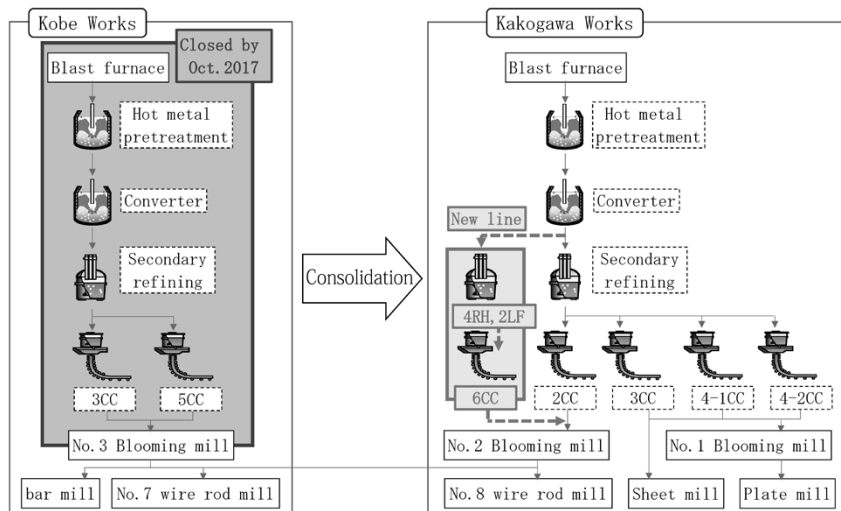


Fig. 1 Changes of steel making production system by upstream process consolidation

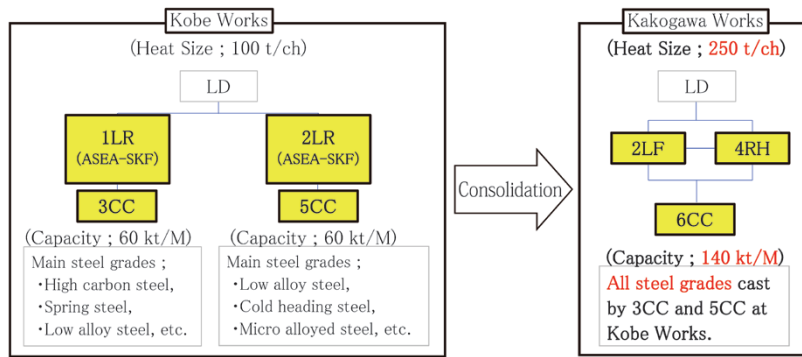


Fig. 2 Change in steelmaking process by upstream process consolidation

Table 1 Challenges in producing special steel

change	Process	Equipment design		Problems	Technology development
		Kobe	Kakogawa		
Raise of heat size Kobe; 100 t/ch ↓ Kakogawa; 250 t/ch	Molten steel refining	ASEA-SKF (ARC, VD)	RH	De-N ₂ during vacuum processing	<ul style="list-style-type: none"> • Circulating by nitrogen gas • Pressure control in vessel
			LF	Quick control of chemical composition of steel	<ul style="list-style-type: none"> • Guidance • Improvement of every equipment
	Continuous casting	2-strand bloom CC × 2 unit	5-strand bloom CC × 1 unit	Composition change of inclusion by strong stirring	<ul style="list-style-type: none"> • Stirring intensity control
				Molten steel cleaning Temperature difference among every strands in tundish Increase work load for maintenance of cooling facility	<ul style="list-style-type: none"> • Slag control • Tundish flow control • Mist nozzle with super wide spreading angle

October 2017, and newly established a special steel production process for wire rods and steel bars at Kakogawa Works. The Steelmaking Department operates 4RH/2LF for secondary refining and 6CC for continuous casting to establish a production system for the steel types of wire rods and steel bars that had been manufactured at Kobe Works.

Fig. 2 shows the process flow from the secondary refining to continuous casting at each ironworks. Kobe Works adopted an ASEA-SKF for the secondary refining process and had two continuous casters (3CC and 5CC) for its continuous casting process with a production capacity of 60 kilo-tonnes/month, in which the apparatuses are selectively used in accordance with their characteristics. With a heat size of 100 tonnes, Kobe Works specialized in small lot production. In the new process, Kakogawa Works, having a heat size of 250 tonnes, was required to have a process from continuous casting to secondary refining with a production capacity of 140 kilo-tonnes/month, while satisfying the quality and productivity of small lots of many steel types for wire rods and steel bars. Hence, the secondary refining process was designed to choose the RH/LF method, which has a high molten steel processing capacity, and the continuous casting process was designed to use a 5-strand continuous bloom caster (6CC) that can cast, with high productivity, high yield, and high quality, all the types of steel that had been cast by Kobe Works

Table 1 shows the challenges in the new process design associated with the upstream consolidation. The challenges were as follows: in the secondary refining, the processing of difficult-to-melt materials and ultra-clean steel that had been processed by the ASEA-SKF at Kobe Works; in the RH, suppressing the denitrification during vacuum processing, and shortening the processing time of steel with narrow composition ranges; and, in the LF, responding to inclusion changes during strong stirring, and the cleaning of molten steel. In addition, the 6CC, which was designed to have 5 strands, had the issues of a temperature difference among the strands, due to the increase in tundish (TD) size, and an increase in the maintenance load of the tertiary cooling equipment (multiple cooling nozzles). These issues were solved by introducing new technologies.

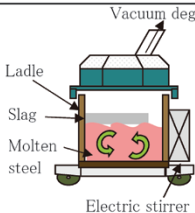
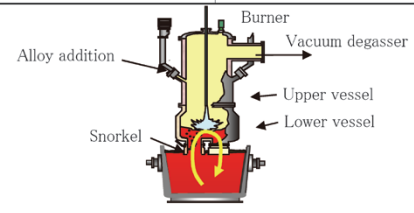
2. Features of each apparatus and concept of quality design

2.1 No.3 molten steel treating equipment (4RH, 2LF)

2.1.1 Outline of 4RH apparatuses

Table 2 compares the vacuum degassing apparatuses of Kobe Works and Kakogawa Works. In the RH method, vigorous stirring and degassing can be performed simultaneously. Therefore, the processing time can be shortened by 45 minutes

Table 2 Comparison of vacuum degassing apparatuses, ASEA-SKF and RH

Apparatus	ASEA(VD)	RH	
		1RH	4RH
			
Degree of vacuum	0.5 torr	0.5 torr	0.5~80 torr
Maintenance device	-	Push car	Turning table
Circulating gas flow rate	(stirrer)	Ar/N ₂ 3,000 NI/min	Ar/N ₂ 5,000 NI/min
Number of alloy hopper	24	17	21
Calculation of amount of alloy	Automatic	Semi-automatic	Automatic
Treatment time	75 min	30 min	30 min
Nitrogen desorption	-	≤ 50 ppm	≤ 50 ppm
Nitrogen adsorption	~160 ppm	~100 ppm	~160 ppm

compared with the ASEA-SKF, in which a separate degassing process is required. In order to shorten the basic processing time further, an automatic alloy adjustment system and a micro-alloying calculator were introduced to enable the equipment to handle steel types specifying narrow composition ranges. The idling time was shortened by newly adopting a slewing-type maintenance cart that can repair refractory online.

In the ASEA-SKF, nitrogen concentration was easily controlled by adding nitrogenized iron alloy under atmospheric pressure. In the RH system, however, the stirring under vacuum promotes denitrification to equilibrium nitrogen concentration, causing a significant challenge in adding nitrogen in the high concentration region. Therefore, in addition to the introduction of high-flow nitrogen gas stirring, a pressure adjustment function was newly provided in the vacuum chamber to accommodate various nitrogen specifications.

2.1.2 Technology for controlling nitrogen concentration

In order to control the nitrogen concentration within the specified range in the RH, a system for calculating and predicting nitrogen concentration was developed taking into account various factors, including reflux gas types, reflux gas flow rate, the degree of vacuum in the vessel, and molten steel composition. The outline of the calculation model that forms the basis of this system is shown by Equation (1)¹⁾. The control accuracy was improved by applying unique measures such as setting various parameters in accordance with the degree of vacuum in the vessel.²⁾

$$\frac{d[N]_V}{dt} = -\frac{Q}{V_V}([N]_V - [N]_L) + R_S + R_{Ar} + R_{N_2} \dots \dots \dots (1)$$

$$\frac{d[N]_L}{dt} = -\frac{Q}{V_L}([N]_V - [N]_L) + R_{leak} \dots \dots \dots (2)$$

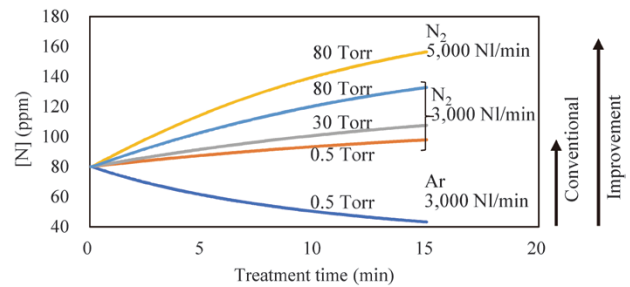


Fig. 3 Influence of RH treatment conditions on [N] content (calculation results)

wherein, $[N]_V$, nitrogen concentration (%) in the vacuum chamber; $[N]_L$, nitrogen concentration (%) in the vessel; V_L , the amount of molten steel in the vessel (m^3); V_V , the amount of molten steel in the vacuum chamber (m^3); t , time (min); Q , the reflux amount of molten steel (m^3/min); R_S , denitrification rate (%/min) at the steel bath surface; R_{Ar} , denitrification rate (%/min) at the interface of Ar bubble for molten steel reflux; R_{N_2} , denitrification rate (%/min) at the interface of nitrogen gas bubble for molten steel reflux; and R_{leak} , nitrogen absorption rate (%/min) due to air intrusion from immersion pipe.

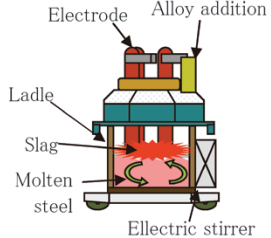
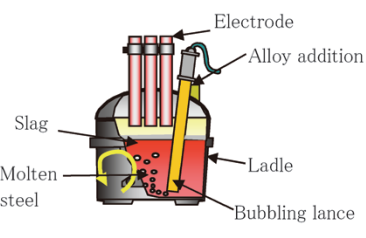
As a method of controlling nitrogen concentration, a dynamic control was introduced in addition to a static control to improve the accuracy. The static control is a method in which the RH treatment conditions (reflux gas types, reflux gas amount, the degree of vacuum) are determined in advance in accordance with the molten steel composition, initial nitrogen concentration, target nitrogen concentration, and treatment time. **Fig. 3** shows the calculation results for each RH treatment condition when the initial nitrogen concentration is 80 ppm.

The dynamic control is a method in which the RH treatment conditions are changed in accordance with the value of nitrogen concentration, analyzed during processing, and the remaining processing time. **Fig. 4**

Table 3 RH treatment conditions with changes of required [N] level in steel, and [N] value obtained after suitable treatment

Steel grade	[N] specification (ppm)	Circulating gas	Gas flow rate (Nl/min)	Degree of vacuum in RH vessel (Torr)	Target [N] value	[N] (measured)	
						Average (ppm)	Standard deviation (ppm)
Case hardening steel, Free-cutting steel	≤80	Ar	3,000	0.5	-	-	-
	80~110	N ₂	3,000	0.5	95	91.4	6.1
	100~120	N ₂	3,000	30	110	108.4	6.6
	120~140	N ₂	3,000	80	130	123.7	7.0

Table 4 Comparison of apparatuses for heating molten steel

Apparatus	ASEA(ARC)	LF	
		1LF	2LF
			
Slag removal	non	Slag dragger	Slag dragger
Circulating gas	(stirrer)	Ar	Ar
Circulating gas flow rate (Nm ³ /h)	—	Soft; 30~60 Hard; ~100	Soft; 15~60 Hard; ~100
Number of alloy hopper	24	21	25
Calculation of amount of alloy	Automatic	Semi-automatic	Automatic
Desulfurization (ppm)	≤50	≤10	≤10

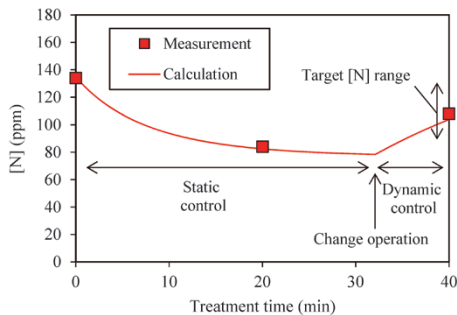


Fig. 4 Behavior of [N] during dynamic control

shows an example of how the deviation from the nitrogen standard, caused by the static control alone, is converged by the dynamic control.

This combined control has enabled the narrow control of nitrogen concentration by gas stirring, allowing the transfer of all the nitrogen-added steel, which had been ASEA-treated at Kobe Works, to the one RH treated at Kakogawa Works. (Table 3).

2.1.3 Outline of 2LF apparatus

Table 4 compares molten-steel heating apparatuses, an ASEA-SKF and two LFs. With the increased heat size, the ASEA-SKF stirrer system lacked the capability of stirring molten steel, and an LF of Ar bubbling type with high stirring power was adopted. In addition, there was a concern that the change in the stirring method might deteriorate

Table 5 Conditions of stirring intensity and slag treatment with changes of steel grades

Steel grade	Stirring intensity	Slag C/S	Slag removal
Clean steel	Soft	High	○
Inclusion control	Soft	Low	○
Sulfur control	Desulfurization	Hard	○
	addition	Soft	Low

cleanliness due to the inclusion of slag, so the design was revised for the method of controlling the slag-metal reaction.

The coarse inclusions containing CaO, which are harmful, mainly originate from the top slag during LF refining, and such inclusions have a strong correlation with the stirring conditions. Equation (3) gives the average flow velocity, U_1 ³⁾ at the molten steel surface approximated from the values of a water model experiment, and no slag entrainment occurs under conditions below the slag entrainment critical flow velocity, $V_{min} = 0.69$ m/s,⁴⁾ determined by Equation (4). A water model and flow analysis were used to verify the lance placement and flow rate, which resulted in an equipment configuration including a regular lance, which performs laminar flow stirring at a low flow rate, and a strong stirring lance, which performs turbulent stirring at a large flow rate. As shown in Table 5, cleaning treatment, inclusion control, and S concentration control were realized by combining slag design and stirring

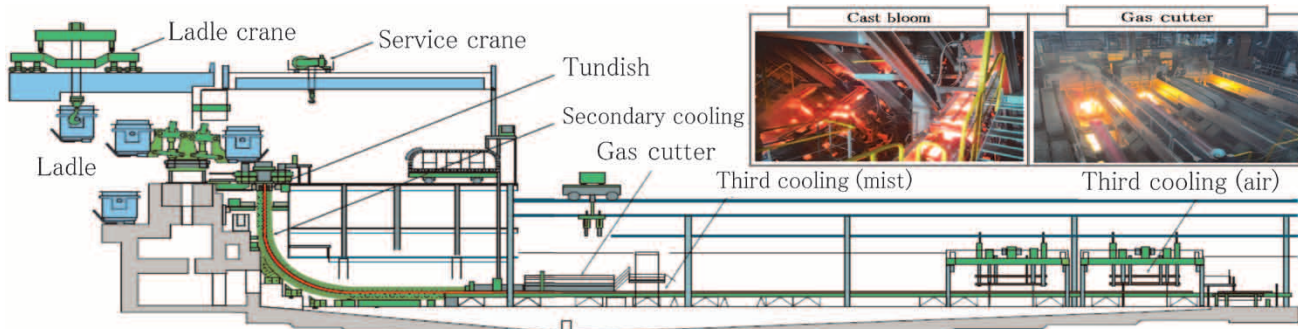


Fig. 5 Schematic diagram of 6CC

Table 6 Design concept and specifications for 6CC

Plant	Kobe Works			Kakogawa Works	
	3CC	5CC	2CC	6CC	Concept
Start	1981.01~ 2017.10	2006.09~ 2017.10	1980.12~	2017.01~	-
Machine type	Verticalbending	Verticalbending	Bending	Verticalbending	Same machine type as Kobe 3CC / 5CC
Number of strands	2	2	4	5	Compatible with Kakogawa heat size
Bloom size	300×430 mm	300×430 mm	380×630 mm	300×430 mm	Same mold size as Kobe 3CC / 5CC
Bending radius	10 m	10 m	15 m	10 m	Same bending radius as Kobe 3CC / 5CC
Machine length	32.3 m	32.4 m	34.4 m	33.4 m	-
Casting speed(max)	1.05 m/min	1.05 m/min	0.90 m/min	1.05 m/min	Same casting speed as Kobe 3CC / 5CC
Vertical length	4.7 m	3.0 m	-	4.0 m	Optimal length to balance surface quality and internal quality
Tundish capacity	20 t	24 t	48 t	63 t	Large tundish enables stable flow control, inclusion removal and easy method to deal with small lot
Third cooling	Mist (on line)	Air (on line)	Water bath (off line)	Mist or Air (on line)	Optimal selection of cooling method with every steel grades (air cooling, mist cooling)

condition.

$$U_1 = 1.54(\varepsilon \cdot R)^{0.43} \dots\dots\dots (3)$$

$$V_{\min} = \sqrt[4]{\frac{48g(\rho_m - \rho_s)\sigma}{\rho_s^2}} \dots\dots\dots (4)$$

wherein, ρ_m , the density of molten steel (kg/m^3); ρ_s , the density of slag (kg/m^3); σ , molten steel/slag interfacial tension (N/m^3); g , the acceleration of gravity (m/s^2); ε , stirring power density (W/t); and R , vessel radius (cm).

With the introduction of these new technologies, the RH equipment capable of N concentration control was combined with the LF equipment, which complements the functions of inclusion control and S concentration control, configuring the No.3 molten steel processing equipment to produce all steel types produced at Kobe Works.

2.2 No.6 continuous caster (6CC)

2.2.1 Equipment outline

Fig. 5 shows the outline of 6CC equipment. This equipment includes a vertical bending-type continuous bloom caster designed by Machinery Business and Iron and Steel Business of Kobe Steel. The bloom size, 300×430 mm, bending radius, 10.0

m, and the casting rate are designed to be the same as those of Kobe Works 3CC and 5CC.⁵⁾

Table 6 shows the design concept and specifications of 6CC. The roll profile of the 6CC has been optimized to further improve the surface and internal quality on the basis of 5CC, which had been casting materials with stringent surface quality. First, in order to prevent bulging under the mold, the bulging that causes internal cracks under the skin, the length of the vertical part including the mold was extended to 4.0 m. The tundish (hereinafter referred to as "TD") is designed to be large enough to accommodate 5 strands and has a shape that allows stable flow control and can handle small lots. The third cooling apparatus was designed such that mist cooling and atmospheric cooling can be selected, and the bloom surface temperature can be controlled over a wide range in accordance with the steel type characteristics.

2.2.2 Tundish

Fig. 6 is a schematic diagram of the tundish for the 6CC (hereinafter the "6CCTD"). The 6CCTD comprises an injection chamber and a strand chamber separated by a weir having a sleeve (weir

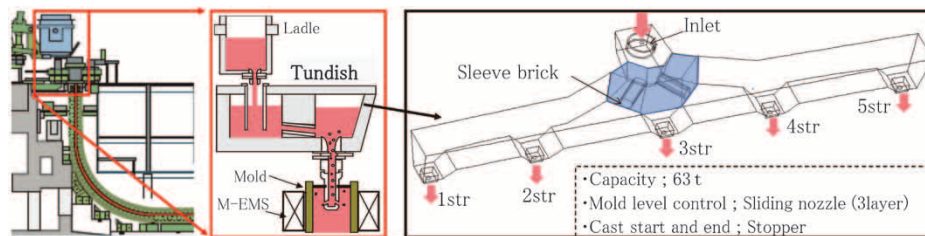


Fig. 6 Schematic view of 6CCTD with large size

Table 7 Tundish shape and simulation results

Operation	Tundish shape	Flow control	Temperature difference among strands (°C)
Simulation	A	×	6.2
Actual	B	○	4.3
	(final)		2.0~5.0

hole) through which molten steel passes. The strand chamber and injection chamber constitute a simple structure, in which, when the weight of the TD is decreased, they are connected by the surface of molten metal so as to secure the dischargeability of steel in the non-steady part. The technological challenge in TD design was the flow control in the stationary part to make molten steel uniform even with a horizontally long shape. The purpose was to promote inclusion floatation and separation by increasing the capacity and to suppress the direct flow to the strand adjacent to the sleeve by the flow control in the lateral direction. Regarding these, a study using simulation and water model experiments was conducted on the sleeve angle and shape.

Table 7 shows the simulation results of molten steel flow in the 6CCTD. The concept⁶⁾ was based on the conventional technology for facilitating inclusion floatation by a large-capacity TD, controlling the flow of molten steel by a sleeve method, and forming an upward whirling flow in the strand chamber. In addition, by adjusting the shape and angle of the sleeve to create a flow in the horizontal direction without any direct flow to the neighboring strand, the optimum structure was realized to ensure the uniformity of the molten steel temperature and inclusion floatation rate in the strand chamber.

As a result, 6CCTD has a simple structure and shape to ensure the satisfactory flow control and dischargeability of steel. In the actual operation, the drop of TD temperature agreed well with the simulation results, and the maximum temperature deviation among the strands was as small as 2.0-5.0°C (Table 7), achieving the effect of reducing the heat deviation by controlling the flow of molten steel in the TD. Furthermore, the secured dischargeability of steel minimized the cropping amount between heats in the non-steady part, achieving the planned

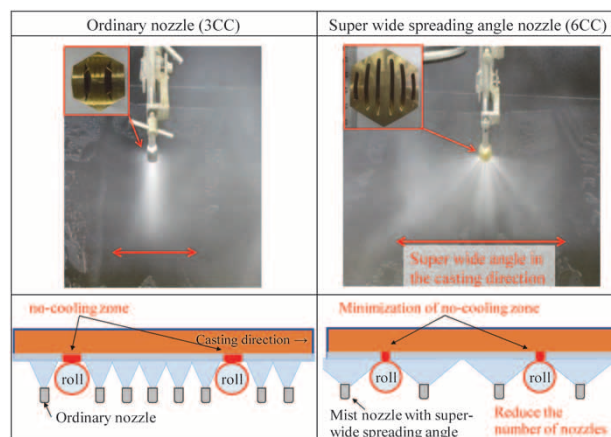


Fig. 7 Mist nozzle with super-wide spreading angle for third cooling

effect.

2.2.3 Third cooling apparatus

The third cooling apparatus is used to cool the bloom such that the surface temperature is lowered below A1 transformation temperature after the bloom cutting and before charging into a heating furnace. This apparatus is provided to refine the microstructure of the bloom surface layer and, thus, to prevent grain boundary cracks from propagating during the bloom rolling. For the 6CC, the cooling method was specified to allow the selection of mist cooling, or air cooling. Furthermore, a cooling zone, disposed in the mist cooling after the bloom cutting, has enabled a uniform cooling without being affected by the casting rate.

In addition, a mist nozzle with a super-wide spreading angle (Fig. 7) was developed to facilitate the maintenance of the mist cooling zone and to ensure more uniform cooling of the lower surface of each bloom. Compared with the conventional 3CC mist nozzle, the new mist nozzle with a super-wide spreading angle has approximately twice the spray width in the casting direction, while maintaining the density of water amount and collision pressure. As a result, the nozzle pitch was increased to approximately twice that of the conventional nozzle, and the number of nozzles was halved. In addition,

Table 8 Effect of applying mist nozzle with super-wide angle

	Number of nozzles in third cooling zone	Ratio of cooling area of undersurface
Ordinary nozzle	>1,000	83 (%)
Mist nozzle with super-wide spreading angle	< 500	93 (%)

Table 9 Results of magnetic particle inspection for billet surface defects

Machine	Index of billet surface defects
3CC/5CC	1.00
6CC	0.89

the uncooled area near the roller contact on the lower bloom surface was reduced by approximately 10% (**Table 8**).

The introduction of these technologies has realized a third cooling apparatus that combines uniform cooling and favorable maintainability, as well as the widely flexible cooling rate. The launch of 6CC has enabled the narrow control of the bloom temperature in the steps from casting to heat furnace charging, using different cooling conditions for each type of cast steel. The results of magnetic particle inspection on a billet surface of a 6CC casting showed a surface quality that is the same or better than that obtained by 3CC or by 5CC (**Table 9**).

3. Construction for upstream process consolidation and status after inauguration

After the decision was made for upstream process consolidation, the 2LF plant was put into operation in October 2015, followed by 4RH and 6CC plants in January 2017 at Kakogawa Works. The 4RH and 6CC of Kobe Works were operated intermittently until the end of October 2017 when the upstream processes in Kobe Works was shut down, while emphasis was placed on the establishment of operation and producing steel for approval (expansion of steel types). In the meantime, work proficiency training was promoted for those who were scheduled to be transferred from Kobe Works. The transferees from Kobe Works were

accepted beginning in November 2017, and the full operation system was established.

After consolidation, the molten steel refining time for 4RH molten steel was shortened, the multiplication of 6CC was promoted and the casting rate was increased; thus, the production capacity was systematically expanded. In March 2019, a crude steel production volume of 148.5 kilo-tonnes/month, the maximum since the launch, was recorded, achieving the initial target production capacity (annual average) of 140 kilo-tonnes/month.

Conclusions

At Kakogawa Works, the No.3 molten steel processing equipment (2LF, 4RH) and No.6 continuous caster (6CC) were newly installed for the purpose of consolidating the upstream process, which has strengthened the system of producing special steels for wire rods and steel bars. The new equipment has been operating steadily since it was launched. The improvements in work proficiency and production capacity have led to stably continuing production under the full production system after the upstream process consolidation, effectively coping with small lot handling and quality improvement.

The future plan is to promote cost minimum production by further improve the compatibility and relaxing the casting restrictions under the two bloom-continuous-caster system of 2CC and 6CC. This is part of Kobe Steel's effort to establish an optimum production system in terms of productivity, quality and cost, to meet the expectations of customers and society for stable supply and quality, and to gain their trust.

References

- 1) S. Nabeshima et al. *Tetsu-to-Hagane*. 2015, Vol.101, No.12, pp.627-635.
- 2) S. Tanaka et al. 7th International Congress on Science and Technology of Steelmaking. 2018.
- 3) S. Asai. 100th and 101st Nishiyama Memorial Seminar. Iron and Steel Institute of Japan.1984, p. 65.
- 4) K. Ogawa et al. *ISIJ. Int.* 1984, p. A181.
- 5) H. Sakai et al. *R&D Kobe Steel Engineering Reports*. 2011, Vol.61, No.1, pp.11-15.
- 6) H. Sakai et al. *R&D Kobe Steel Engineering Reports*. 2006, Vol.56, No.3, pp.9-13.

Improving Control Accuracy of Steel Plate Temperature by Accelerated Cooling with Columnar Water Jets

Takahiro OHARA*¹, Keiichi YAMASHITA*¹, Kiichiro TASHIRO*², Kensuke UENISHI*³, Taketsugu OSAKA*⁴,
Dr. Masahiko MITSUDA*⁵

*¹ Process Engineering Development Section, Research & Development Laboratory, Iron & Steel Business

*² Sheet & Plate Products Development Department, Research & Development Laboratory, Iron & Steel Business

*³ Plate Production Department, Kakogawa Works, Iron & Steel Business

*⁴ Production Systems Research Laboratory, Technical Development Group

*⁵ Kobelco Research Institute, Inc.

The amount of cooling water, which affects the heat transfer characteristics, and the height of residual water on the steel plate surface, the height that changes in accordance with the steel plate size, were modeled for the accelerated cooling of steel plates with cylindrically-arranged multi jet. In addition, the heat transfer characteristics associated with the height of residual water were investigated by laboratory experiments to model the heat transfer coefficient, which is an index of heat transfer characteristics. Furthermore, the heat transfer coefficient model was optimized by the actual temperatures measured at multi-points on a steel plate in an actual machine, which enabled the accurate prediction of the plate temperature. A water flow rate control function was newly developed on the basis of the temperature prediction results and was introduced into the actual machine, which improved the accuracy of the plate temperature control.

Introduction

In the cooling step of the thermo-mechanical control process (TMCP),¹⁾ a typical process for producing steel plates, each steel plate must be cooled uniformly at a desired cooling rate (CR) to a finishing cooling temperature by an accelerated-cooling device to realize the target material structure and properties. In the cooling control, it is necessary to consider how the flow and boiling mode of cooling water affect the heat transfer characteristics, so as to properly set the longitudinal and width directions of the steel plate and the cooling water flow on its upper and lower surfaces. Several steel plate producers have also developed cooling devices and cooling control technologies to more accurately control the steel plate in the cooling process.^{2), 3)} The flow rate control sets the required cooling water flow rate on the basis of the calculated predictive values of the temperature of a steel plate in the cooling process. This means that the accuracy of the predictive calculation affects the accuracy of the temperature control.

Hence, Kobe Steel focused on the behavior of the

cooling water on the upper surface of a steel plate, which affects the characteristics of heat transfer between the cooling water and the steel plate. In order to improve the accuracy of the predictive calculation, a prediction model was constructed for the height distribution of cooling water accumulated on the upper surface of a steel plate (hereinafter referred to as "residual water"). A heat transfer model taking into account the height of the residual water was constructed as well. Moreover, the constructed models were optimized and adapted for the cooling control of the actual machine to improve the accuracy of the temperature control of the steel plate.

This paper relates to the construction of a heat transfer model and describes the construction of a prediction model for the height distribution of residual water on the upper surface of a steel plate and the effect of the residual water height on the heat transfer characteristics. Also introduced are the results of evaluating the accuracy of the newly constructed heat transfer model.

1. Temperature prediction of steel plates in cooling process

For predicting the steel plate temperature in the cooling process, the steel plate temperature on the entrance side of a cooling header (start cooling temperature, hereinafter referred to as "SCT") is regarded as the starting point for predicting the steel plate temperature on the exit side of the cooling header (finishing cooling temperature, hereinafter referred to as "FCT"). In the cooling control, the calculated predictive value of the steel plate temperature is used as the basis for determining the flow rate of cooling water and other parameters that satisfy the desired FCT and CR. At this time, it is necessary to ensure the accuracy of the heat transfer model used in the predictive calculation. The heat transfer characteristics between the cooling-target surface (of a steel plate) and the cooling water vary greatly depending on the amount of cooling

water, its flow on the upper surface of the steel plate, the changes in boiling mode, the cooling water temperature and the surface texture of the steel plate.⁴⁾ In particular, the flow of cooling water on the upper surface of a steel plate is considered to vary greatly in accordance with the cooling conditions (size of the steel plate, water flow, and the like). Hence, a small testing machine simulating the actual cooling header was used to observe the flow of cooling water to develop a model for predicting the height distribution of cooling water staying on the upper surface of the steel plate. In the meantime, a cooling experiment was conducted to study the effect of residual water heights on the heat transfer characteristics and to develop a heat transfer model taking into account the height of residual water. Moreover, actual temperatures were measured at multi points in the cooling process to adjust the model parameters so as to optimize the heat transfer model being developed.

1.1 Model for predicting height of residual water on upper surface of steel plate

The cooling header used for cooling the upper surfaces of steel plates in Kobe Steel's steel plate mill comprises a repeated arrangement of a nozzle injection part for injecting high-pressure cooling water from densely disposed columnar water jets nozzles and an injection part without any nozzle. The heat-transfer coefficient during water cooling is affected by the flow state of the cooling water staying on the upper surface of the steel plate. Hence, the flow state of cooling water was examined by a cooling water flow observation test was performed.

Fig. 1 depicts the outline of the test, and **Fig. 2** shows the flow state of the cooling water on the upper surface of a steel plate during the test. The testing apparatus consists of a cooling header with a group of columnar water jets nozzles and an acrylic plate simulating a steel plate (hereinafter referred to as a "simulation plate") disposed under the header, while a half-width model was used in consideration of symmetry. An acrylic wall plate is placed at the symmetry boundary plane, and residual water is discharged from the end of the simulation plate. In order to observe the flow of residual water, the simulation plate and wall plate are made transparent. In this cooling water flow observation test, the distance between the nozzle tip and the simulation steel plate was 300 mm, the nozzle diameter was 3 mm, the nozzles were 500 jets/m², and the header size was 1,000 × 2,000 mm. The flow of residual water varies depending on

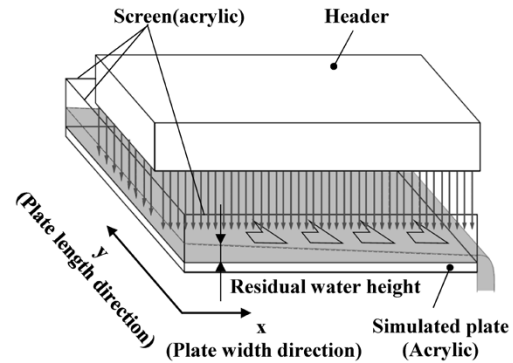


Fig. 1 Schematic diagram of test for observing flow of cooling water

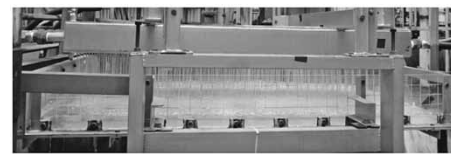


Photo from conveyance direction



Photo from direction orthogonal to conveyance direction

Fig. 2 Columnar water jets and residual water flow in experiment

the cooling water flow per unit area (water flow density) and the plate width. For this reason, the water density was set to 3 levels, the widths of the simulation plates were 1,500 mm and 2,000 mm, and the length was 1,000 mm. The distribution in the width direction of the residual water height was measured, and the results are shown in **Fig. 3**. The residual water height increases with increasing water flow density and plate width. On the other hand, the residual water height decreases from the center of the plate width toward the end of the plate width. From these results, the heat transfer characteristics are considered to change depending on the plate width, water flow density, and position on the plate surface.

Hence, the residual water height distributions were measured while changing the water flow density and plate width and, on the basis of the results, a model was developed to predict the residual water height at any position on the steel plate (**Fig. 4**). Here, the plate width direction is the x-axis, the plate longitudinal direction is the y-axis, the nozzle region length is a , the plate width is b , and the non-nozzle region length is c . Taking into account the symmetry, a 1/4 region for each was used as an analysis region.

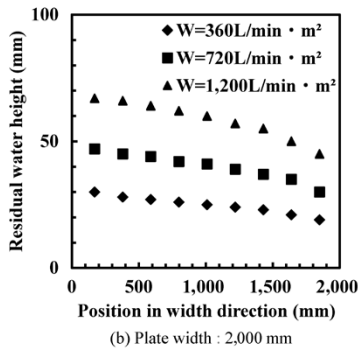
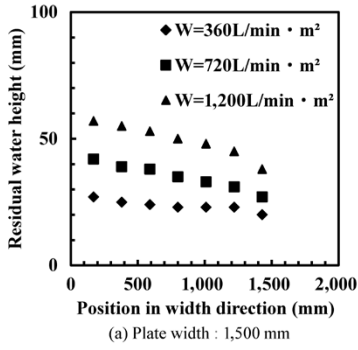


Fig. 3 Distribution of residual water height

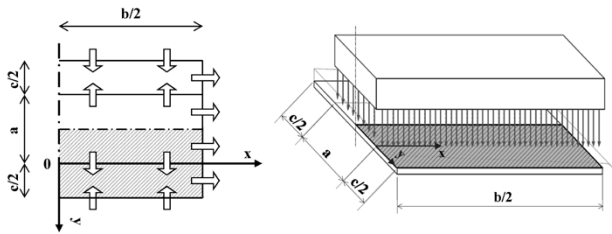


Fig. 4 Analysis model for residual water height prediction

The equations governing the analysis model are expressed by Equations (1) to (4).

The equations of continuity are given by Equations (1), (2):

for the nozzle injection region;

$$\partial(hu)/\partial x + \partial(hv)/\partial y = \gamma \quad (1)$$

for the non-nozzle-injection region;

$$\partial(hu)/\partial x - \partial(hv)/\partial y = 0 \quad (2)$$

The energy equation is given by Equation (3):

$$q^2 = (hu)^2 + (hv)^2 \quad (3)$$

The Bernoulli's equation is expressed by Equation (4):

$$H = h + (u^2 + v^2)/2g = h + q^2/2gh^2 \quad (4),$$

wherein h is the height of residual water (m); u , the flow velocity in the x direction (m/s); v , the flow velocity in the y direction (m/s); γ , water flow density (m/s); q , water flow rate (m²/s); H , total head (m); g , the acceleration of gravity (m/s²).

The Bernoulli's equation holds only when the

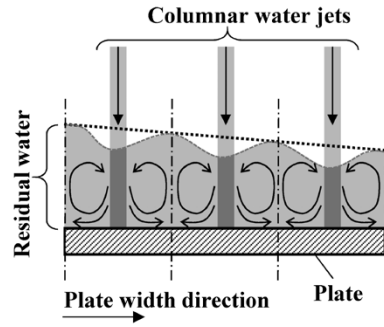


Fig. 5 Flow behavior in nozzle injection region

nozzle jet flow is mixed so as not to give friction to the flow from the upstream of residual water and cannot sufficiently express the flow behavior. Therefore, the flow behavior of the nozzle injection part (Fig. 5) is taken into account to expand Equation (4) so as to express the momentum redistribution and loss due to frictional force, as follows:

$$H = h + q^2/2gh^2 + Kq/gh \quad (5)$$

wherein K is the friction coefficient (m/s).

Since q reaches the maximum at the position of $x = b/2$ and $y = 0$, the residual water height, h , becomes minimum at this position. Here, according to the concept of critical flow, $dq/dh = 0$ holds at the position of $x = b/2$ and $y = 0$, and Equation (5) becomes Equation (6):

$$h^3 - Hh^2 + q^2/2g + Kqh/g = 0 \quad (6)$$

Thus,

$$(K/gh + q/g)(dq/dh) + 3h^2 - 2Hh + Kq/g = 0 \quad (7)$$

Therefore, representing the critical flow by the subscript cr gives

$$3h_{cr}^2 - 2Hh_{cr} + kq_{cr}/g = 0 \quad (8)$$

$$h_{cr}^3 - Hh_{cr}^2 + kq_{cr}h_{cr}/g + q_{cr}^2/2g = 0 \quad (9)$$

wherein h_{cr} is the critical residual water height; q_{cr} , critical water flow rate.

Here, using a dimensionless constant, C , based on a dimensional analysis, the friction coefficient, K , is expressed by Equation (10):

$$K = Cq_{cr}/2h_{cr} \quad (10)$$

wherein the critical residual water height, h_{cr} , the critical water flow rate, q_{cr} , and the total head, H , are given by Equations (11) to (13), respectively:

$$q_{cr} = \gamma(a/2)(b^2 + c^2)^{1/2}/(a + c) \quad (11)$$

$$h_{cr} = \{(2 + C)q_{cr}^2/2g\}^{1/3} \quad (12)$$

$$H = (3 + 2C)h_{cr}/(2 + C) \quad (13)$$

The water flow rate q is given by Equations (14) and

(15):

$$q = \{2\gamma/(a+c)\} \{c^2(a/2+x)^2 + (ay)^2\}^{1/2} : x < 0 \dots (14)$$

$$q = \{2\gamma/(a+c)\} \{a^2(c/2-x)^2 + (ay)^2\}^{1/2} : x \geq 0 \dots (15)$$

To determine the residual water height, h , it is necessary to find the roots of the cubic equation, Equation (6). Hence, taking Equation (16) into consideration, an approximate expression satisfying Equations (17) and (18) is derived as Equation (19):

$$dh/dq = -(Kh+q) / \{Kq+g(3h^2-2Hh)\} \dots (16)$$

$$h = H, dh/dq = -K/(gH) : q = 0 \dots (17)$$

$$h = h_{cr}, dh/dq = -\infty : q = q_{cr} \dots (18)$$

$$h = h_{cr} + 2 \{H - h_{cr} - Kq_{cr}/(gh)\} \{1 - q/q_{cr}\}^{1/2} - \{H - h_{cr} - 2Kq_{cr}/(gh)\} \{1 - q/q_{cr}\} \dots (19)$$

In particular, the measured value of the residual water height distribution in the width direction during the water model experiment is located at $y = c/2$, and q is expressed by Equation (20):

$$q = 2\gamma ax / (a+c) \dots (20)$$

Therefore, Equation (19) is expressed as Equation (21):

$$h = h_{cr} + 2 \{H - h_{cr} - Kq_{cr}/(gh)\} \{1 - ax\}^{1/2} - \{H - h_{cr} - 2Kq_{cr}/(gh)\} \{1 - ax\} \dots (21)$$

$$a = \{2\gamma a / (a+c)\} / q_{cr} = 4 / (b^2 + c^2)^{1/2} \dots (22)$$

The value calculated by Equation (21) and value measured were used to determine C. Fig. 6 shows the measurement results and model prediction results for residual water height. As shown in this figure, the changes in residual water height with respect to the changes in water flow density and plate width can be predicted using the model equation, which is an expanded Bernoulli's equation.

1.2 Effect of residual water height on heat transfer characteristics

In the construction of the heat transfer model taking into account the residual water height, the effect of residual water height on heat transfer characteristics was examined by a cooling experiment using a down-sized apparatus simulating the cooling process used at Kobe Steel's steel plate mill (Fig. 7). The experimental apparatus consists of a heating furnace, a conveying table, a descaler, and a cooling header (Fig. 8). The descaler is a high-pressure water injection device for removing oxide scale, which is an influential factor

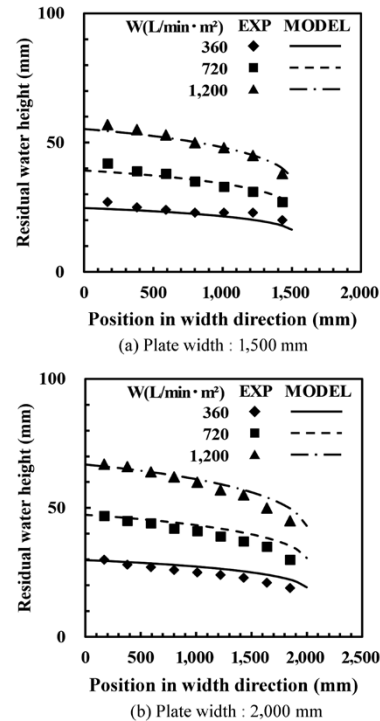


Fig. 6 Predicted and measured distributions of residual water height

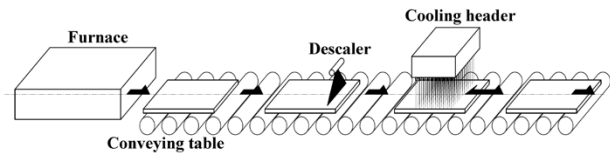


Fig. 7 Main components of small-sized apparatus for cooling experiment

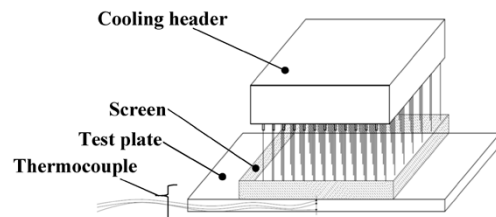


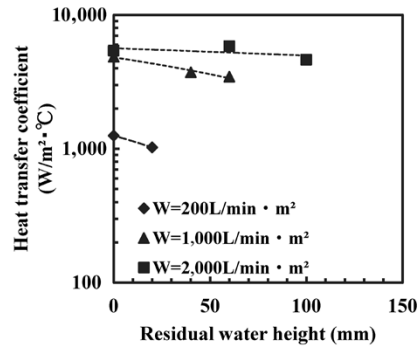
Fig. 8 Schematic of cooling header

in heat transfer characteristics. The cooling header is a cooling device with a group of columnar water jets nozzles. Here, the distance from the nozzle tip to the test plate was 300 mm, the nozzle diameter was 3 mm, the number of nozzles was 500 jets/m², and the header size was 500 × 500 mm. The residual water height was simulated by changing the height of the weir provided on the upper surface of the test plate. Table 1 shows the set values of the weir height corresponding to each water flow density. The temperature of the test material was measured by thermocouples installed at multiple points in the thickness direction inside the plate.

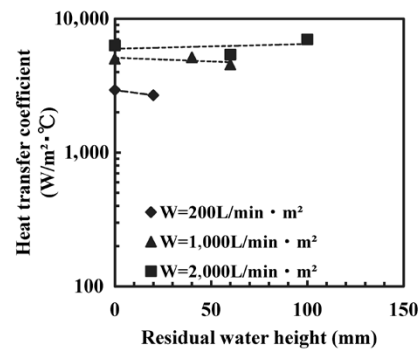
In the cooling test, the test material was heated to 900°C or higher in a heating furnace, taken onto the

Table 1 Relationship between water flow density and set value of screen height

Water flow density (L/min · m ²)	Height of screen (mm)
200	0(Not set), 20
1,000	0(Not set), 40, 60
2,000	0 (Not set), 60, 100



(a) Surface temperature in high temperature range:750 - 600°C



(b) Surface temperature in low temperature range:400 - 250°C

Fig. 9 Effect of residual water height on HTC (heat transfer coefficient)

transfer table, transferred to the descender to remove the scale, and then transferred to the cooling header. The cooling was conducted by oscillate cooling in order to simulate the actual cooling process.

The heat-transfer coefficient, which is an evaluation index of heat transfer characteristics, was calculated by solving the inverse problem of the heat conduction equation at each temperature measurement point. Fig. 9 shows the relationship between the heat-transfer coefficient and the calculated residual water height. This relationship confirms that the heat-transfer coefficient changes in accordance with water flow density and residual water height. When the water flow density is low (200 L/min · m²), the heat-transfer coefficient decreases as the residual water height increases, and this trend is observed in both the high temperature range (600°C or higher) and the low temperature range (400°C or lower). This is presumably because the impact pressure of the nozzle jet decreases with increasing residual water height.

On the other hand, when the water flow density

is high (1,000 L/min · m², 2,000L/min · m²), only a small decrease in heat-transfer coefficient is associated with increasing residual water height. In particular, when the water flow density is 2,000 L/min · m², the heat-transfer coefficient becomes almost constant in the high temperature range regardless of the increase in residual water height. The results show only a slight increase in the heat-transfer coefficient in the low temperature range. This is presumably because the stirring effect of the residual water has been improved, although the collision pressure immediately below the nozzle jet has decreased with the increase of the residual water height. This trend has also been observed in experiments with a single cylindrical jet nozzle,⁵⁾ and similar results are obtained for the group of cylindrical jet nozzles.

A heat transfer model was constructed by combining these cooling test results with the residual water height model described in Section 1.1. The spray's cooling experimental equation⁴⁾ has been adapted for the basic model and has been expanded as shown in Equation (23), in consideration of the effect of residual water height on the heat transfer characteristics:

$$\log HTC = c_1 + c_2 \log W + c_3 T_s - d \log h \dots\dots\dots (23)$$

wherein *HTC* is the heat-transfer coefficient (W/m² · °C); *W*, water flow density (L/min · m²); *T_s*, steel plate surface temperature (°C); *h*, residual water height (m); and *c*₁, *c*₂, and *c*₃ are constants.

It should be noted that the residual water height, which affects the heat transfer characteristics, changes depending on the water flow density, and, therefore, the coefficient *d* is regarded as a function of water flow density.

In order to take into account the change in cooling capacity due to the boiling state of cooling water, the steel plate temperature was divided into two regions; i.e., high temperature region and low temperature region. The heat-transfer coefficient was formulated in each of these two temperature regions, and the two temperature regions were expressed by interpolating the respective equations.

In addition to the heat transfer model of the nozzle injection part described above, another heat transfer model was constructed for the non-nozzle-injection part between the cooling headers. That is, this model calculates the flow rate of the drainage flow from the center to the edge of the steel plate, which is in accordance with the residual water height distribution on the upper surface of the steel plate, on the basis of the difference in the residual water height, and thereby predicts the heat-transfer coefficient of the non-nozzle-injection part.

From these, the water flow density and the residual water height, which changes with the plate width at any position on the steel plate, can be predicted by a semi-theoretical equation. Hence, a heat transfer model has been constructed to predict the heat-transfer coefficient at any position of the steel plate, the coefficient that varies with the water flow density and the site on the steel plate.

2. Optimization of heat transfer model and accuracy evaluation

On the basis of the heat transfer model of the nozzle injection part on the upper surface of the steel plate described in section 1.2, heat transfer models were constructed for different areas (upper / lower cooling, nozzle injection part and non-nozzle-injection part) of the actual cooling header. Moreover, a temperature prediction model for cooling was constructed by combining the heat transfer models of the regions. The model parameters related to the influence factors, such as water flow density and steel plate surface temperature in the heat transfer model, have been determined by a cooling test using a small experimental apparatus. In order to compensate for the difference between the small experimental apparatus and the actual machine, the model parameters were optimized based on the temperatures measured at multiple points of the actual machine in the cooling process.

Fig.10 shows the values calculated by the temperature prediction model and the values measured. The multi-point measurement values obtained by adding the values measured for SCT and FCT and the temperature values measured^(Note) on the upper and lower surfaces of the steel plate in the recuperation process right after the cooling header were used as the basis for optimizing the model parameters such that the deviation between the calculated temperature values and the measured values was minimized. Since the cooling process is expressed by the heat transfer model for each region with different cooling conditions, it is necessary to set the model parameters for each region. For this reason, the model parameter was optimized using the particle swarm optimization (PSO) method,⁷⁾ which is one of the optimization techniques for multi-variables, so as not to fall into local solutions.

Note) The measurements employed a normal thermometer for measuring the upper surface of a steel plate and a thermometer for measuring temperature on the lower steel plate surface introduced to actual machines.⁶⁾

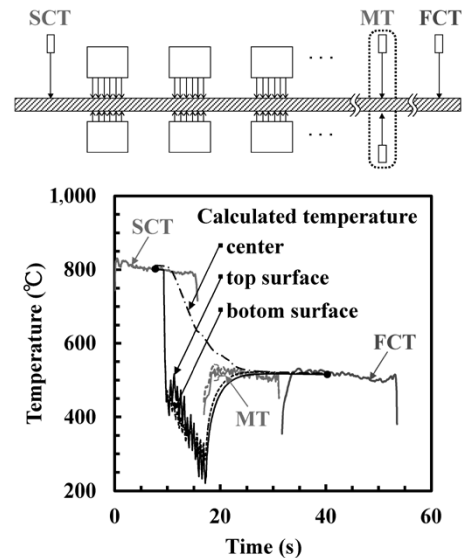


Fig.10 Calculated and measured temperatures

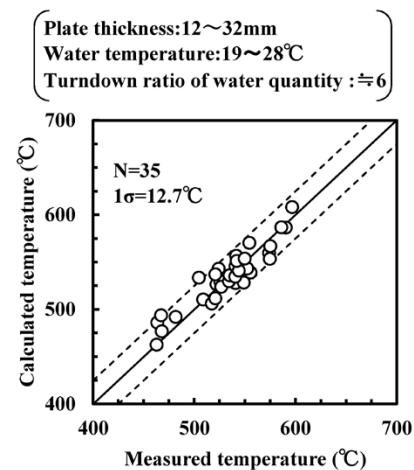


Fig.11 Calculated and measured FCTs

Fig.11 shows the calculated and measured values of the finishing cooling temperature based on the optimized temperature prediction model. Here, the prediction accuracy, 1σ , is 12.7°C . As the steel plate temperature decreases due to cooling, the boiling state transits from film boiling to nucleate boiling (transition boiling region). In the transition boiling region, the cooling capacity increases rapidly, making it difficult for conventional methods to predict the temperature. Therefore, a heat transfer model considering the flow state of the cooling water was used for the optimization based on the actual steel plate temperatures measured. This has enabled the prediction of the finishing cooling temperature with high accuracy even in the finishing cooling temperature range including cooling in the transition boiling region. Fig.12 shows an example of the newly developed heat transfer model applied to the cooling control of an actual machine. The predictive values of temperature calculated by the heat transfer

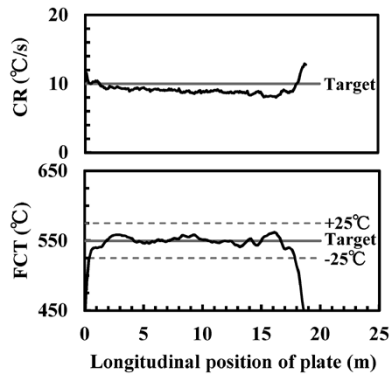


Fig.12 Results of online cooling control using developed heat transfer model (Plate thickness: 20 mm, FCT=550°C, CR=10°C/s)

model were used for setting the amount of cooling water satisfying the desired FCT and CR. Fig.12 shows the results of FCT and CR when the plate thickness is 20 mm, the target FCT is 550°C, and the target CR is 10°C/s. It is shown that highly accurate control has been realized with the FCT of the longitudinal steady-state portion of the steel plate, excluding the leading edge falling within $\pm 25^\circ\text{C}$, and the CR for the same falling within $\pm 1^\circ\text{C/s}$ of the target value. Based on this, it has been confirmed that highly accurate temperature control is possible by applying the newly developed heat transfer model.

Conclusions

A study was conducted to improve the accuracy of the temperature control for steel plates in the accelerated-cooling header of Kakogawa Works steel plate mill. A prediction model for the height distribution of the cooling water on the upper surface of a steel plate was constructed along with a heat transfer model taking into account the flow state, the residual water height. The constructed heat transfer model was applied to the cooling control of an actual machine, which confirmed the feasibility of highly accurate temperature control.

Kobe Steel will work on to improve the control accuracy in a wide range of temperature control conditions and steel plate size conditions, and contribute to the commercialization, yield improvement and quality stabilization of new high-value-added steel plates.

References

- 1) I. Kozasu. Controlled Rolling · Controlled Cooling. Chijinshokan Co., Ltd. 1997.
- 2) Y. Serizawa et al. Nippon steel technical report. 2014, Vol.400, No.4, pp.18-25.
- 3) A. Fujibayashi et al. JFE Technical Report. 2004, No.5, pp.8-12.
- 4) Boiling heat transfer and cooling, The Japan Society of Mechanical Engineers. JAPAN INDUSTRIAL PUBLISHING CO., LTD. 1989.
- 5) Y. Haraguchi et al. CAMP-ISIJ. 2012, Vol.25, p.1042.
- 6) T. Ohara. CAMP-ISIJ. 2018, Vol.31, p.257.
- 7) Y. Oguma et al. Transactions of the Society of Instrument and Control Engineers. 2009, Vol.10, pp.512-521.

On-line Inter-stand Tension Monitor System for Bar Mill

Dr. Masanori KOBAYASHI*¹, Tomohide TAIRA*², Masakazu KATO*³, Hiroshi NAKAMURA*³, Dr. Yoshio MORIMOTO*⁴, Dr. Shusuke YANAGI*⁵

*¹ Process Engineering Development Section, Research & Development Laboratory, Iron & Steel Business

*² MONODZUKURI(Production System Innovation) Planning and Promotion Department

*³ Wire Rod & Bar Rolling Department, Kobe Works, Iron & Steel Business

*⁴ Kobelco Research Institute, Inc.

*⁵ Materials Research Laboratory, Technical Development Group

In wire rod and bar mills, it is important to optimize inter-stand tensions in order to prevent problems during rolling and to prevent dimensional variations in the longitudinal direction. The stabilization of inter-stand tension, however, has hitherto been dependent on the adjustment skills of operators. This paper relates to a method that was developed to estimate inter-stand tensions on the basis of a model for wire rod rolling. This model uses the values of motor current, which can easily and constantly be obtained during rolling without relying on the skills of the operators. A tension monitor system was newly developed to provide the rolling mill operators with inter-stand tension estimated in real time using the above method, and this monitor was introduced to the bar rolling mill at the Kobe Works of Kobe Steel. As a result, the system has facilitated the motor speed adjustment performed by the operators. This contributes to the stabilization of the inter-stand tension in actual operation and to the reduction of operational troubles.

Introduction

For the rolling of steel-bar products, it is important to maintain the inter-stand tensions between the stands of rolling trains within an appropriate range so as to prevent problems including rolling troubles such as cobbles, surface defects such as scab, and the dimensional variation of leading/tailing ends. In the case of steel bar rolling, only a certain type of stand can adapt a tension adjustment mechanism by loop control due to the size of the material being rolled. Hence, rolling mill operators adjust each inter-stand tension to an appropriate tensile/compressional state by manipulating the rotations of rolls. They determine the tension/compression of the material between the stands of rolling trains from the changes in the electric current of the main electric motor that drives the rolls during the process from the tension-free state on the exit side, when the tip of the rolling material is bitten, to the tension-loaded state on the exit side, when the tip is bitten into the next stand. There are, however, challenges in that the ammeter must be monitored while the material tip passes through, and that the change in electric current is instantaneous and difficult to recognize at the

downstream stands where the rolling speed is high, which are not easy tasks for an operator with little operating experience.

The proposed methods for quantifying inter-stand tensions include a method¹⁾ of directly detecting the force acting on roll chocks in the rolling direction, and another method^{2), 3)} involving the calculation of rolling torques from the rolling load measured by load cells to estimate tension. Each of these methods, however, requires a load cell, which complicates the equipment configuration, and the soundness of the sensors must be maintained.

Hence, Kobe Steel has developed a system to monitor and grasp tension more easily. This system not only allows less experienced operators to easily adjust the tension, but also can automatically read the changes in the driving current before and after the biting by the next stand, and, moreover, can estimate the tension values on the basis of a rolling model and display them. By referring to these values, the operators can easily adjust the rotational speed of rolls and stabilize the inter-stand tension. This paper outlines this tension monitor system for steel-bar rolling.

1. Outline of steel-bar rolling line

The steel-bar rolling line at Kobe Works of Kobe Steel consists of a heating furnace, a roughing train (8 stands), an intermediate train (4 stands), a finishing train (4 stands) and a block mill (5 stands) (Fig. 1). Billets of 155 mm square or 182 mm square are rolled into steel bars of ϕ 17 mm to ϕ 108 mm in diameter. A loop control mechanism is introduced between the intermediate train and the finishing

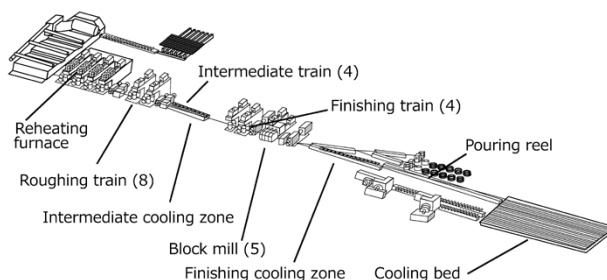


Fig. 1 Layout of bar mill in Kobe Works

train, and tension-free rolling is performed on the entry side of the finishing train. However, there is no loop mechanism for the trains further upstream. As a result, tensile force or compressive force may be exerted on the rolled material between adjacent stands, depending on the relationship between the rotational speeds of the rolls in them.

2. Development of tension monitor

2.1 Concept of tension monitor

In the continuous rolling of a steel bar, tension (tensile force or compressive force) is applied to the rolled material between the stand on the upstream side and the subsequent stand (on the downstream side) at the moment when the tip of the rolled material is bitten by the subsequent stand. Due to this inter-stand tension, the roll drive torque of the stand on the upstream side changes, causing a change in the motor current (differential current) in the motor that drives the rolls (Fig. 2). That is, when a tensile force occurs, the differential current of the motor on the upstream stand becomes negative, and when a compressive force occurs, it becomes positive. Hence, a roller operator memorizes the motor current value for the tension-free state before the tip of the rolled material is bitten by the subsequent stand and estimates the state of tension between the stands from the change in the motor current immediately after the biting to adjust the rotational speed. This adjustment method, however, requires continuous monitoring so as not to miss the change in the electric current value at the time of biting, and this interferes with other tasks such as monitoring the condition of passing material. Also, in the inter-stands with high rolling

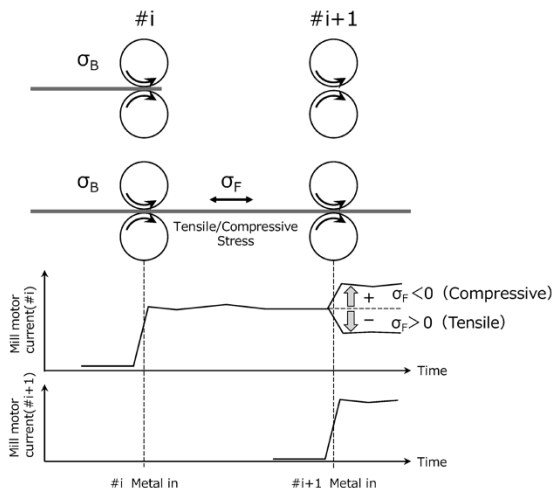


Fig. 2 Method of measuring inter-stand tension using difference of motor currents between #i and #i+1

speed, the movement from one stand to the next is instantaneous, and it is difficult to visually recognize the differential current.

Hence, Kobe Steel has constructed a system that allows easy adjustment of the rotations to obtain an appropriate tension by grasping the inter-stand tension, which is difficult to measure. In this system, the automatically detected change in motor load is converted into tension using a rolling model and is displayed in an easy-to-recognize manner.

2.2 Inter-stand tension model

A model for wire rod rolling was used as an analysis technique to estimate the tension from the differential current.⁴⁻⁶⁾ The rolling load, P_0 , and rolling torque, G_0 , in the tension-free state are calculated by the rectangle conversion method proposed by Saito et al.⁴⁾

$$P_0 = Q_p \cdot k_{fm} \cdot F_D \quad \dots \dots \dots (1)$$

$$G_0 = 2 \xi \cdot l_d \cdot P_0 \quad \dots \dots \dots (2)$$

wherein Q_p , is the roll-separating force function; k_{fm} , average deformation resistance; F_D , projection area of contact; ξ , torque arm coefficient; and l_d , contact arc length.

Next, the rolling state under tension is calculated by the method proposed by Noguchi et al.,^{5, 6)} and the rolling load, P , under tension is expressed by Equation (3):

$$P = P_0 \times \left(1 + a_1 \frac{\sigma_F}{k_{fm}} + a_2 \frac{\sigma_B}{k_{fm}} \right) \quad \dots \dots \dots (3)$$

wherein P is the load (tension loaded); P_0 , load (tension free); σ_F , forward tension; σ_B , backward tension; and a_1, a_2 , influence coefficients.

The rolling torque (driving torque) G under tension is given by Equation (4):

$$G = G_0 \left\{ 1 + \frac{R_m}{G_0} (F_0 \sigma_B - F_1 \sigma_F) \right\} \quad \dots \dots \dots (4)$$

wherein G_0 is the torque (tension load); R_m , average roll diameter; F_0 , cross sectional area of material on the entry side; and F_1 , cross sectional area of material on the exit side.

In wire rod rolling, the flow of material in the width direction is greater and expands the dimension in the direction orthogonal to the rolling direction after rolling (width expansion).

The relationship between the rolling conditions and the width expansion is expressed by Equation (5).⁵⁾

$$b = b_0 \left[1 - \frac{B}{b_0} \left(0.025 \frac{\sigma_f}{k_{fm}} + 0.769 \frac{\sigma_b}{k_{fm}} \right) \right] \quad \dots \dots \dots (5)$$

wherein H and B are the material height and width,

respectively, on the entry side; b_0 , material width on the exit side (tension free); and h and b , material height and width, respectively, on the exit side (with tension loaded).

The width expansion is expressed by equation (6).

$$\Delta b = \frac{\partial b}{\partial \sigma_F} \Delta \sigma_F + \frac{\partial b}{\partial \sigma_B} \Delta \sigma_B \dots\dots\dots (6)$$

Equation (4) becomes $G = \text{Func}(H, B, h, b, k_{fm}, \sigma_F, \sigma_B)$. Therefore, assuming that there is no change in the material dimensions on the entry side and deformation resistance before and after the biting, the change in rolling torque, ΔG , at the stand on the upstream side when the material is bitten by the next stand is given by:

$$\Delta G = \frac{\partial G}{\partial \sigma_F} \Delta \sigma_F + \frac{\partial G}{\partial \sigma_B} \Delta \sigma_B + \frac{\partial G}{\partial b} \Delta b + \frac{\partial G}{\partial h} \Delta h \dots\dots\dots (7)$$

In hot rolling, the change in backward tension due to the change in forward tension is generally small, and, assuming that the change does not exist ($\Delta \sigma_B = 0$), the following holds:

$$\left. \begin{aligned} \Delta G &= \frac{\partial G}{\partial \sigma_F} \Delta \sigma_F + \frac{\partial G}{\partial b} \frac{\partial b}{\partial \sigma_F} \Delta \sigma_F \\ \therefore \Delta \sigma_F &= \Delta G / \left(\frac{\partial G}{\partial \sigma_F} + \frac{\partial G}{\partial b} \frac{\partial b}{\partial \sigma_F} \right) \end{aligned} \right\} \dots\dots\dots (8)$$

From the relational equation between the rolling torque and drive motor current, $G = \eta VI / (2\pi N)$, Equation (8) is expressed as Equation (9):

$$\Delta \sigma_F = \left(\frac{\eta V \Delta I}{2\pi N} \right) / \left(\frac{\partial G}{\partial \sigma_F} + \frac{\partial G}{\partial b} \frac{\partial b}{\partial \sigma_F} \right) \dots\dots\dots (9)$$

wherein V is the rated voltage of the motor; N , rotational speed of the motor; I , motor current; ΔI , differential current; and η , efficiency.

The partial derivatives, such as $(\partial G / \partial \sigma_F)$, are calculated in advance by numerical differentiation of the torque model equation (4) as in the example of Equation (10).

$$\frac{\partial G}{\partial \sigma_F} = \frac{G(\sigma_F + \Delta \sigma_F) - G(\sigma_F - \Delta \sigma_F)}{2\Delta \sigma_F} \dots\dots\dots (10)$$

From Equation (9), the inter-stand tension $\Delta \sigma_F$ can be estimated from the change in the electric current ΔI when the material is bitten by the next stand.

Fig. 3 shows the flow of the model for calculating the inter-stand tension using the above equations. As described, by combining conventionally proposed equations while assuming that the mill rigidity is large and there is no tension propagation from the downstream side to the upstream side stand, the inter-stand tension is obtained by a simple equation.

2.3 Processing of current values and examples of inter-stand tension calculation

As an example of obtaining the inter-stand tension described in Section 2.2, **Fig. 4** shows the electric current data during actual rolling. **Fig. 4** (a) is a case where the inter-stand tension is compressive. First, the load begins to be applied to the motor when the rolled material is bitten by the #1 stand (here, $i = 1$). It is shown that, when the rolled material is bitten by the #(i+1) stand on the downstream side at a later time, the current value of the #i stand increases stepwise, increasing the motor load of the #i stand. The current value of the motor for the tension-free state ((A) in **Fig. 4** (a)) is acquired

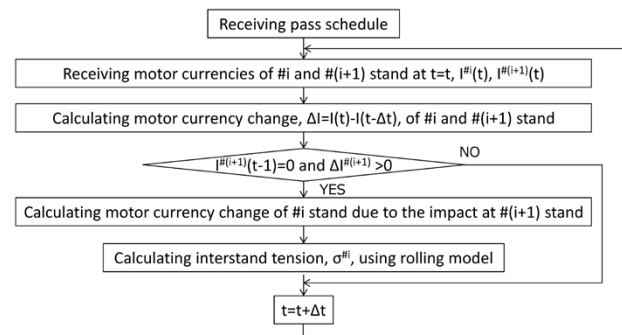


Fig. 3 Flow of calculating inter-stand tension

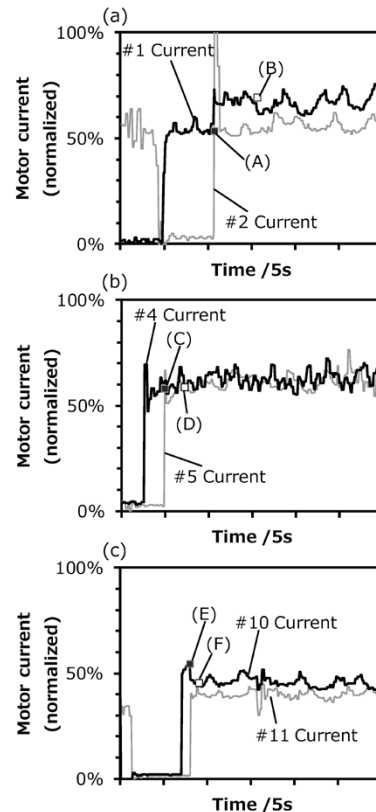


Fig. 4 Example of detection of inter-stand tension (detected stress of (a); compression, (b); neutral, (c); tension)

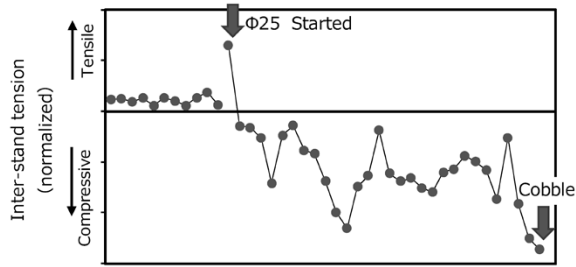


Fig. 5 Inter-stand tension between #10 and #11 stands in cobbling

at the moment when the rolled material is bitten by the # $(i+1)$ stand. Let this current value be I_A . The motor current value after the biting by # $(i+1)$ stand is obtained when a certain time has elapsed after the biting by # $(i+1)$ stand ((B) in Fig. 4 (a)).

Let this current value be I_B . On the basis of the difference between the two current values ($\Delta I = I_A - I_B$), the inter-stand tension is calculated by the method described in the previous section. It should be noted that I_A is the average current value of several points before the biting by # $(i+1)$ stand. Similarly, I_B is the average current value of several points after the biting by # $(i+1)$ stand. The acquisition timing of I_A and I_B was optimized for each stand and line speed, excluding the moment of impact. Such processing has enabled the estimation of reasonable tensions from the current values with large fluctuations.

Fig. 4 (b) shows a case where # i -# $(i+1)$ inter-stand tension is almost 0 (in this case, $i = 4$), and (c) shows a case where # i -# $(i+1)$ inter-stand tension is tensile ($i = 10$ in this case). In these figures, (C) and (E) are just before the biting by the next stand, and (D) and (F) are the electric current values of # 4 and # 10 stands after the biting and their acquisition timing, respectively. In either case, this technique has been confirmed to stably detect proper motor current values.

In order to confirm the validity of this technique, the transition of tension was examined for the case where cobble occurred due to poor adjustment of the rotational speed (Fig. 5). In Fig. 5, the product dimension rolled for the 12th run is changed to $\Phi 25$ mm, at which time the hole type of the rolls was changed (type setting). At the 30th run after the type setting, the compressive force increased between the #10 and #11 stands, causing buckling and cobbling. The transition of tension during this period indicates that the tension between the #10 and #11 stands after type setting has shifted to the compressive direction. It is conceivable that, if the worker could recognize that such a compressive stress state is continuing, the cobble caused by buckling would have been avoided.

3. Overview of tension monitor system

Fig. 6 shows the configuration of the constructed tension monitor system. The monitor system acquires rolling command information from the process computer, and also acquires the motor speed and current value for each stand from the controller. The inter-stand tension model described in Section 2.3 is implemented in the monitor system, which calculates the forward tension at the upstream stand immediately after the material is bitten by the next stand. When one of the inter-stand tensions is renewed, the monitor system replaces the tension value displayed on the tension monitor screen (operator assistance screen shown in Fig. 7) with the latest one. The assistance screen displays the most recent 20 tensions along with the inter-stand tensions of the material currently being rolled (bottom of the screen). In addition, the past results of inter-stand tension for the same size are displayed as a histogram (middle of the screen), making it easier for the operator to determine whether the current tension state is appropriate. These past results for the tension are updated sequentially.

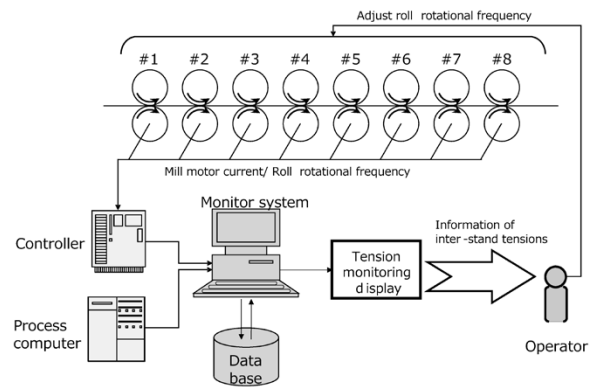


Fig. 6 System configuration for monitoring inter-stand tension of bar rolling mill

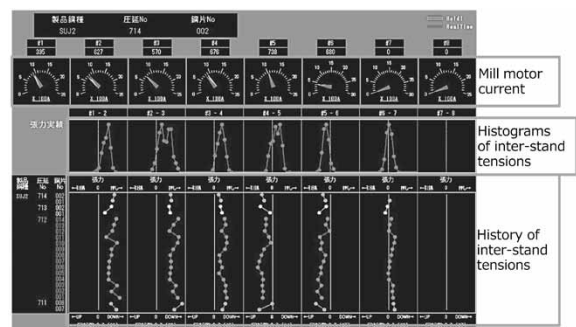


Fig. 7 Monitor image of inter-stand tension for operator

4. Results of tension monitor system application

This tension model was incorporated into a tension monitor system, which comprises an achievement collection function and a screen display function, and the system was launched. Fig. 8 shows the transition, after the introduction of this system, of the variation in the tension actually applied after being calculated by this system. The target product types were: a) $\Phi 30$ mm bearing steel and b) $\Phi 23$ - 27 mm cold heading steel, both with large rolling reductions. For each rolled material, the standard deviation of the tension value obtained at each inter-stand for #1 to #5 was calculated every 3 months. At this time, the results were standardized assuming the standard deviation of tension between # 2 and # 3 in 2012 1Q to be 1.

Although there are differences depending on the stands, the standard deviation of the measured tension values has decreased since 1Q, i.e., during 2Q to 4Q, immediately after the introduction. Conventionally, operators observed the change in the current value when a rolled material was bitten to measure the timing for adjusting the rotations as the material passed each stand. The introduction of the tension monitor system has enabled the current values to be displayed as calculated tension values on one screen and be displayed also as a trend in the order of rolling. It is perceived that this has enabled

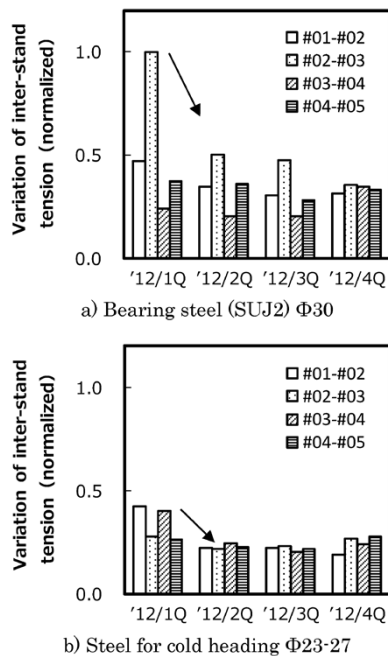


Fig. 8 Changes of inter-stand tensions

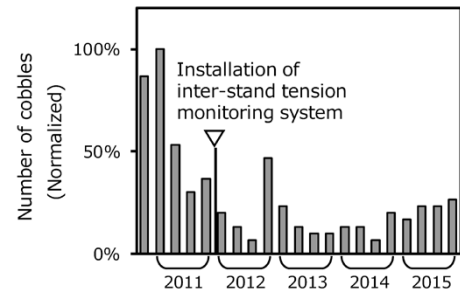


Fig. 9 Changes in number of cobbles in bar mill

the operators to grasp the situation of multiple stands at a glance with any timing and has facilitated the adjustment of the rotational speed, which has led to the stabilization of inter-stand tension.

Fig. 9 shows the cobble frequency before and after the introduction of this tension monitor system. The frequency of occurrence was tabulated every 3 months and standardized with the maximum occurrence frequency as 100%. Cobble is known to occur due to various reasons, including improper adjustment of the roll speed, and has decreased significantly since the application of the monitor system.

Conclusions

A technique was developed to calculate the inter-stand tension from the differential current using a steel-bar rolling model. A tension monitor system that displays the tension calculated by this technique was introduced into the steel bar plant of Kobe Works, Kobe Steel. This monitor system is used by the operators to adjust the rotational speed of the rolling train motor, and, as a result, variations in tension setting have been reduced, contributing to the reduction of cobble.

References

- 1) M. Asakawa et al. Journal of the Japan Society for Technology of Plasticity. 1979, Vol.20, No.224, p.841.
- 2) M. Uemura et al. Tetsu-to-Hagane. Iron and Steel Institute of Japan. 1985, Vol.71, No.12, S1127.
- 3) M. Uemura et al. Tetsu-to-Hagane, Iron and Steel Institute of Japan. 1986, Vol.72, No.12, S1243.
- 4) Y. Saito et al. Journal of the Japan Society for Technology of Plasticity. 1983, Vol.24, No.273, p.1070.
- 5) Y. Noguchi et al. The 31st Sokaren Koron. 1980, p.395.
- 6) Y. Noguchi et al. The 32nd Sokaren Koron. 1981, p.29.

Technology for Reducing Strip Meandering in Tandem Cold Mill

Shigeto KOIZUMI*¹, Dr. Shusuke YANAGI*², Dr. Masanori KOBAYASHI*³

*¹ Sheet Production Department, Kakogawa Works, Iron & Steel Business

*² Materials Research Laboratory, Technical Development Group

*³ Process Engineering Development Section, Research & Development Laboratory, Iron & Steel Business

Strip meandering in a tandem cold mill causes strip breakage troubles and must be suppressed. The issue of meandering has been studied for a long time, but many of the studies focused on runout of the strip tail end with tension released, or on the inter-stand meandering behavior during tandem rolling. On the other hand, even at the entry side of a tandem cold mill with a tension lower than that of inter-stand, strips may meander due to various disturbances and cause problems. Hence, an analysis model of meandering behavior was constructed while considering the restraint by bridle rolls disposed on the entry side of a tandem cold mill. The effect of entry-side tension on meandering behavior was investigated, and the calculation results were verified by rolling experiments. It was found that the tension enhancement on the entry-side was effective for the suppression of meandering. Consequently, the entry-side tension of the tandem cold mill of Kakogawa Works was increased, and this has reduced the problems due to meandering.

Introduction

Tandem cold rolling is an intermediate process that supplies semi-products to the annealing and galvanizing processes and is important in creating the thickness of cold-rolled and surface-treated steel products. In tandem cold rolling, it is essential to stably supply semi-product to the subsequent process. One of the factors that inhibit stable production in the tandem cold rolling is that a steel strip may be rolled off-center in the rolling mill (hereinafter referred to as "meandering"). If this happens, there is a risk that the steel strip will be partially buckled, folded into a roll bite and broken. Once a steel strip breaks, the clean-up takes a long time, resulting in a significant loss of opportunity, as well as economic losses caused by yield loss and roll damage. Hence, the reduction of meandering is a challenge that must be addressed for the stable operation of cold-rolling mills.

The problem of meandering in strip rolling has been studied for a long time, including the construction of analysis models, experimental verifications, and the development of techniques for controlling meandering.¹⁾⁻⁷⁾ Many of these studies focused on "runout of strip tail end," in which tension is released at the tail end of the coil,

and "inter-stand meandering behavior" in tandem rolling. On the other hand, since the tension on the entry side of tandem rolling is lower than the inter-stand tension, meandering may easily be caused by non-symmetric components such as a difference in mill rigidity between the work side (WS) and drive side (DS), leveling difference in roll gap, wedging of hot-rolled strip (thickness difference between left and right sides), and camber. Particularly in the case of high-tensile-strength steel, which causes greater roll-separating force, the effect of asymmetry in rolling becomes even more significant.

Hence, an analysis was performed to see how the entry-side tension of the rolling mill influences meandering. The effect of the entry-side tension was evaluated by the laboratory and rolling experiments using an actual apparatus, and it was clarified that the strip meandering can be suppressed by increasing the entry-side tension of the mill. On the basis of these results, the tension on the entry side of the tandem cold rolling mill at Kakogawa Works was increased; making this change has greatly reduced the troubles caused by strip meandering. This paper reports on the outline of that approach.

1. Analysis of strip meandering behavior during rolling

The hitherto proposed methods for analyzing strip meandering during rolling include the deformation analysis of the rolling mill, deformation analysis of material and the relational expressions between the incident angle or left/right speed difference and meandering. Each analytical method has led to an examination result showing that the amount of meandering gradually increases if there is an initial irregularity such as a roll gap leveling difference (the difference in the gap between the left and right sides of the rolling mill, hereinafter referred to as "leveling difference").¹⁾⁻⁷⁾ On the entry side of the tandem rolling mill, however, the strip is restrained gently by tension, and meandering rarely continues to increase, even when an initial irregularity such as a leveling difference exists. Thus, the conventional methods of analysis do not necessarily represent the actual phenomena.

Hence, the model shown in **Fig. 1** was devised

on the assumption that there is a meandering retention mechanism involving tension. Fig. 1 shows an example where there is an initial irregularity of leveling difference. If the rolled material is not restrained at its rear (Fig. 1, bottom), the rolled material rotates around a point directly below the roll and enters the roll bite at an incident angle of θ_s (Fig. 1 (a)), as is the case with conventional analytical methods. On the entry side of the tandem rolling mill, however, the rolled material is fixed by a bridle roll in the width and traveling directions and cannot rotate on the entry side of the rolling mill. Due to this constraint, a tension distribution, $\sigma'_E(x)$, is formed on the entry side of the rolling mill (Fig. 1(b)). This entry-side tension is generated by the in-plane bending back of the strip, and the distribution is such that the tension on the narrow side of the roll gap is low and the tension on the wide side of the roll gap is high. Due to such a tension distribution, the load on the side with a narrow roll gap increases, and, while the load on the side with a wide roll gap decreases so as to cancel the difference in the roll gap. If the rolling is further continued and the rolled material meanders more, the difference in tension between the left and right sides increases, and the initial leveling difference between the left and right sides disappears completely. As a result, the rolled material enters the rolling mill at an incident angle of 0, and meandering stops (Fig. 1 (c)).

Fig. 2 shows the numerical calculation method for analyzing meandering on the basis of the above concept. First, assumptions are made for initial irregularities such as the leveling difference, wedging, and initial amount of meandering. Next, taking the bridle roll on the entry side of the tandem rolling mill as a rigid support, the deformation of the strip between the bridle roll and the head stand is calculated to determine the tension distribution at the entry side of the head stand. This entry-side tension distribution is used to calculate the

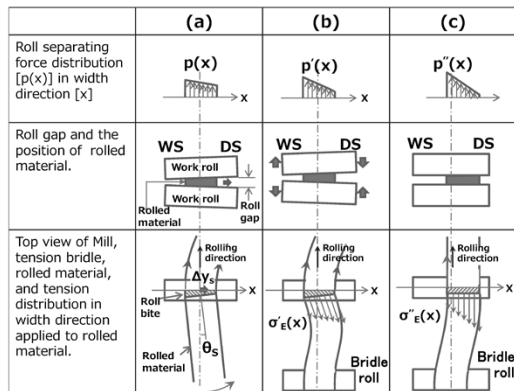


Fig. 1 Analytical model of strip meandering at entry side of tandem cold mill

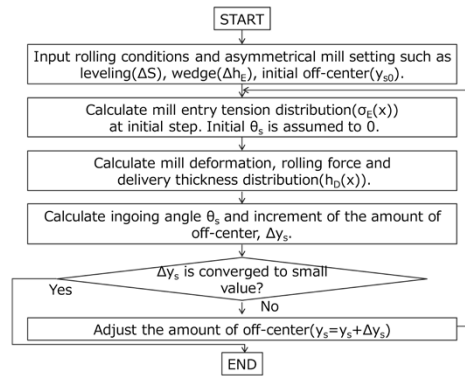


Fig. 2 Method of calculating strip meandering at entry side of cold strip mill⁸⁾

deformation of the rolling mill, the rolling load distribution, the strip thickness distribution on the exit side, and the difference in reduction ratio between the left and right sides. The incident angle θ_s is obtained from the difference in reduction ratio between the left and right sides, and the meandering increment Δy_s during the minute time Δt is added to the initial value or the amount of meandering obtained in the previous calculation. The entry-side tension distribution is calculated for the renewed amount of meandering. Similarly, the meandering behavior of the strip is calculated by repeatedly calculating the load distribution, strip thickness distribution, reduction ratio difference, and amount of meandering increment. It should be noted that the incident angle θ_s and meandering increment Δy_s are calculated using the following geometric equation, in which v_s is the strip speed on the entry side of the rolling mill.

$$\Delta y_s = v_s \cdot \tan \theta_s \cdot \Delta t \dots\dots\dots (1)$$

Fig. 3 shows a calculation example for the amount of strip meandering and the tension distribution in the strip width direction at the entry side of a rolling mill. The calculation conditions are shown in the figure. Considering the availability of material for comparison of the calculation results with those of laboratory rolling described later, aluminum is used here. Referring to Fig. 3, when the strip meanders on the entry side of the rolling mill, a compressive stress is formed toward the inside of the bend and a tensile stress is formed toward the outside of the bend due to the in-plane bending of the strip. These stresses are added to the initially loaded tension. As the amount of meandering increases, the stress toward the inside of the bend (the left side of each graph in Fig. 3) becomes compressive even after the addition to the loaded tension (Fig. 3 (b)). The strip does not buckle when the compressive stress is small; however, when under a compressive stress above a certain level,

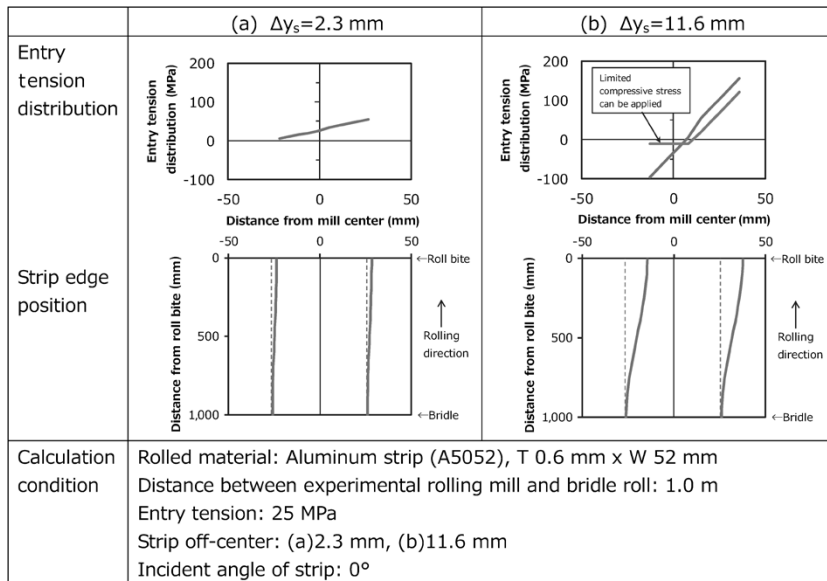


Fig. 3 Examples of calculation of tensile distribution caused between off-center value of rolled strip and entry side of rolling mill

Table 1 Conditions of strip meandering calculation

Experimental Rolling mill	4H, Work roll: Φ 50 mm x L 200 mm Back up roll: Φ 200 mm x L 200 mm
Rolled Material	Aluminum, A5052 T 0.6 mm x W 52 mm
Reduction	24%
Entry tension	(1)(2)30 MPa (3)100 MPa
Delivery tension	50 MPa
Roll gap leveling	(1)50 μ m (2)(3)250 μ m
Length between entry side bridle roll and Rolling mill center	1,000 mm

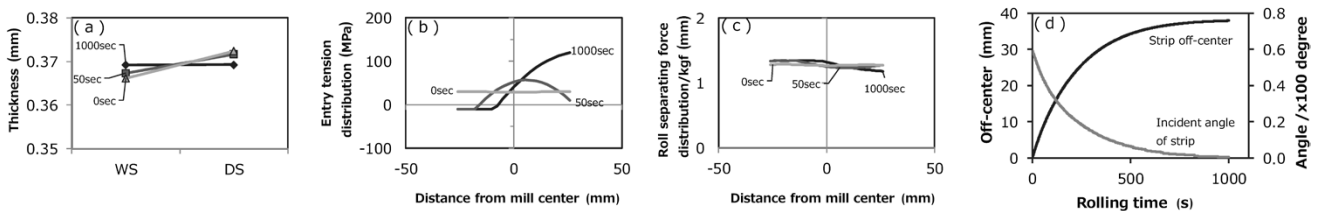


Fig. 4 Analytical result (1) with small initial roll gap leveling difference.

- (a) Thickness of rolled material at exit side of roll bite.
 (b) Tension distribution along width direction at entry side of roll bite.
 (c) Roll separating force distribution along width direction. (d) Strip meandering and incident angle.

out-of-plane deformation of the strip occurs due to local buckling. It is estimated that the compressive stress at which no local buckling occurs (allowable compressive stress) depends on the strip thickness and strip width; hence, this analysis employed an adjustment parameter determined by experiments and other means.

The strip thickness distribution, load distribution, tension distribution, and amount of meandering were sequentially calculated in accordance with the flow in Fig. 2. Table 1 shows the analysis conditions. Here, leveling difference is taken up

as an asymmetry factor. Fig. 4 shows the analysis results when the leveling difference is 50 μ m, Fig. 5 shows the analysis results when it is 250 μ m, and Fig. 6 shows the analysis results when the leveling difference is 250 μ m and the entry-side tension is 100 MPa. Since there is a leveling difference in either case, a difference in strip thickness is found between the left and right sides at the beginning of the sequential calculation (Fig. 4-6 (a): rolling time=0s). As the calculation is repeated, the strip gradually meanders to the wide side of the gap (Fig. 4-6 (d)), increasing the tension difference

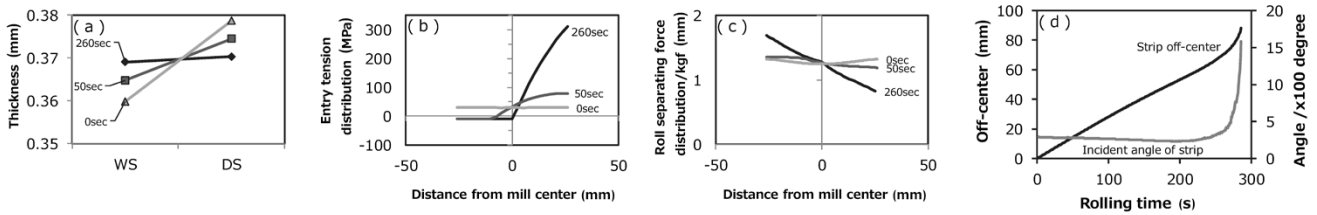


Fig. 5 Analytical result (2) with large initial roll gap leveling difference.

- (a) Thickness of rolled material at delivery side of roll bite.
- (b) Tension distribution along width direction at entrance of roll bite.
- (c) Roll separating force distribution along width direction.
- (d) Strip meandering and incident angle.

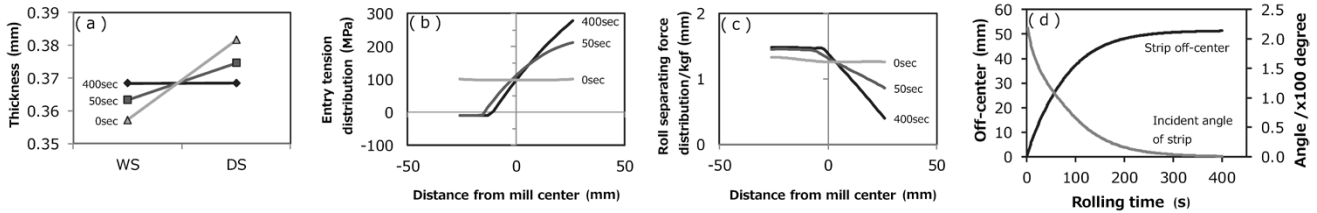


Fig. 6 Analytical result (3) with large tension being applied to strip at entry side of roll bite.

- (a) Thickness of rolled material at exit side of roll bite.
- (b) Tension distribution along width direction at entry side of roll bite.
- (c) Roll separating force distribution along width direction.
- (d) Strip meandering and incident angle.

between the left and right sides (rolling time=50s). As a result, the rolling load on the side where the strip meanders decreases (Fig. 4-6 (c)), and the difference in strip thickness between the left and right sides gradually decreases (Fig. 4-6 (a): rolling time=1,000, 260, 400s). Through such a process, when the given leveling difference is small (Fig. 4) and after the meandering of about 40 mm, the thickness difference between the left and right sides is eliminated, the incident angle becomes zero, and the meandering stops. Under the condition of a great leveling difference (Fig. 5), when the amount of meandering increases, the compressive stress due to in-plane bending of the strip increases, expanding the region with compressive stress exceeding the allowable range. Further expansion of this region does not increase the tension difference between the left and right sides, and the load difference between the left and right sides does not increase. As a result, the meandering continues to propagate without resolving the thickness difference of the strip (divergence of meandering).

On the other hand, when the entry-side tension is increased (Fig. 6), even if the strip greatly meanders, the differences in tension and load between the left and right sides can be increased without expanding the region where compressive stress exceeds the allowable range. As a result, the difference in strip thickness is eliminated, the incident angle becomes 0 degrees, and the meandering stops (Fig. 6).

2. Method of meandering experiment using test rolling, experimental results and discussion

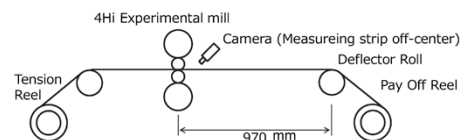
In order to confirm the validity of the method of analyzing meandering, testing was conducted using an experimental rolling mill. **Table 2** shows a diagram of the experimental rolling mill and the testing conditions. The strip was filmed by a camera installed above the entry side of the rolling mill, and the amount of meandering of the strip was calculated by reading the position of the strip end in the captured image.

Fig. 7 shows the experimental and analytical results of the meandering behavior when the leveling difference is changed. In the case of the experimental rolling mill, meandering stopped under the conditions where the leveling difference was

Table 2 Schematic diagram of experimental rolling mill and experimental conditions

Experimental Rolling mill	4H, Work roll: Φ 50 mm \times L 200 mm Back up roll: Φ 200 mm \times L 200mm
Rolled Material	Aluminum, A5052 T 0.6 mm \times W 52 mm
Reduction	33 %
Entry tension	10-80 MPa
Delivery tension	24 MPa
Roll gap leveling	0-200 μ m

Schematic diagram of experimental rolling



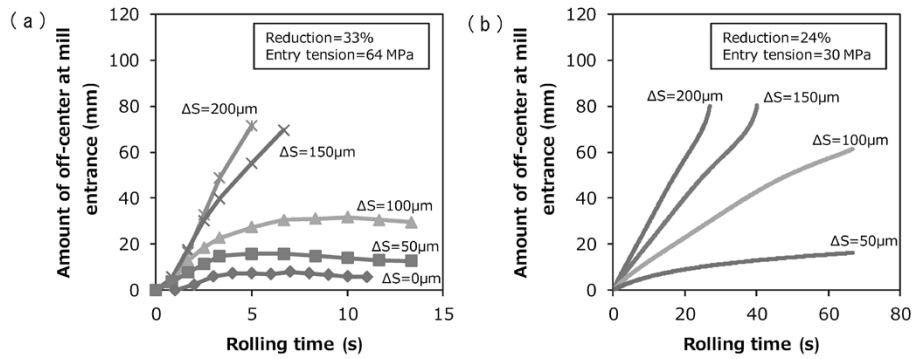


Fig. 7 Relationship between roll gap leveling difference ΔS and strip off-center, (a) experimental result and (b) analytical result

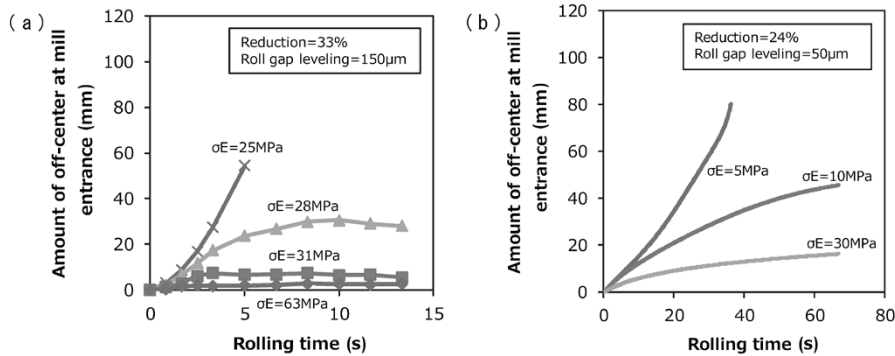


Fig. 8 Relationship between entry-side tension σE and strip off-center, (a) experimental results and (b) analytical results

small (less than $100 \mu\text{m}$). When a certain threshold (between $100 \mu\text{m}$ and $150 \mu\text{m}$) was exceeded, however, the meandering rate (the increase in meandering when rolling for a certain length) rapidly increased and the meandering diverged. In the meandering analysis also, meandering stopped when the leveling difference was $50 \mu\text{m}$, and diverged when the leveling difference was $150 \mu\text{m}$ or greater. When the leveling difference was intermediate, $100 \mu\text{m}$, however, the amount of meandering continued to increase while the meandering rate gradually slowed down.

Fig. 8 shows the experimental and analytical results of the meandering behavior when the entry-side tension is changed. In the case of the experiment using the rolling mill for testing (Fig. 8 (a)), meandering stops when the tension is high, as in the case where the leveling difference is changed. As the tension is gradually decreased, however, the amount of meandering when the strip meandering ends gradually increases, and when the tension falls below a certain threshold (28 MPa), meandering increases rapidly and diverges. Meanwhile, in the analysis, meandering stops when the tension is high, and amount of meandering increases and gradually diverges when the tension is low. There is, however, no clear transition between diverging and stopping as in the experimental results.

The meandering behavior on the entry side

of a tandem rolling mill will be discussed while considering the above experimental and analytical results. First, the strip starts meandering due to initial irregularities such as a slight leveling difference, wedging, and a difference in mill stiffness (Fig. 9 (a)). If the initial irregularity that induces such meandering is small, the entry-side tension distribution generated by slight left-and-right meandering of the strip eliminates the difference in thickness between the left and right sides of the strip, and the meandering stops (Fig. 9 (b)). Normally, it is considered that rolling is performed in such a manner.

On the other hand, when the initial irregularity is great, the compressive stress in the longitudinal direction caused by the in-plane bending of the strip exceeds the critical limit of buckling, and the tension difference between the left and right side does not increase. As a result, the difference in rolling load between the left and right sides does not increase, the difference in thickness between the left and right sides of the strip is not eliminated, and the meandering continues to propagate (divergence of meandering) (Fig. 9 (c)). Increasing the entry-side tension prevents buckling from occurring because the region where compressive stress is formed is limited to a narrow range even if the tension difference between the left and right sides is increased. Therefore, the differences in the tension

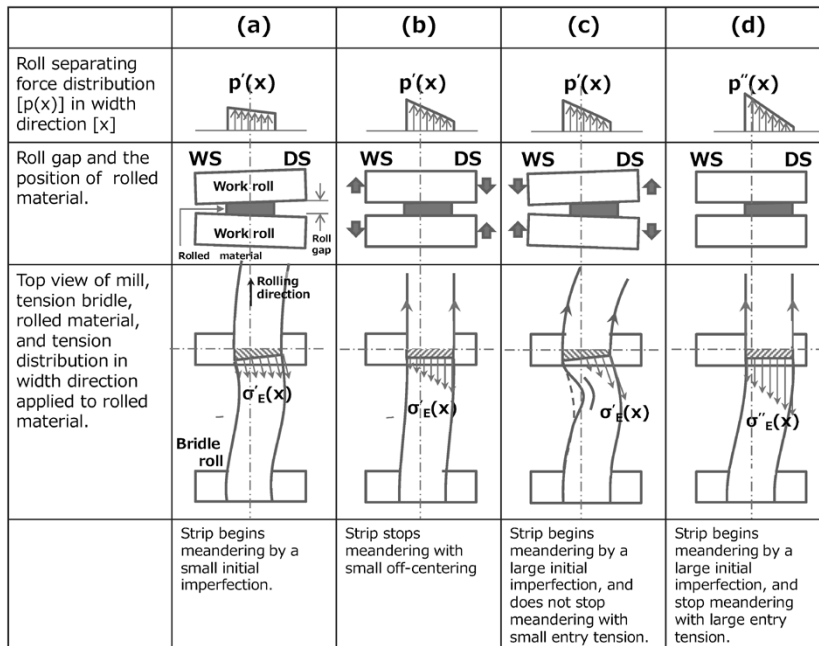


Fig. 9 Mechanism of retention and divergence in strip meandering phenomenon at tandem cold mill

and load continue to be corrected until the thickness difference between the left and right sides of the strip is eliminated and the meandering stops (Fig. 9 (d)).

Moreover, the experimental and analytical results (Figs. 7 and 8) show a difference in the propagation time of meandering. This is considered to be due to the following reasons: When there is an initial irregularity in the rolling conditions, the advance rate and reverse rate differ on the left and right, causing a left-and-right-side difference in the length of the entry side material entering the roll bite. In the experiment, the difference in entry-side length on the left and right sides accumulates as rolling proceeds, while the analysis does not take into account the accumulation of this difference in length. Therefore, the out-of-plane deformation due to entry side compressive stress occurs earlier in the case of the experiment, and meandering propagates. Also, since the ultimate tension distribution is reached earlier in the experiment, the time before stopping becomes shorter than that in the analysis.

If meandering follows the above mechanism, the following facts are considered to hold:

- (1) When the strip is thick on the entry side, the allowable compressive stress is increased, making buckling less likely to occur, which makes it easier to stop meandering.
- (2) When the strip is wide, a slight meandering causes a difference in an in-plane tension that is greater than that for a narrow strip between the left and right sides, which makes meandering less likely.

- (3) Even if the distance between the rolling mill and entry side restraint rolls, such as bridle rolls, is made smaller, the difference in tension between the left and right sides during meandering is increased, making meandering more likely to stop.
- (4) If the original strip is not flat enough when entering the rolling mill and becomes wavy on the entry side of the rolling mill, a large in-plane tension difference cannot be formed, making meandering likely to diverge.

It is difficult to change the equipment layout of the existing tandem rolling mill. From the above considerations, however, it is thought that the tension can be increased on the entry-side of the rolling mill, where the strip is relatively thick, and thereby the meandering can be stopped without its diverging.

3. Suppression of meandering by increasing entry-side tension of actual tandem cold mill

3.1 Equipment outline of tandem cold mill

Fig.10 shows the overview of the tandem cold mill at Kakogawa Works of Kobe Steel. The rolling mill comprises a total of 5 stands, and entry-side tension is imparted by the bridle rolls on the entry side of the mill. Tension-meter rolls for measuring the strip tension are disposed on the entry and exit sides of each stand and is controlled so that the tension value inputted beforehand in a table is imparted.

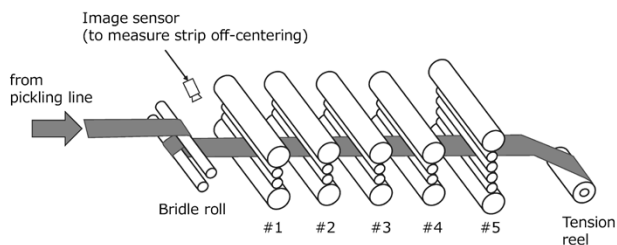


Fig.10 Overview of tandem cold mill in Kakogawa Works

The motor output that imparts the tension is 8,000 kW for each stand, while that of the bridle roll on the mill entry side is 360 kW. Thus, the entry side of the mill is configured to impart a tension smaller than the tension imparted between the stands.

3.2 Experimental method

In order to confirm that increased entry-side tension has a suppressive effect on meandering, the relationship between the mill entry-side tension and amount of meandering was investigated using an actual cold tandem rolling mill.

The rolling was performed using the actual cold tandem mill in a steady state with stable rolling conditions. Next, a leveling difference of $150\ \mu\text{m}$ was applied to the #1 stand so as to initiate meandering, and the applied leveling difference was maintained for 15 seconds after the start of operation in order to measure the amount of meandering of the strip rolled during that period. A CCD camera was fixedly disposed at the middle position of the center-position-control device, the strip roll closest to the #1 stand of the tandem rolling mill, and the amount of meandering was measured on the image of the strip, the strip-edge position having been extracted using an image processing apparatus. Since the strip centering is performed by the center-position-control device, the amount of strip meandering measured at the intermediate position is considered to be about half of the amount of strip meandering directly under the #1 stand.

The experimental conditions are shown in Table 3. The tested material was a 980MPa grade high-tensile-strength steel, the strip thickness at the entry side of the #1 stand was 2.3 mm, the strip width was 1,250 mm, and the rolling load was 1,500 tonnes. The mill entry-side tension was set at 2 levels, a reference condition and 0.7 times the reference condition.

3.3 Experimental results

Fig.11 shows the measurement results for strip meandering in the cases where a leveling difference of $150\ \mu\text{m}$ was imparted for each condition and the

Table 3 Conditions of strip meandering experiment using actual mill

Rolled material	980 MPa class high tensile strength steel T 2.3 mm \times W 1,250 mm
Rolling force	1,400 tonf
Roll gap leveling	$150\ \mu\text{m}$
Tension at entry side of #1	Standard tension, Standard tension \times 0.7
Tension between #1 and #2	Standard tension
Rolling speed	50 mpm
Lubricant	Emulsion
Measuring method of strip off-centering	Measured by image sensor (KEYENCE CV-3500)

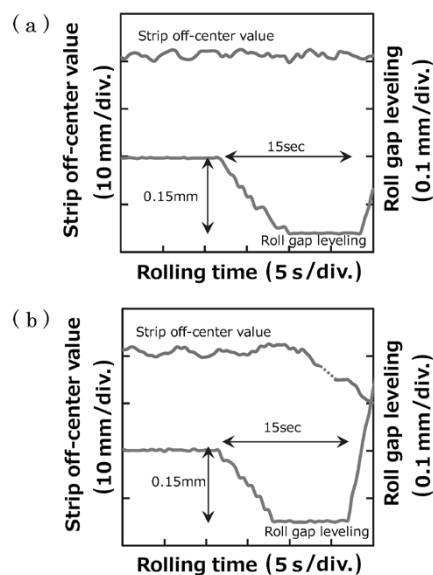


Fig.11 Result of strip meandering experiment with actual mill ((a)standard tension (b)standard tension \times 0.7)

plate-feed state was maintained for 15 seconds after the start of operation.

When the entry-side tension was in the reference condition, the amount of meandering remained almost unchanged for 15 seconds after the leveling difference had been imparted. On the other hand, when the entry-side tension was 0.7 times the reference condition, the amount of meandering exceeded 10 mm. These results suggest that meandering can be suppressed by increasing the tension even in the actual tandem rolling mill.

3.4 Results of actual machine improvement

On the basis of the test results on the mill entry-side tension and amount of strip meandering, the entry-side tension was increased for the tandem rolling mill at the cold strip mill of Kakogawa Works. The outline of this reinforcement is given in Table 4. The motor output of the bridle roll for imparting tension at the entry side of the #1 stand was increased from 360 kW to 1,410 kW.

On the basis of the analysis of the constructed meandering model, the conditions that would

Table 4 Reinforcement of tension bridle at entry side of tandem cold mill in Kakogawa Works

	Before reinforcement	After reinforcement
Motor power of tension bridle	Total 360 kW	Total 1,410 kW

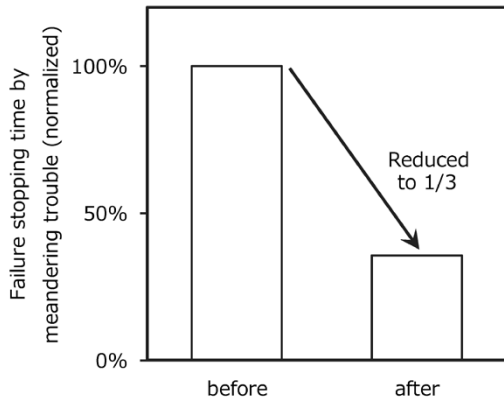


Fig.12 Change in failure downtime caused by meandering trouble before and after reinforcement of tension bridle

stop meandering were found even for the initial irregularities that can occur in operation, and the tension conditions on the entry side of the rolling mill were set for each rolling specification.

Fig.12 compares the failure shut-down rates due to strip meandering at the #1 stand before and after the entry-side tension enhancement. After the entry-side tension was increased, the time consumed by meandering trouble in #1 stand was reduced to 1/3 of what it had been before the increase, which greatly contributed to stable production.

Conclusions

Taking into account the tension distribution on the entry side of a rolling mill, a model was constructed to analyze the meandering phenomena in the entry side of a tandem cold mill, and the validity of the analysis was confirmed by laboratory rolling.

The analysis revealed that the meandering of the strip during rolling can be stopped by increasing the entry-side tension, and the meandering phenomenon was confirmed to stop in an actual cold rolling mill.

On the basis of this knowledge, the electric motor was strengthened in the entry-side bridle roll of the cold tandem rolling mill at Kakogawa Works and the entry-side tension of the mill was optimized. As a result, meandering troubles in the rolling mill have been reduced.

References

- 1) C. Hayashi et al. Tetsu-to-Hagane. 1977, Vol.63, No.2, A21-24.
- 2) K. Nakajima et al. Proceedings of the Japanese Spring Conference for the Technology of Plasticity, Japan Soc. for Technology of Plasticity, 1980, p.61.
- 3) Y. Oike et al. Proceedings of the Japanese Spring Conference for the Technology of Plasticity, Japan Soc. for Technology of Plasticity, 1983, p.377.
- 4) T. Ishikawa et al. Trans. ISIJ. 1988, Vol.28, No.6, p.485.
- 5) H. Furumoto et al. Journal of JSTP.1997, Vol.38, No.442, pp.996-1006.
- 6) A. Ishii et al. CAMP-ISIJ, 2005, Vol.18, p.1164.
- 7) H. Matsumoto et al. The Proceedings of the 53rd Japanese Joint Conference for the Technology of Plasticity. 2002-11-22/24, Japan Soc. for Technology of Plasticity, 2002, p.117.
- 8) S. Yanagi et al. CAMP-ISIJ. 2018, Vol.31, p.724.

Influence of Modified Oxide Inclusions on Initiation of Rolling Contact Fatigue Cracks in Bearing Steel

Masaki SHIMAMOTO*¹, Dr. Eiichi TAMURA*¹, Akihiro OWAKI*², Akihiro MATSUGASAKO*²

*¹ Material Research Laboratory, Technical Development Group

*² Wire Rod & Bar Products Development Department, Research & Development Laboratory, Iron & Steel Business

In order to elucidate the mechanism by which the modification of oxide inclusions in bearing steel leads to the improvement of rolling contact fatigue (RCF) properties, a study was conducted with particular attention to the difference in the crack initiation time. Compared with normal Al-killed steel, non-Al-killed steel with modified oxide inclusions has been confirmed to exhibit improved rolling contact fatigue properties. Investigations using ultrasonic testing (UT) and acoustic emission (AE) have revealed that the non-Al-killed steel has a smaller number of defects detected by UT and the number of signals detected by AE, both indicating the suppressed initiation of initial cracks. A study done on the reasons shows that SiO₂-based inclusions generated in the non-Al-killed steel have excellent adhesion between each inclusion and the matrix, with a smaller difference in Young's modulus between them. Therefore, it is conceivable that the non-Al-killed steel experiences a decreased amount of the strain change that occurs in the vicinity of inclusions during rolling load, which suppresses the initiation of initial cracks and improves the rolling contact fatigue properties.

Introduction

Bearing parts are used in various industrial machines and automobiles and require high reliability. Hence, excellent rolling contact fatigue properties are required for the bearing steel used in bearing parts, and various researches have been conducted focusing on non-metallic inclusions (hereinafter referred to as "inclusions"), which can become the origin of fatigue fracture.

As a result of previous studies, flaking due to rolling contact fatigue originated from inclusions is considered to occur through the following process:¹⁾

- (1) Initiation of cracks from inclusions as points of origin.
- (2) Steady propagation of cracks.
- (3) Flaking due to the rapid propagation of cracks.

Of these cracks, those that are initiated from inclusions as points of origin are considered to occur very early in rolling contact fatigue. Udagawa et al.²⁾ reported that the initiation time of cracks from oxide inclusions as the points of origin is 1×10^4 cycles.

Tsuchida et al.³⁾ discussed the initiation mechanism of cracks from inclusions as the points of origin. They clarified that not only the size of

the inclusions but also the Young's modulus of the inclusions and the adhesion state of the interface between the inclusions and the matrix must be considered for the initiation of cracks.

Hashimoto et al.⁴⁾ prepared normal Al-killed steel and another kind of steel made by a modified deoxidation method and observed the characteristics of the interface between the inclusions and matrix. According to their report, there are gaps in the periphery of each Al₂O₃ inclusion in the normal Al-killed steel, whereas Al₂O₃ · SiO₂ based inclusions in the steel produced by the modified deoxidation method adhere well with the matrix, and the steel prepared by the modified method has a longer life.

However, it has not been clarified how modifying the oxide inclusions by changing the deoxidation method makes a difference in the crack initiation time.

Hence, Kobe Steel focused particularly on the difference in crack initiation time, with the aim of elucidating the mechanism through which rolling contact fatigue properties are improved by modifying oxide inclusions, a type of inclusion. Also, the reason for the difference in crack initiation time was discussed from the viewpoints of inclusion size, adhesion between the inclusions and matrix, and Young's modulus of inclusions, which are considered to be factors affecting crack initiation.

1. Experimental method

Samples AL-1 and AL-2 were prepared as normal Al-killed steel. In addition, samples Non-AL-1 and Non-AL-2 were prepared as non-Al-killed steel to modify oxide inclusions. **Table 1** shows the chemical compositions of the samples. AL-1, Non-AL-1, and Non-AL-2 were melted in an induction melting furnace (melting capacity: 170 kg), and then hot-forged and hot-rolled into material with a diameter of 65 mm. A billet produced in the actual process was used to prepare AL-2, which was hot-rolled into material with a diameter of 65 mm. Each hot-rolled material was cut, spheroidizing annealed (795°C × 6 h), quenched (840°C × 30 min), tempered (160°C × 2 h), and final polished into specimens for a thrust-type rolling contact fatigue test.

Thrust-type rolling contact fatigue tests were conducted on AL-1 and Non-AL-1 under the

Table 1 Chemical compositions and deoxidation type of steel samples^{5), 6)}

No.	Deoxidation type	C	Si	Mn	Cr	Al	P	S	O
		wt%	wt%	wt%	wt%	wt%	wt%	wt%	ppm
AL-1	Al-killed	1.08	0.25	0.36	1.47	0.017	0.013	0.005	4
AL-2	Al-killed	1.00	0.25	0.31	1.47	0.022	0.011	0.005	3
Non AL-1	Non Al-killed	1.01	0.25	0.35	1.47	<0.001	0.016	0.001	16
Non AL-2	Non Al-killed	1.02	0.25	0.35	1.47	0.001	0.014	0.001	13

Table 2 Conditions of thrust-type rolling contact fatigue test^{5), 6)}

Ball diameter	9.53 mm(SUJ2)
Number of balls	3
Contact surface pressure	5.24 GPa
Rolling contact frequency	1,500 rpm
Number of specimens	16
Maximum number of cycles	2×10^8

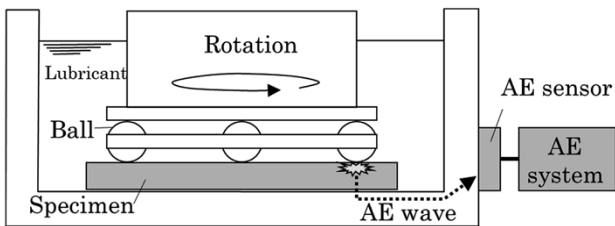


Fig. 1 Schematic diagram of thrust-type rolling contact fatigue test and AE sensor

conditions shown in **Table 2** to investigate the effect of modified oxide inclusions on the rolling contact fatigue properties. Also, in order to investigate how the modification of oxide inclusions affects the crack initiation time, thrust-type rolling contact fatigue tests were conducted on AL-2 and Non-AL-2 under the conditions in Table 2. AL-2 and Non-AL-2 were subjected to ultrasonic testing (hereinafter referred to as "UT") during the rolling contact fatigue test. The UT was performed under a frequency of 125 MHz, and the conditions were adjusted such that the specimen surface layer of 0.05 to 0.45 mm thick fell within the detection range. The entire surface of each specimen was regarded as the observation surface for UT, and the number of defects immediately below the transfer surface of each steel sphere was examined.

Furthermore, in order to investigate the crack initiation time and propagation status as needed, an acoustic emission (hereinafter referred to as "AE") apparatus was installed in the specimen holder of the thrust-type rolling contact fatigue test machine (**Fig. 1**) to detect AE signals emitted from inside the specimens during the rolling contact fatigue test.

2. Experimental results

2.1 Properties of thrust-type rolling contact fatigue

Fig. 2 shows the results of rolling contact fatigue tests. The non-Al-killed steel (Non-AL-1) has an L_{10} life^{Note)} of 2.0×10^8 cycles or higher, an improvement compared with the 6.1×10^6 cycles of the Al-killed steel (AL-1). Thus, the rolling contact fatigue properties have been improved by changing the deoxidation method. It should be noted that none of the Non-AL-1 specimens exhibited flaking, and the test was aborted at a load count of 2.0×10^8 cycles.

2.2 Crack initiation time (UT, AE evaluations)

The Al-killed steel (AL-2) was evaluated by UT at the initial stage of the rolling contact fatigue test (load count, 1.0×10^6 cycles). As a result, 20 defects were detected immediately below the rolling contact surface (**Fig. 3 (a)**). In addition, as the load count increased, the number of defects detected by UT increased (**Fig. 3 (b)**, load count 6.3×10^6 cycles). It should be noted that flaking occurred in the AL-2 specimen at the load count of 6.3×10^6 cycles, and the test was aborted.

On the other hand, in the case of the non-Al-

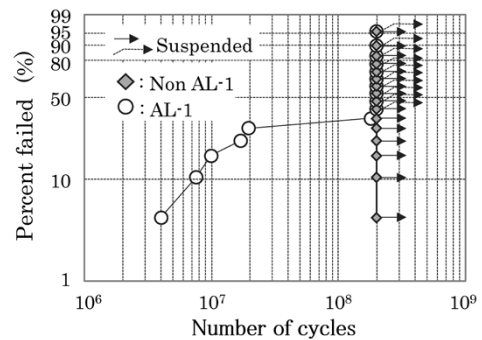


Fig. 2 Results of thrust-type rolling contact fatigue test on AL-1 and Non-AL-1⁵⁾

Note) Number of load cycles with a cumulative failure probability of 10%

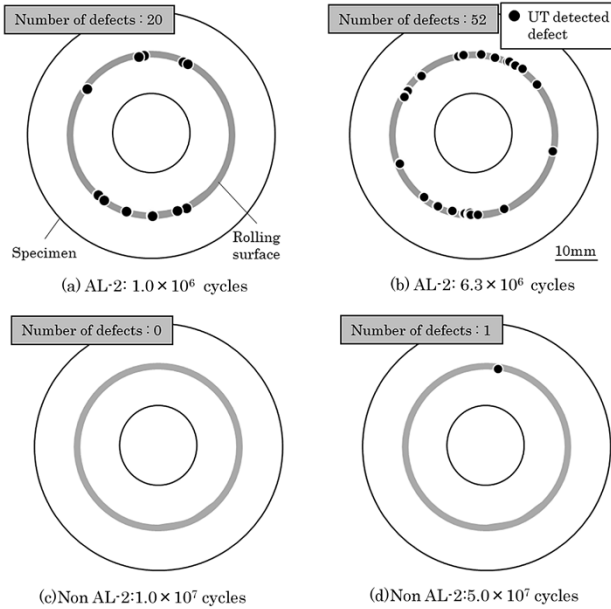


Fig. 3 UT test results of rolling contact fatigue test specimens⁶⁾

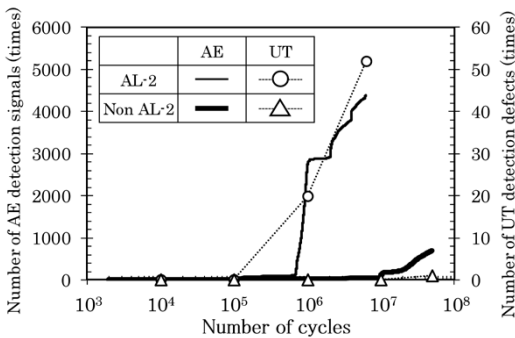


Fig. 4 Relationship between rolling contact fatigue cycles and number of AE signals and UT defects⁶⁾

killed steel (Non-AL-2), no defects were detected by UT at the load count of 1×10^7 cycles (Fig. 3 (c)), and one defect was detected by the same at the load count of 5×10^7 (Fig. 3 (d)).

Next, Fig. 4 shows the changes in the number of signals detected by AE. For the Al-killed steel (AL-2), the total number of AE signals exceeded 100 at the load count of 5.7×10^5 cycles, whereas, for the non-Al-killed steel (Non-AL-2), the total number of AE signals exceeded 100 at the load count of 1.0×10^7 cycles. Fig. 4 also shows the transition of the number of defects detected by UT, and it was found that the non-Al-killed steel (Non-AL-2) had fewer AE signals and UT defects than the Al-killed steel (AL-2), and the time of detection was late in each case.

3. Effect of modifying oxide inclusions on crack initiation time

As described in Section 2, the non-Al-killed steel with modified oxide inclusions has improved rolling

contact fatigue properties compared with the normal Al-killed steel. The results of UT and AE evaluations indicate that the Al-killed steel shows an increase in the number of UT defects and the number of AE signals in the initial stage of the rolling contact fatigue test. On the other hand, the non-Al-killed steel had fewer UT defects and AE signals, and the time of detection was also late in each case. From these results, cracks initiated from oxide inclusions are considered to be suppressed in the non-Al-killed steel. This has led to tests and discussions as to the reasons why the modification of oxide inclusions causes a difference in crack initiation time.

3.1 Modification of inclusions

In order to confirm the modification of inclusions brought about by the change in deoxidation method, the inclusion before the thrust-type rolling contact fatigue test was observed with a scanning electron microscope (SEM) (Fig. 5). Inclusion compositions were analyzed using energy dispersive X-ray spectroscopy (EDS), and, as a result, complex inclusions consisting of Al_2O_3 -base inclusions and MnS were observed in the Al-killed steel (AL-1). On the other hand, in the non-Al-killed steel (Non-AL-1), no Al_2O_3 -based inclusions were observed, but SiO_2 -based inclusions were.

3.2 Inclusion size

The effect of inclusion size was investigated, as it is considered to be a factor affecting the initiation of cracks. The inclusion size is expressed by the following equation:

$$\sqrt{a \times b} \dots \dots \dots (1),$$

wherein a (μm) is the minor axis diameter of an inclusion, and b (μm) is the major axis diameter of the inclusion. The maximum sizes of the inclusions in the Al-killed steel (AL-1) and non-Al-killed steel (Non-AL-1) were predicted by extreme value statistics.

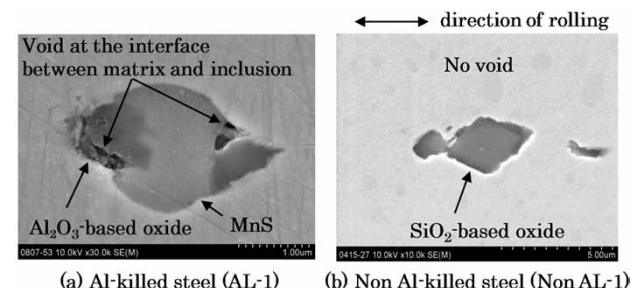


Fig. 5 SEM observation results of non-metallic inclusion before rolling contact fatigue test⁵⁾

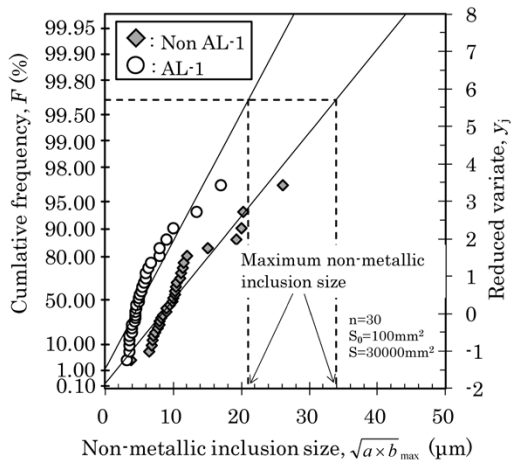


Fig. 6 Predicted maximum size of non-metallic inclusions in AL-1 and Non-AL-1

The analysis results are shown in Fig. 6. The vertical axes of the graph represent cumulative distribution function F and standardized variable y_j . The maximum inclusion size for the Al-killed steel (AL-1) was $21.0 \mu\text{m}$ and that for the non-Al-killed steel (Non-AL-1) was $33.9 \mu\text{m}$.

The inclusion size for the Al-killed steel is smaller than that for the non-Al-killed steel, thus inclusion size cannot explain why crack initiation was suppressed in the non-Al-killed steel.

3.3 Adhesion between inclusions and matrix

The adhesion between inclusions and matrix was investigated. As shown in Fig. 5, gaps were observed at the interface between inclusion and matrix in the Al-killed steel (AL-1). The gaps exist at both ends of each inclusion and lie in the hot rolling direction. On the other hand, in the non-Al-killed steel (Non-AL-1), no gap was observed at the inclusion-matrix interface nor in the SiO_2 -based inclusions.

In other words, the modified inclusions in the non-Al-killed steel were found to adhere better to the matrix than the inclusions generated in the Al-killed steel.

3.4 Young's modulus of inclusions

The Young's moduli of inclusions were investigated. In the case of the Al-killed steel, the Young's modulus of Al_2O_3 generated as Al_2O_3 -based inclusions is approximately 380 GPa.⁷⁾ The Young's modulus of MnS generated at the same time is reported to be 137 GPa, and the Young's modulus of matrix is reported to be 206 GPa⁸⁾. The difference $\Delta E (E_{\text{Matrix}} - E_{\text{Inclusion}})$ between the Young's modulus of the matrix, E_{Matrix} , and the Young's modulus of an inclusion, $E_{\text{Inclusion}}$, is approximately -174 GPa for

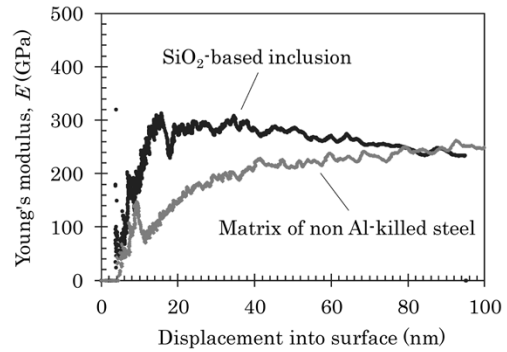


Fig. 7 Nanoindentation test result of SiO_2 -based inclusion and matrix of non Al-killed steel (Non-AL-1)

Al_2O_3 and 69 GPa for MnS.

On the other hand, the Young's modulus of the inclusions modified in the SiO_2 system (hereinafter referred to as "modified inclusions") generated in the non-Al-killed steel (Non-AL-1) is unknown, so the Young's modulus of modified inclusions was measured by the nanoindenter continuous stiffness method under the conditions of excitation vibration amplitude 2 nm and strain rate 0.05 s^{-1} (Fig. 7). According to the reading of the Young's modulus in the indentation depth range where its value was relatively stable, the Young's modulus of the modified inclusions in the non-Al-killed steel was 250 to 300 GPa (indentation depth of 20 nm or more). The Young's modulus of the matrix measured simultaneously was 200 to 250 GPa (indentation depth of 40 nm or deeper) as shown in Fig. 7. That is, the ΔE of modified inclusions of the non-Al-killed steel is -100 to 0 GPa, and the absolute value of the ΔE is smaller than that of the Al_2O_3 -based inclusions observed in the Al-killed steel (AL-1).

3.5 Effect of inclusion-matrix adhesion and Young's modulus of inclusions on crack initiation

The modified inclusions in the non-Al-killed steel have greater adhesion between inclusions and matrix compared with Al_2O_3 -based inclusions generated in the Al-killed steel and have a smaller difference in Young's modulus between the matrix and inclusions. In order to investigate how these features affect the initiation of rolling contact fatigue crack with inclusions as the points of origin, the strain distribution near the inclusion under the rolling load was analyzed using the technique used by Tsuchida et al.³⁾

In the analysis, the inclusions were assumed to have a circular shape with a diameter of $20 \mu\text{m}$, and the adhesion between the inclusion and matrix was categorized as two states: a bonded state and a flaking state. In addition, the Young's modulus of inclusions, $E_{\text{Inclusion}}$, was set to three levels: 100 GPa

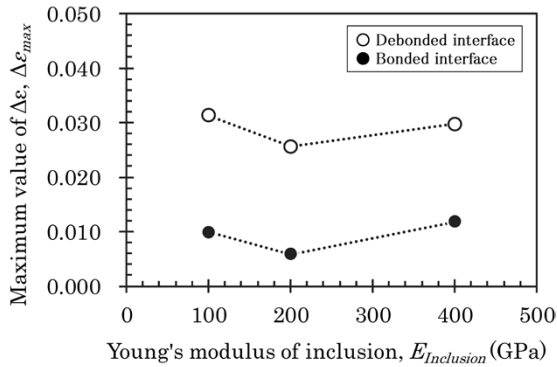


Fig. 8 Influence of interface conditions and Young's modulus of inclusions on maximum value of $\Delta\epsilon$

(simulating MnS), 200 GPa (simulating the modified inclusions in the non-Al-killed steel), and 400 GPa (simulating the Al_2O_3 -based inclusions). The crack from an inclusion as the point of origin was assumed to be initiated by mode I deformation, and from the analysis results, the change in strain, $\Delta\epsilon$, of the tensile composition in an arbitrary direction was obtained and the maximum value $\Delta\epsilon_{max}$ of $\Delta\epsilon$ was calculated.

The analysis results are shown in Fig. 8. When the inclusion-matrix adhesion is in a bonded state, $\Delta\epsilon_{max}$ is smaller in all calculating conditions (Young's modulus) than in the flaking state. Even in the case of a bonded state, it was found that $\Delta\epsilon_{max}$ takes a minimum value when Young's modulus of inclusion is close to that of the matrix (i.e., for simulated modified inclusions in the non-Al-killed steel).

In the analysis simulating Al_2O_3 -based inclusions generated in the Al-killed steel (in the flaking state, $E_{Inclusion} = 400$ GPa), $\Delta\epsilon_{max}$ is 3.0×10^{-2} , whereas, in the analysis simulating modified inclusions in the non-Al-killed steel (adhesion state, $E_{Inclusion} = 200$ GPa), $\Delta\epsilon_{max}$ decreases, becoming as small as 5.8×10^{-3} . For

this reason, cracks with inclusion as their point of origin are considered difficult to initiate from the modified inclusions of the non-Al-killed steel.

4. Mechanism of improving rolling contact fatigue life by modified oxide inclusions

The Al-killed steel had gaps between the inclusions and matrix before the fatigue test, and there was a large difference in Young's modulus between the Al_2O_3 -based inclusions and matrix. In such a case, the strain change in the tensile composition near the inclusions during rolling load increases and the initial crack with an inclusion as the point of origin is likely to be initiated.

On the other hand, the non-Al-killed steel has no gap between inclusions and matrix, which are in a bonded state. Because the difference is small between the modified inclusions in the non-Al-killed steel and the Young's modulus of the matrix, the strain change of the tensile composition near the inclusions is small. As a result, the initial cracks were suppressed, and the non-Al-killed steel was considered to have improved rolling contact fatigue properties compared with the Al-killed steel (Fig. 9).

Conclusions

Kobe Steel focused on and studied the difference in crack initiation time with the aim of elucidating the mechanism by which rolling contact fatigue properties are improved by modified oxide inclusions.

As a result, the non-Al-killed steel was found to have improved rolling contact fatigue properties compared with the Al-killed steel. The modified

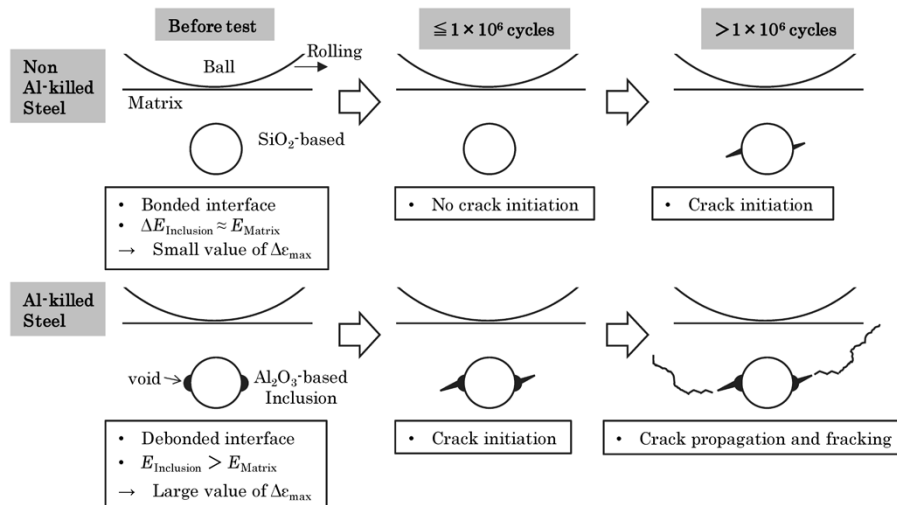


Fig. 9 Mechanism for suppressing rolling fatigue crack initiation by oxidation inclusion change

inclusions of non-Al-killed steel were found to have excellent adhesion with the matrix with a small difference in Young's modulus between the inclusions and matrix. According to the analysis, the amount of strain change that occurs near the inclusions during rolling load is reduced in the non-Al-killed steel. This was found to suppress the initial crack initiation and improve the rolling contact fatigue properties.

References

- 1) O. Umezawa. Fundamental Studies on Technologies for Steel Materials with Enhanced Strength and Functions, Proceedings of the 2nd Symposium. 2012, pp.111-112.
- 2) T. Udagawa et al. Aichi Steel technical review. 2013, Vol.30, pp.29-36.
- 3) T. Tsuchida et al. *R&D Kobe Steel Engineering Reports*. 2011, Vol.61, No.1, pp.62-65.
- 4) K. Hashimoto et al. CAMP-ISIJ. 2008, Vol.21, p.1388.
- 5) M. Shimamoto et al. ASTM Int. STP1580. 2014, pp.173-188.
- 6) A. Owaki et al. ASTM Int. STP1600. 2017, pp.487-501.
- 7) M. Ashizuka et al. Journal of the Ceramic Society of Japan. 1989, Vol.97, pp.544-548.
- 8) T. Fujimatsu et al. Tetsu-to-Hagane. 2008, Vol.94, pp.13-20.